Acta
Technica
Jaurinensis

Vol. 14, No. 1, pp. 1–23, 2021
DOI: 10.14513/actatechjaur.00562

Study of the TP transformation via the inverted pendulum example

A. Wéber, M. Kuczmann

Széchenyi István University, Department of Automation
Egyetem tér 1., 9026, Győr
E-mail: andrea.weber.gyor@gmail.com

Submitted: 04/09/2020; Accepted: 16/11/2020; Published online: 09/12/2020

Abstract: This study decribes the Tensor Product (TP) based model construction through the nonlinear dynamic system of the inverted pendulum. It presents the steps of TP modeling, various weighting functions and the Linear Matrix Inequality (LMI) based approach. LMI control has been used to stabilize the nonlinear system. This study shows the quasi-Linear Parameter-Varying (qLPV) state-space modeling and the Higher-Order Singular Value Decomposition (HOSVD) based TP model transformation. Some research in this issue already exists, but only the furuta, rotary, single and parallel-type double pendulum have been examined. In this paper the TP model transformation of the inverted pendulum is analyzed in terms of stability.

Keywords: *tensor product based control; nonlinear dynamic systems; linear matrix inequality; inverted pendulum*

1. Introduction

Modeling and control of complicated nonlinear systems with multiple objectives are actually a challenge in control engineering. Many researchers investigate the H_2, H_∞ [1], LQ-optimization, pole-placement [2] methods in control theory, which can be solved by LMI based approaches. Application of LMIs can reduce a wide species of problems appearing in systems and control engineering [3].

This paper introduces a qLPV model [4] of the inverted pendulum. The LPV systems [5] approach the nonlinear system in linear way, however the properties of

the qLPV system are equivalent the nonlinear properties. It enables the representation of the nonlinear system without a complicated linearization method. LPV systems appear in the structure of Linear-Time Invariant (LTI) state-space representations. In this paper the LTI vertex system of the problem, the LMI design technique through the Parallel Distributed Compensation (PDC) and the HOSVD based TP transformation have been used. Close to Normalised (CNO) type weighting functions for an example have been applied MATLAB TP Toolbox [6]. TP transformation of pendulum has been investigated in some research for example rotary [7], furuta [8], single [9] [10] and parallel-type double pendulum [11]. This example is a good task to examine the TP model transformation and the stability of the nonlinear system.

The paper is organised as follows: in Section 2, the TP model transformation has introduced through the HOSVD based approach, the weighting functions and the qLPV model. Section 3 presents the LMI based controller design to obtain stable closed loop system based on the Lyapunov stability conditions. Due to nonlinearity, stable controller has been designed via LMI stability conditions. In Section 4, TP model transformation of the inverted pendulum has been presented, based on the Section 2-3.

2. TP model transformation

Control design of the TP model transformation was proposed by Baranyi et al. [12] [13]. The TP model structure [14] represents a multivariable tensor function. In fact, the TP model representation is a finite element convex polytopic representation [15] [16] [17]. In this paper the nonlinear system has approximated by the TP model transformation. The mathematical structure of this method is based on the HOSVD theory.

Singular value decomposition (SVD) [18] is a two dimensional matrix method used in the field of linear algebra. It is widespread in mathematics but this method is not suitable for analyzing multidimensional data. For multidimensional problems HOSVD methods [19] can be used. Multidimensional arrays or tensors represent data structures with more than two dimensions.

The HOSVD based computation extends its application to the qLPV model's continuos multivariable function. This produces numerically the TP model. TP transformation of HOSVD based approach generates the weighting funcions and the LTI vertex systems. The steps of transformating the TP model are the following [13]:

- The given qLPV model must be discretized, which means the system matrix $\mathbf{S}(\mathbf{p})$ is converted numerically into a tensor representation, where $\mathbf{p} = \mathbf{p}(t) \in \Omega$ is a time-varying parameter vector within the closed hypercube $\Omega = [a_1,b_1] \times [a_2,b_2] \times ... \times [a_n,b_n] \subset \mathbb{R}^n$. At first the problem space Ω is defined, which is a closed hypercube and the TP model is interpretable only in this space. M denotes the discretization grid defined in Ω.
- The TP model sctructure is extracted via the HOSVD structure to obtain the tensor product form.
- Weighting functions are defined. It is a computational method on HOSVD that can be converted numerically the qLPV model into that frame. The qLPV state-space representation is able to describe nonlinear systems because of combinating the LTI vertices and the nonlinear weighting functions $w_i = w_i(\mathbf{p}(t))$ i.e. weighting functions depend on the parameters. Types of the weighting functions are [13] [14]:
  - (SN) Sum Normalised: the weighting function is SN if the sum of weighting functions for all $\mathbf{p}(t) \in \Omega$ is equal to 1;
  - (NN) Non-Negative: values of the weighting functions are non- negative;
  - (NO) Normalised: if the weighting function is SN and NN type and its largest value is 1;
  - (CNO) Close to Normalised: if it is SN and NN type and its largest value is 1 or close to 1;
  - (INO) Inverse Normalised: the weighting function is INO if its smallest value is 0;
  - (RNO) Relaxed Normalised: the weighting function is RNO if its largest value is SN and NN type and that value is only between 0 and 1;
  - (IRNO) Inverse Relaxed Normalised: the weighting function is IRNO if its smallest value is 0 and its largest value is SN and NN type and that value is only between 0 and 1.

The conditions of convexity is not satisfied via HOSVD method [20] [21]. Thus, the convex hull created by the TP vertex system must be manipulated. The CNO type weighting function is used in this work to determine TP transformation of the inverted pendulum, see in Section 4.

The continuous systems [22] are written by this form:

$$\dot{\mathbf{x}}(t) = \mathbf{A}(\mathbf{p}(t))\mathbf{x}(t) + \mathbf{B}(\mathbf{p}(t))\mathbf{u}(t), \tag{1}$$

$$\mathbf{y}(t) = \mathbf{C}(\mathbf{p}(t))\mathbf{x}(t) + \mathbf{D}(\mathbf{p}(t))\mathbf{u}(t), \tag{2}$$

where $\mathbf{x}(t) \in \mathbb{R}^n$ is the state vector, $\mathbf{u}(t) \in \mathbb{R}^m$ is the input vector, $\mathbf{y}(t) \in \mathbb{R}^q$ is the output vector [14]. Equations (1) and (2) can be defined by combinating LTI systems. Thus, the representation can be written for instance:

$$\dot{\mathbf{x}}(t) = \sum_{i=1}^{r} w_i(\mathbf{p}(t))(\mathbf{A}_i\mathbf{x} + \mathbf{B}_i\mathbf{u}), \tag{3}$$

$$\mathbf{y}(t) = \sum_{i=1}^{r} w_i(\mathbf{p}(t))(\mathbf{C}_i\mathbf{x} + \mathbf{D}_i\mathbf{u}), \tag{4}$$

where $\mathbf{A_i}(t) \in \mathbb{R}^{n\times n}$, $\mathbf{B_i}(t) \in \mathbb{R}^{n\times m}$, $\mathbf{C_i}(t) \in \mathbb{R}^{q\times n}$, $\mathbf{D_i}(t) \in \mathbb{R}^{q\times m}$ and r is the vertex number. Equation (3) is the TP transformation. Weighting functions w_i have two important properties that satisfy convexity [13]:

$$w_i(\mathbf{p}(t)) \in [0,1], \tag{5}$$

$$\sum_{i=1}^{r} w_i(\mathbf{p}(t)) = 1. \tag{6}$$

If parameter $\mathbf{p}(t)$ does not contain elements of $\mathbf{x}(t)$, it is an LPV system. If parameter $\mathbf{p}(t)$ contains elements of $\mathbf{x}(t)$, it is a qLPV model because of the nonlinearity. The qLPV model representation of state-space configuration (1) is:

$$\mathbf{S}(\mathbf{x}(t)) = \begin{bmatrix} \mathbf{A}(\mathbf{x}(t)) & \mathbf{B}(\mathbf{x}(t)) \\ \mathbf{C}(\mathbf{x}(t)) & \mathbf{D}(\mathbf{x}(t)) \end{bmatrix}, \tag{7}$$

i.e.

$$\begin{pmatrix} \dot{\mathbf{x}} \\ \mathbf{y} \end{pmatrix} = \mathbf{S}(\mathbf{p}) \begin{pmatrix} \mathbf{x} \\ \mathbf{u} \end{pmatrix}. \tag{8}$$

3. LMI based optimization

In control science, application of LMI, especially in the field of dynamic system is related to Lyapunov [23]. This section presents the LMI based [2] control design approach. Many problems arise in control system design that are reduced by researchers to convex or quasi-convex optimization problem involving LMIs. LMIs are applied to solve many automation problems, optimization problems and system identification that are generally difficult to solve but it can be possible to solve by convex optimizing.

LMIs can solve in polynomial time. Many variety of systems and control problems can revise as LMI problems. These problems may be state-feedback synthesis, robustness design, H_2 and H_∞ control [2]. It is reducible to convex problems. The variables are often matrices, therefore application of Lyapunov-inequality is the basic structure of the LMI method [31]:

$$\mathbf{A}^T\mathbf{P}\mathbf{A} - \mathbf{P} \prec 0, \tag{9}$$

where $\mathbf{P} = \mathbf{P}^T$ is the variable. Finding $\mathbf{K}$ is the problem of control design. The closed-loop system is quadratically stable:

$$[\mathbf{A} - \mathbf{B}\mathbf{K}]^T\mathbf{P}[\mathbf{A} - \mathbf{B}\mathbf{K}] - \mathbf{P} \prec 0, \tag{10}$$

The above inequality is multiplied on the left and right via $\mathbf{P}^{-1}$, and $\mathbf{X} = \mathbf{P}^{-1}$ $\mathbf{M} = \mathbf{K}\mathbf{X}$:

$$\mathbf{P}^{-1}[\mathbf{A} - \mathbf{B}\mathbf{K}]^T\mathbf{P}[\mathbf{A} - \mathbf{B}\mathbf{K}]\mathbf{P}^{-1} - \mathbf{P}^{-1}\mathbf{P}\mathbf{P}^{-1} \prec 0, \tag{11}$$

i.e.

$$\mathbf{X}[\mathbf{A}-\mathbf{BK}]^T\mathbf{X}^{-1}[\mathbf{A}-\mathbf{BK}]\mathbf{X}-\mathbf{X}\prec 0, \tag{12}$$

finally

$$\mathbf{X}-[\mathbf{AX}-\mathbf{BM}]^T\mathbf{X}^{-1}[\mathbf{AX}-\mathbf{BM}]\succ 0. \tag{13}$$

It can be transformed into the LMI form:

$$\begin{bmatrix}\mathbf{X} & (\mathbf{AX}-\mathbf{BM})^T\\ (\mathbf{AX}-\mathbf{BM}) & \mathbf{X}\end{bmatrix}\succ 0. \tag{14}$$

This form is defined by Schur complements. Defining the Schur complements [2] of a partitioned $\mathbf{A}$ matrix can be written as:

$$\mathbf{A}=\begin{bmatrix}A_{11} & A_{12}\\ A_{21} & A_{22}\end{bmatrix}, \tag{15}$$

For example if A_{11} is nonsingular, $A_{22}-A_{21}A_{11}^{-1}A_{12}$ is the Schur complement of A_{11}. It can be denoted by $S_{ch}(A_{11})$. Thus, matrix $\mathbf{A}$ can be written as:

$$\mathbf{A}=\begin{bmatrix}A_{11} & 0\\ 0 & S_{ch}(A_{11})\end{bmatrix}. \tag{16}$$

3.1. Presenting LMI based approach

PDC is a model based design procedure that was suggested by Tanaka and Wang [24]. They designed for Takagi-Sugeno (TS) fuzzy decision [31] models so their procedure was to develop a fuzzy controller from a TS fuzzy model. Combination of LMI optimization and PDC framework can be accomplished with convex optimization. The PDC design structures are defined one LTI feedback gain $\mathbf{k}$ to all LTI vertex systems.

Therefore, the TP controller is:

$$\mathbf{u}(t) = -\sum_{i=1}^{r} w_i(\mathbf{p}(t))\mathbf{k}_i\mathbf{x}(t) = -\left(\sum_{i=1}^{r} w_i(\mathbf{p}(t))\mathbf{k}_i\right)\mathbf{x}(t) = -\mathbf{k}^T\mathbf{x}(t). \quad (17)$$

Substituting (17) into (3) the following representation is obtained:

$$\dot{\mathbf{x}}(t) = \sum_{i=1}^{r} w_i[\mathbf{A}_i\mathbf{x}(t) + \mathbf{B}_i(-\sum_{j=1}^{r} w_j\mathbf{k}_j\mathbf{x}(t))], \quad (18)$$

$$\dot{\mathbf{x}}(t) = \sum_{i=1}^{r}\sum_{j=1}^{r} w_i w_j[\mathbf{A}_i - \mathbf{B}_i\mathbf{k}_j]\mathbf{x}(t), \quad (19)$$

where i,$j = 1...r$, r is the total number of LTI systems. It can be rewritten into this form:

$$\dot{\mathbf{x}}(t) = \sum_{i=1}^{r} w_i w_i[\mathbf{A}_i - \mathbf{B}_i\mathbf{k}_i]\mathbf{x}(t) + 2\sum_{i=1}^{r}\sum_{i<j}^{r} w_i w_j\mathbf{G}_{ij}\mathbf{x}(t), \quad (20)$$

where $\mathbf{G}$ is:

$$\mathbf{G}_{ij} = \frac{[\mathbf{A}_i - \mathbf{B}_i\mathbf{k}_j] + [\mathbf{A}_j - \mathbf{B}_j\mathbf{k}_i]}{2}. \quad (21)$$

3.2. The Lyapunov theory

The LMI based approach began with Lyapunov [23] based stability conditions. In the case of nonlinear dynamic systems, stability analysis methods developed for linear systems, are not applicable. The Lyapunov methods are used to get suifficent conditions for stability of the equilibrium point of a linear system.

Consider a system $\dot{\mathbf{x}} = \mathbf{f}(\mathbf{x},t)$, where $\mathbf{f}$ is continuos. To study the stability of nonlinear dynamic systems, the Lyapunov theorem can be applied. If there exists a function $V(\mathbf{x},t)$ what can be derived around an equilibrium point $\mathbf{x} = 0$ and satisfies the following conditions:

- $V(\mathbf{0},t) = 0$ and $V(\mathbf{x},t) > 0$ if $V(\mathbf{x},t)$ is a positive defitine function,
- $\dot{V}(\mathbf{x},t) \leq 0$, i.e. $\dot{V}(\mathbf{x},t)$ is a negative semidefinite function,
- $\dot{V}(\mathbf{x},t) < 0$, i.e. $\dot{V}(\mathbf{x},t)$ is a negative definite function.

If first and second conditions are existed, then the system is stable, and if the first and third conditions are existed the system is asymptotically stable. The function V in Lyapunov theorem is the energy function assigned to the system.

Consider a system $\dot{\mathbf{x}} = \mathbf{f}(\mathbf{x},\mathbf{u})$ with control inputs u, where $\mathbf{x}(t) \in \mathbb{R}^n$, $\mathbf{u}(t) \in \mathbb{R}^m$. Consider the candidate Lyapunov function $V(\mathbf{x})$ for every fixed $\mathbf{x} \neq 0$ there exists and acceptable value $\mathbf{u}$ for the control in such a way as to:

$$\nabla V(\mathbf{x}) \cdot \mathbf{f}(\mathbf{x},\mathbf{u}) < 0. \tag{22}$$

Regard the following candidate Lyapunov function [31] $V(\mathbf{x}(t)) = \mathbf{x}^T(t)\mathbf{P}\mathbf{x}(t)$ where $\mathbf{P} \succ 0$, thus:

$$\begin{aligned}\dot{\mathbf{V}}(\mathbf{x}(t)) &= \sum_{i=1}^{r}\sum_{j=1}^{r} w_i w_j \mathbf{x}^T(t)[(\mathbf{A}_i - \mathbf{B}_i\mathbf{k}_j)^T\mathbf{P} + \mathbf{P}(\mathbf{A}_i - \mathbf{B}_i\mathbf{k}_j)]\mathbf{x}(t) \\ &= \sum_{i=1}^{r} w_i^2 \mathbf{x}^T(t)[\mathbf{G}_{ii}^T\mathbf{P} + \mathbf{P}\mathbf{G}_{ii}]\mathbf{x}(t) + \sum_{i=1}^{r}\sum_{i<j} 2w_i w_j \mathbf{x}^T(t) \\ &\times \left[\left(\frac{\mathbf{G}_{ij} + \mathbf{G}_{ji}}{2}\right)^T\mathbf{P} + \mathbf{P}\left(\frac{\mathbf{G}_{ij} + \mathbf{G}_{ji}}{2}\right)\right]\mathbf{x}(t).\end{aligned} \tag{23}$$

3.3. Stable controller design with LMI based stability conditions

Consider the stability of an open-loop system via Lyapunov stability concept, where the equilibrium of TP system (19) via $\mathbf{u}(t) = 0$ is globally asymptotically stable, then there is a common positive definite matrix $\mathbf{P}$ for instance

$$\mathbf{A}_i^T\mathbf{P} + \mathbf{P}\mathbf{A}_i \prec 0, \tag{24}$$

for $\forall i = 1, \cdots, r$. Examine stability of an closed-loop system, as:

$$\dot{\mathbf{x}}(t) = \sum_{i=1}^{r} \sum_{j=1}^{r} w_i w_j (\mathbf{A}_i - \mathbf{B}_i \mathbf{K}_j) \mathbf{x}(t), \tag{25}$$

$$\dot{\mathbf{x}}(t) = \sum_{i=1}^{r} w_i w_i [\mathbf{A}_i - \mathbf{B}_i \mathbf{K}_i] \mathbf{x}(t) + 2 \sum_{i=1}^{r} \sum_{i<j}^{r} w_i w_j \mathbf{G}_{ij} \mathbf{x}(t), \tag{26}$$

Let us use the following notations:

$$\mathbf{G}_{ij} = \mathbf{A}_i - \mathbf{B}_i \mathbf{K}_j, \tag{27}$$

$$\mathbf{G}_{ji} = \mathbf{A}_j - \mathbf{B}_j \mathbf{K}_i, \tag{28}$$

where $i = 1, \cdots, r$. The equilibrium point of the TP system (9) is globally asymptotically stable if there is a common positive definite matrix $\mathbf{P}$:

$$\mathbf{G}_{ii}^T \mathbf{P} + \mathbf{P} \mathbf{G}_{ii} \prec 0, \tag{29}$$

and

$$\left(\frac{\mathbf{G}_{ij} + \mathbf{G}_{ji}}{2} \right)^T \mathbf{P} + \mathbf{P} \left(\frac{\mathbf{G}_{ij} + \mathbf{G}_{ji}}{2} \right) \preceq 0. \tag{30}$$

Multiplying inequelity (29) on the left and right by $\mathbf{P}^{-1}$ and denote $\mathbf{X} = \mathbf{P}^{-1}$ and $\mathbf{M_i} = \mathbf{K_i X}$:

$$\left(\mathbf{P}^{-1} \mathbf{A}_i \mathbf{P} - \mathbf{P}^{-1} \mathbf{B}_i \mathbf{K}_i \mathbf{P} \right)^T + \left(\mathbf{P}^{-1} \mathbf{P} \mathbf{A}_i - \mathbf{P}^{-1} \mathbf{P} \mathbf{B}_i \mathbf{K}_i \right) \prec 0, \tag{31}$$

finally

$$\begin{aligned}&\left(\mathbf{P}^{-1}\mathbf{A}_i\mathbf{P}\mathbf{P}^{-1}-\mathbf{P}^{-1}\mathbf{B}_i\mathbf{K}_i\mathbf{P}\mathbf{P}^{-1}\right)^T\\&+\left(\mathbf{P}^{-1}\mathbf{P}\mathbf{A}_i\mathbf{P}^{-1}-\mathbf{P}^{-1}\mathbf{P}\mathbf{B}_i\mathbf{K}_i\mathbf{P}^{-1}\right)\prec 0,\end{aligned}\tag{32}$$

Substituting $\mathbf{X}=\mathbf{P}^{-1}$ and $\mathbf{M_i}=\mathbf{K_i}\mathbf{X}$, then:

$$-\mathbf{X}\mathbf{A}_i^T-\mathbf{A}_i\mathbf{X}+\mathbf{X}\mathbf{K}_i^T\mathbf{B}_i^T+\mathbf{B}_i\mathbf{K}_i\mathbf{X}\succ 0,\tag{33}$$

the following LMI stability condition is got:

$$-\mathbf{X}\mathbf{A}_i^T-\mathbf{A}_i\mathbf{X}+\mathbf{M}_i^T\mathbf{B}_i^T+\mathbf{B}_i\mathbf{M}_i\succ 0.\tag{34}$$

Equations (27) and (28) are applied, and denote $\mathbf{X}=\mathbf{P}^{-1}$ and $\mathbf{M_i}=\mathbf{K_i}\mathbf{X}$:

$$\begin{aligned}&\left(\frac{\mathbf{A}_i-\mathbf{B}_i\mathbf{K}_j+\mathbf{A}_j-\mathbf{B}_j\mathbf{K}_i}{2}\right)^T\mathbf{P}+\mathbf{P}\\&\left(\frac{\mathbf{A}_i-\mathbf{B}_i\mathbf{K}_j+\mathbf{A}_j-\mathbf{B}_j\mathbf{K}_i}{2}\right)\preceq 0,\end{aligned}\tag{35}$$

then multiplying inequelity (30) on the left and right by $\mathbf{P}^{-1}$, then the following equation is got:

$$\begin{aligned}&\left(\frac{\mathbf{A}_i\mathbf{P}-\mathbf{B}_i\mathbf{K}_j\mathbf{P}+\mathbf{A}_j\mathbf{P}-\mathbf{B}_j\mathbf{K}_i\mathbf{P}}{2}\right)^T\\&+\left(\frac{\mathbf{P}\mathbf{A}_i-\mathbf{P}\mathbf{B}_i\mathbf{K}_j+\mathbf{P}\mathbf{A}_j-\mathbf{P}\mathbf{B}_j\mathbf{K}_i}{2}\right)\preceq 0,\end{aligned}\tag{36}$$

$$\left(\frac{\mathbf{P}^{-1}\mathbf{A}_i\mathbf{P}-\mathbf{P}^{-1}\mathbf{B}_i\mathbf{K}_j\mathbf{P}+\mathbf{P}^{-1}\mathbf{A}_j\mathbf{P}-\mathbf{P}^{-1}\mathbf{B}_j\mathbf{K}_i\mathbf{P}}{2}\right)^T + \left(\frac{\mathbf{P}^{-1}\mathbf{P}\mathbf{A}_i-\mathbf{P}^{-1}\mathbf{P}\mathbf{B}_i\mathbf{K}_j+\mathbf{P}^{-1}\mathbf{P}\mathbf{A}_j-\mathbf{P}^{-1}\mathbf{P}\mathbf{B}_j\mathbf{K}_i}{2}\right) \preceq 0, \tag{37}$$

$$\left(\frac{\mathbf{P}^{-1}\mathbf{A}_i\mathbf{P}\mathbf{P}^{-1}-\mathbf{P}^{-1}\mathbf{B}_i\mathbf{K}_j\mathbf{P}\mathbf{P}^{-1}+\mathbf{P}^{-1}\mathbf{A}_j\mathbf{P}\mathbf{P}^{-1}-\mathbf{P}^{-1}\mathbf{B}_j\mathbf{K}_i\mathbf{P}\mathbf{P}^{-1}}{2}\right)^T + \left(\frac{\mathbf{P}^{-1}\mathbf{P}\mathbf{A}_i\mathbf{P}^{-1}-\mathbf{P}^{-1}\mathbf{P}\mathbf{B}_i\mathbf{K}_j\mathbf{P}^{-1}+\mathbf{P}^{-1}\mathbf{P}\mathbf{A}_j\mathbf{P}^{-1}-\mathbf{P}^{-1}\mathbf{P}\mathbf{B}_j\mathbf{K}_i\mathbf{P}^{-1}}{2}\right) \preceq 0, \tag{38}$$

Substituting $\mathbf{X}=\mathbf{P}^{-1}$ and $\mathbf{M_i}=\mathbf{K_i}\mathbf{X}$:

$$\left(\frac{\mathbf{X}\mathbf{A}_i-\mathbf{X}\mathbf{B}_i\mathbf{K}_j+\mathbf{X}\mathbf{A}_j-\mathbf{X}\mathbf{B}_j\mathbf{K}_i}{2}\right)^T + \left(\frac{\mathbf{A}_i\mathbf{X}-\mathbf{B}_i\mathbf{K}_j\mathbf{X}+\mathbf{A}_j\mathbf{X}-\mathbf{B}_j\mathbf{K}_i\mathbf{X}}{2}\right) \preceq 0, \tag{39}$$

$$-\mathbf{X}\mathbf{A}_i^T-\mathbf{A}_i\mathbf{X}-\mathbf{X}\mathbf{A}_j^T-\mathbf{A}_j\mathbf{X}+\mathbf{X}\mathbf{K}_j^T\mathbf{B}_i^T+\mathbf{B}_i\mathbf{K}_j\mathbf{X}+\mathbf{X}\mathbf{K}_i^T\mathbf{B}_j^T+\mathbf{B}_j\mathbf{K}_i\mathbf{X} \succ 0, \tag{40}$$

after this, another LMI stability condition is got:

$$-\mathbf{X}\mathbf{A}_i^T-\mathbf{A}_i\mathbf{X}-\mathbf{X}\mathbf{A}_j^T-\mathbf{A}_j\mathbf{X}+\mathbf{M}_j^T\mathbf{B}_i^T+\mathbf{B}_i\mathbf{M}_j+\mathbf{M}_i^T\mathbf{B}_j^T+\mathbf{B}_j\mathbf{M}_i \succeq 0. \tag{41}$$

Equations (34) and (41) are the LMI stability conditions and these are applied for the inverted pendulum example by equations (66) and (67).

4. TP transformation of the inverted pendulum

The center of mass of the inverted pendulum [25] is above its pivot point. Control designing of this nonlinear system has been the subject of many studies and researchers in the recent period [26] [27] [28].

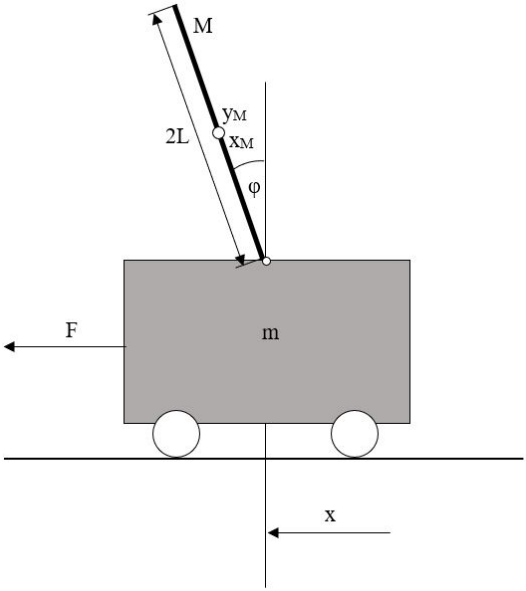

Figure 1. Inverted Pendulum

4.1. Modeling of inverted pendulum

The illustration of the inverted pendulum installed on a cart is given in Fig 1. The lenght of the rod on the car is $2L = 0.35$, the mass of the rod is $M = 1.2$, the mass of the cart $m = 0.2$ in a coherent unit system SI and the generalized coordinates are x and φ. The system equations of the nonlinear system are written by Euler-Lagrange

equation [29]:

$$\frac{d}{dt}\frac{\partial K}{\partial \dot{q}_i} - \frac{\partial K}{\partial q_i} + \frac{\partial P}{\partial q_i} = \tau_i, \tag{42}$$

where K is the kinetic energy, P is the potential energy, q_i is the generalized coordinate and τ_i is the generalized force. The moment of inertia of the rod belonging to the center of mass is $\Theta = \frac{ML^2}{3}$. The center of gravity of the rod mass is given by the coordinates $x_M = x + LS_\varphi$ and $y_M = LC_\varphi$ and the velocity is v_M. Let's denote $S_\varphi = \sin(\varphi)$ and $C_\varphi = \cos(\varphi)$ [29] [26] [32]. After derivating x_M and y_M, the following results can be got:

$$\dot{x}_M = \dot{x} + \dot{\varphi} L C_\varphi, \tag{43}$$

$$\dot{y}_M = -\dot{\varphi} L S_\varphi, \tag{44}$$

$$v_M^2 = \dot{x}_M^2 + \dot{y}_M^2 = \dot{x}^2 + 2LC_\varphi \dot{x}\dot{\varphi} + L^2\dot{\varphi}^2. \tag{45}$$

Determining kinetic energy and potential energy as follows:

$$\begin{aligned} K &= \frac{1}{2}m\dot{x}^2 + \frac{1}{2}Mv_M^2 + \frac{1}{2}\Theta\dot{\varphi}^2 \\ &= \frac{1}{2}m\dot{x}^2 + \frac{1}{2}M(\dot{x}^2 + 2LC_\varphi\dot{x}\dot{\varphi} + L^2\dot{\varphi}^2) + \frac{1}{2}\Theta\dot{\varphi}^2, \end{aligned} \tag{46}$$

$$P = MgLC_\varphi. \tag{47}$$

After obtaining the partial derivatives of K and P, and applying mathematical manipulations, the following equations are given:

$$\frac{d}{dt}\frac{\partial K}{\partial \dot{x}} = (m+M)\ddot{x} + MLC_\varphi\ddot{\varphi} - MLS_\varphi\dot{\varphi}^2, \tag{48}$$

$$\frac{d}{dt}\frac{\partial K}{\partial \dot{\varphi}} = MLC_{\varphi}\ddot{x} - MLS_{\varphi}\dot{x}\dot{\varphi} + (\Theta + ML^2)\ddot{\varphi}. \tag{49}$$

Using Euler-Lagrange equation (42), the following equations are got:

$$\frac{d}{dt}\frac{\partial K}{\partial \dot{x}} - \frac{\partial K}{\partial x} + \frac{\partial P}{\partial x} = F, \tag{50}$$

$$\frac{d}{dt}\frac{\partial K}{\partial \dot{\varphi}} - \frac{\partial K}{\partial \varphi} + \frac{\partial P}{\partial \varphi} = 0, \tag{51}$$

i.e.

$$(M+m)\ddot{x} + MLC_{\varphi}\ddot{\varphi} - MLS_{\varphi}\dot{\varphi}^2 = F, \tag{52}$$

$$MLC_{\varphi}\ddot{x} + (\Theta + ML^2)\ddot{\varphi} - MgLS_{\varphi} = 0. \tag{53}$$

After some mathematical manipulations the following equations are given:

$$\ddot{x} = \frac{F - MLC_{\varphi}\ddot{\varphi} + MLS_{\varphi}\dot{\varphi}^2}{m+M}, \tag{54}$$

$$\ddot{\varphi} = \frac{gS_{\varphi} - \frac{C_{\varphi}}{m+M}(F + MLS_{\varphi}\dot{\varphi}^2)}{L\left(\frac{4}{3} - \frac{MC_{\varphi}^2}{m+M}\right)}. \tag{55}$$

Then the following state-space representation is defined:

$$\dot{x}_1 = x_2, \tag{56}$$

$$\dot{x}_2 = \frac{\frac{4}{3}MLsin(x_3)x_4^2 - Mgcos(x_3)sin(x_3) + \frac{4}{3}F}{\frac{4}{3}(m+M) - Mcos^2(x_3)}, \tag{57}$$

$$\dot{x}_3 = x_4, \tag{58}$$

$$\dot{x}_4 = \frac{MLsin(x_3)cos(x_3)x_4^2 + cos(x_3)F - (m+M)gsin(x_3)}{MLsin^2(x_3) - \frac{4}{3}(m+M)L}, \tag{59}$$

where the state-space variables are $x_1 = x$, $x_2 = \dot{x}$, $x_3 = \varphi$, $x_4 = \dot{\varphi}$.

4.2. TP transformation

It is an important purpose of transforming TP to convert the given state-space model (1) into a convex TP model. In this model the LTI systems create a tight convex hull [30]. Consider the following state-space structure:

$$\dot{\mathbf{x}}(t) = \mathbf{A}(\mathbf{x})\mathbf{x} + \mathbf{B}(\mathbf{x})u, \tag{60}$$

Elements of matrix $\mathbf{A}(\boldsymbol{x})$ (61) and vector $\mathbf{B}(\mathbf{x})$ (62) depend on only the state variables x_3 and x_4, i.e. nonlinearity is caused by x_3 and x_4. For TP model transfromation the transformation space $\Omega = [(-45/180)\pi,(45/180)\pi] \times [(-45/180)\pi,(45/180)\pi]$ is defined and discretized by $M_1 \times M_2 = 136 \times 136$ grid points. The components of matrix $\mathbf{A}(\boldsymbol{x})$ and vector $\mathbf{B}(\mathbf{x})$ have been defined numerically and they are stored in a four dimensional tensor $S \in R^{136\times136\times4\times5}$,

$$\mathbf{A}(\boldsymbol{x}) = \begin{bmatrix} 0 & 1 & 0 & 0 \\ 0 & 0 & \frac{-Mgcos(x_3)}{\frac{4}{3}(m+M)-Mcos^2(x_3)}\frac{sin(x_3)}{x_3} & \frac{\frac{4}{3}MLsin(x_3)}{\frac{4}{3}(m+M)-Mcos^2(x_3)}x_4 \\ 0 & 0 & 0 & 1 \\ 0 & 0 & -\frac{(m+M)g}{MLsin^2(x_3)-\frac{4}{3}(m+M)L}\frac{sin(x_3)}{x_3} & \frac{MLsin(x_3)cos(x_3)}{MLsin^2(x_3)-\frac{4}{3}(m+M)L}x_4 \end{bmatrix}, \tag{61}$$

$$\mathbf{B}(\mathbf{x}) = \begin{bmatrix} 0 \\ \frac{\frac{4}{3}}{\frac{4}{3}(m+M)-Mcos^2(x_3)} \\ 0 \\ \frac{cos(x_3)}{MLsin^2(x_3)-\frac{4}{3}(m+M)L} \end{bmatrix}. \tag{62}$$

Applying HOSVD, the singular values are $\sigma_1 = 1909$, $\sigma_2 = 201$, $\sigma_3 = 23$, $\sigma_4 = 2$ for the variable x_3 and $\sigma_1 = 1920$, $\sigma_2 = 23$ for the variable x_4. After using HOSVD

on $\mathbf{S}(\mathbf{x}(t))$ and CNO type weighting function, the following TP model transformation describes inverted pendulum system:

$$\dot{\mathbf{x}} \cong \sum_{i_1=1}^{r_1} \sum_{i_2=1}^{r_2} w_{i_1}(x_3) w_{i_2}(x_4)(\mathbf{A}_{i_1,i_2}\mathbf{x} + \mathbf{B}_{i_1,i_2}u), \tag{63}$$

where $w_{i_1}(x_3)$ and $w_{i_2}(x_4)$ are the CNO type weighting functions, $\mathbf{A}_{i_1,i_2}$ and $\mathbf{B}_{i_1,i_2}$ are state independent system matrix and vector. This nonlinear system is possible to be approximated by the combinations of $r_1 r_2$ LTI systems. It can be written as follows:

$$\dot{\mathbf{x}} \cong \sum_{i_1=1}^{5} \sum_{i_2=1}^{2} w_{i_1}(x_3) w_{i_2}(x_4)(\mathbf{A}_{i_1,i_2}\mathbf{x} + \mathbf{B}_{i_1,i_2}u), \tag{64}$$

$$\dot{\mathbf{x}} \cong \sum_{i=1}^{r} w_i(x_3,x_4)(\mathbf{A}_i\mathbf{x} + \mathbf{B}_i u). \tag{65}$$

where $r = r_1 r_2$ is the number of LTI systems via $5 \times 2 = 10$ LTI vertex models. Weighting functions $w_{i_1}(x_3)$ and $w_{i_2}(x_4)$ are shown in Fig. 2-3. Thus, the system is decomposed in angular velocity $\dot{\varphi}$ into 2 weighting functions, and in angular position φ into 5 weighting functions.

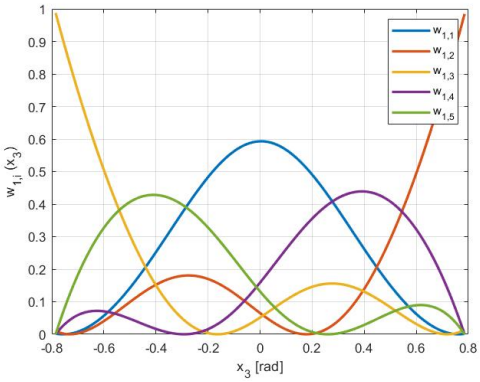

Figure 2. CNO type weighting functions for x_3

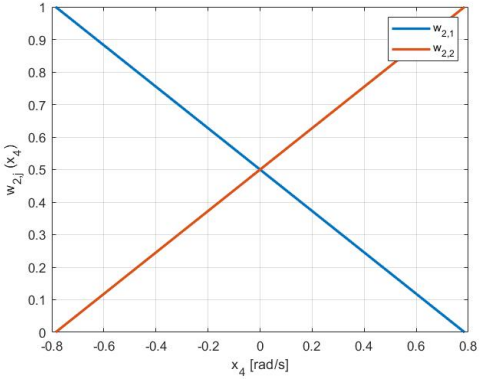

Figure 3. CNO type weighting functions for x_4

The controller vector $\mathbf{k}_i$ can be numerically defined by LMI. Using stability conditions (31) and (41), determining asymptotic stability of the system. Thus, the stabilization controller can be found:

$$-\mathbf{X}\mathbf{A}_i^T - \mathbf{A}_i\mathbf{X} + \mathbf{M}_i^T\mathbf{B}_i^T + \mathbf{B}_i\mathbf{M}_i \succ 0, \tag{66}$$

$$-\mathbf{X}\mathbf{A}_i^T - \mathbf{A}_i\mathbf{X} - \mathbf{X}\mathbf{A}_j^T - \mathbf{A}_j\mathbf{X} + \mathbf{M}_j^T\mathbf{B}_i^T + \mathbf{B}_i\mathbf{M}_j + \mathbf{M}_i^T\mathbf{B}_j^T + \mathbf{B}_j\mathbf{M}_i \succeq 0, \tag{67}$$

$$\mathbf{k}_i = \mathbf{M}_i\mathbf{X}^{-1}, \tag{68}$$

where $i = 1, \cdots, r$ and $j = i+1, \cdots, r$, and r is the number of LTI vertex systems.

The control signal is shown in Fig. 6. and state variables x_1 and x_3 are shown in Fig. 4-5. The initial condition is $\mathbf{x}(0) = [0.3,0,0,0]$.

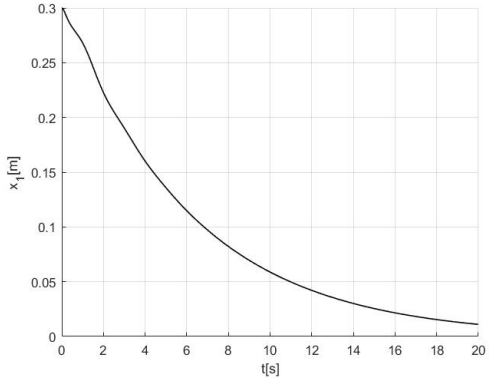

Figure 4. State variable x_1

It can be seen in Fig. 4-6. that functions x_3 and u return to a steady state after a few oscillations. The system get into the stable position around 10 seconds. This will result that LMI approach should improve to stabilize better this nonlinear system.

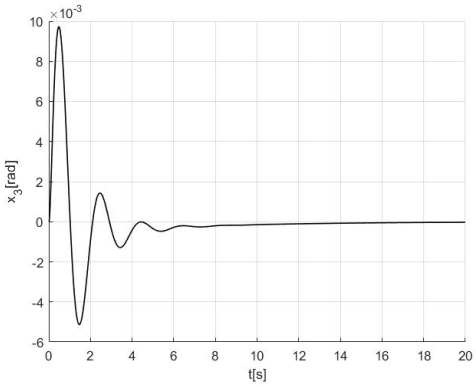

Figure 5. State variable x_3

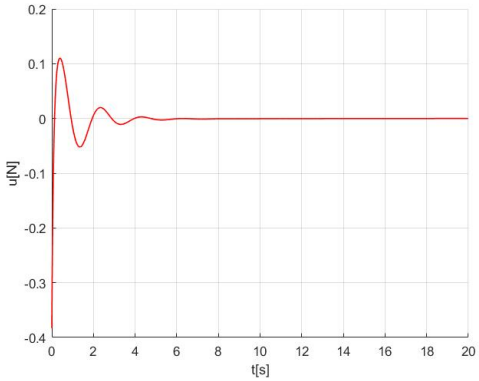

Figure 6. Control signal u

5. Conclusion

This paper describes a study of the HOSVD based TP transformation with CNO type weighting functions using LMI solver and a solution to a problem by applying these methods through an inverted pendulum example. In this example there are 10 LTI vertex systems of the qLPV model. This paper shows an example to analyse global asymptotic stability. Therefore in the future the decay rate for the inverted pendulum and H_2, H_∞ controllers will be analysed.

References

[1] S. Iles, F. Kolonic, J. Matusko, Linear Matrix Inequalities Based H_∞ Control of Gantry Crane using Tensor Product Transformation, Proceedings of the 18th International Conference on ProcessControl, Tatranská Lomnica, Slovakia, 2011, pp. 92–99.

[2] D. Guang-Ren, Y. Hai-Hua, LMIs in Control Systems: Analysis, Design and Applications, 1st Edition, CRC Press, Taylor and Francis Group, Boca Raton, 2013.
doi: https://doi.org/10.1201/b15060

[3] X. Liu, X. Xin, Z. Li, Z. Chen, Near Optimal Control Based on the Tensor-Product Technique, *IEEE Transactions on Circuits and Systems II: Express Briefs* 64 (5) (2017) pp. 560–564.
doi: https://doi.org/10.1109/TCSII.2016.2592986

[4] A. Szollosi, P. Baranyi, Influence of the Tensor Product model representation of qLPV models on the feasibility of Linear Matrix Inequality, *Asian Journal of Control* 18 (4) (2015) pp. 1328–1342.

[5] B. Lantos, Theory and Design of Control Systems III., Academic Press, Budapest, 2018.

[6] Sz. Nagy, Z. Petres, P. Baranyi, TP tool - A MATLAB toolbox for TP model transformation, 8th International Symposium of Hungarian Researchers on Computational Intelligence and Informatics, CINTI (2007), Budapest, Hungary pp. 483–495.

[7] S. Iles, J. Matusko, F. Kolonic, Furuta Pendulum - a Tensor Product Model-based Design Approach Case Study, 2011 Proceedings of the 34th International Convention MIPRO, Opatija, Croatia, 2011.

[8] P. Grof, Y. Yam, TP transformation based control of rotary pendulumy, IEEE International Conference on Systems, Man, and Cybernetics (2015) pp. 2620–2625.
doi: https://doi.org/10.1109/SMC.2015.458

[9] J. Matusko, V. Lesic, F. Kolonic, S. Iles, Tensor product based control of the Single Pendulum Gantry process with stable neural network based friction compensation, Advanced Intelligent Mechatronics (AIM), 2011 IEEE/ASME International Conference, Budapest.
doi: https://doi.org/10.1109/AIM.2011.6027152

[10] F. Kolonic, A. Poljugan, Experimental Control Design by TP Model Transformation, 2006 IEEE International Conference on Mechatronics, Budapest, Hungary, 2006.
doi: https://doi.org/10.1109/ICMECH.2006.252605

[11] Sz. Nagy, Z. Petres, P. Baranyi, TP model transformation based controller design for the parallel-type double inverted pendulum, 2008 IEEE International Conference on Fuzzy Systems (IEEE World Congress on Computational Intelligence), Hong Kong, China, 2008.
doi: https://doi.org/10.1109/FUZZY.2008.4630551

[12] P. Baranyi, TP- Model Transformation Based Control Design Frameworks, Control Engineering, Springer Book, 2016.
ISBN: 978-3-319-19605-3

[13] P. Baranyi, Y. Yam, P. Várlaki, Tensor Product Model Transformation in Polytopic Model Based Control, 1st Edition, Automation and Control Engineering, CRC Press, Taylor and Francis Group, 2018.
doi: https://doi.org/10.1201/9781315218045

[14] P. Baranyi, Extracting LPV and qLPV Structures from State-Space Functions: A TP Model Transformation Based Framework, *IEEE Transactions on Fuzzy Systems* 28 (3) (2017) pp. 499–509.
doi: https://doi.org/10.1109/TFUZZ.2019.2908770

[15] P. Korondi, Tensor Product Model Transformation-based Sliding Surface Design, *Acta Polytechnica Hungarica* 3 (4) (2006) pp. 23–35.

[16] F. Kolonic, A. Poljugan, I. Petrovic, Tensor Product Model Transformation-based Controller Design for Gantry Crane Control System-an Application Approach, *Acta Polytechnica Hungarica* 3 (4) (2006) pp. 95–112.

[17] P. Varkonyi, D. Tikk, P. Korondi, P. Baranyi, A New Algorithm for RNO-INO Type Tensor Product Model Representation, 2005 IEEE International Conference on Intelligent Engineering Systems, Cruising on the Mediterranean Sea, Spain, 2005, pp. 263–266.
doi: https://doi.org/10.1109/INES.2005.1555170

[18] Y. Yam, P. Baranyi, C.T. Yamg, Reduction of Fuzzy Rule Base via Singular Value Decomposition, *IEEE Transactions on Fuzzy Systems* 7 (2) (1999) pp. 120–132.
doi: https://doi.org/10.1109/91.755394

[19] G. Bergqvist, E. Larsson,The Higher Order Singular Value Decomposition: Theory and an Application, *IEEE Signal Processing Magazine* 27 (3) (2010) pp. 151–154.
doi: https://doi.org/10.1109/MSP.2010.936030

[20] P. Baranyi, P. Szeidl, P. Várlaki, Y. Yam, Definition of the HOSVD Based Canonical Form of Polytopic Dynamic Models, Proceedings of the 2006 IEEE International Conference on Mechatronics, Budapest, 2006 pp. 660–665.
doi: https://doi.org/10.1109/ICMECH.2006.252604

[21] P. Szeidl, P. Várlaki, HOSVD Based Canonical Form for Polytopic Models of Dynamic Systems, *Journal of Advanced Computational Intelligence and Intelligent Informatics* 13 (1) (2009) pp. 52–60.

[22] M. Kuczmann, Signals and Systems, Universitas- Győr Nonprofit Kft., Győr, 2010.

[23] V. C. S. Campos, F. O. Souza, L. A. B. Torres, R. M. Palhares, New Stability Conditions Based on Piecewise Fuzzy Lyapunov Functions and Tensor Product Transformations, *IEEE Transactions on Fuzzy Systems* 21 (4) (2013) pp. 784–760.
doi: https://doi.org/10.1109/TFUZZ.2012.2230178

[24] H. O. Wang, K. Tanaka, M. F. Griffin, Parallel Distributed Compensation of Nonlinear Systems by Takagi-Sugeno Fuzzy Model, Proceedings of 1995 IEEE International Conference on Fuzzy Systems, Yokohama, Japan, 1995 pp. 531–538.
doi: https://doi.org/10.1109/FUZZY.1995.409737

[25] B. P. Lal, T. Barjeev, O. G. Hari, Optimal Control of Nonlinear Inverted Pendulum System using PID Controller and LQR: Performance Analysis without and with Disturbance Input, *International Journal of Automation and Computing* (2014) pp. 661–670.

[26] M. Kuczmann, Comprehensive Survey of PID Controller Design for the Inverted Pendulum, *Acta Technica Jaurinensis* 12 (1) (2019) pp. 55–81.
doi: https://doi.org/10.14513/actatechjaur.v12.n1.492

[27] G. Zhao, Z. Wang, Z. Song, A Novel Tensor Product Model Transformation-based Adaptive Variable Universe of Discourse Controller, *Journal of the Franklin Institute* 353 (17) (2016) pp. 4471–4499.
doi: https://doi.org/10.1016/j.jfranklin.2016.08.026

[28] S. Kuntanapreeda, Tensor Product Model Transformation Based Control and Synchronization of a Class of Fractional-Order Chaotic Systems, *Asian Journal of Control* 17 (2) (2015) pp. 371–380.
doi: https://doi.org/10.1002/asjc.839

[29] B. Lantos, Theory and Design of Control Systems I., Academic Press, Budapest, 2009.

[30] Z. Petres, B. Reskó, P. Baranyi, TP Model Transformation Based Control of the TORA System, Production Systems and Information Engineering (2004) pp. 159–175.

[31] K. Tanaka, H. O. Wang, Fuzzy Control Systems Design and Analysis: A linear Matrix Inequality Approach, John Wiley and Sons, 2001.
doi: https://doi.org//10.1002/0471224596.ch2

[32] M. Kuczmann, State Space Based Linear Controller Design for the Inverted Pendulum, *Acta Technica Jaurinensis* 12 (2) (2019) pp. 130–147.
doi: https://doi.org/10.14513/actatechjaur.v12.n2.499

Acta
Technica
Jaurinensis

Vol. 14, No.1, p. 24-35, 2021
DOI: 10.14513/actatechjaur.00576

OEE measurement at the automotive semi-automatic assembly lines

P. Dobra[1,*], J. Jósvai[2]

[1]Adient Hungary Kft
Hammerstein u. 2, 8060 Mór, Hungary
[2]Széchenyi István University, Department of Vehicle Manufacturing
Egyetem tér 1, 9026 Győr, Hungary
[*]e-mail: peter.dobra@freemail.hu

Submitted: 24/11/2020; Accepted: 07/01/2021; Published online: 18/01/2021

Abstract: Manufacturing companies continuously evaluate their achieved performance based on different Key Performance Indicators (KPI). This article gives an overview about the OEE values. The study aims to provide practical OEE data of semi-automatic assembly lines used in the automotive industry. Its novelty is the revealed relationship between seat assembly lines and seat subassembly lines. Firstly, a literature review shows the scientific relevance and several cases are collected to increase OEE percentage. Secondly, the connection between chassis, tracks, recliner and mechanism assembly lines is described. Each part of OEE (availability, performance, quality) are analysed in terms of their impact.

Keywords: KPI; OEE; MES; assembly line

1. Introduction

Nowadays (when industry develops day by day), manufacturing companies are facing increasing standards and complexity regarding productivity, quality and cost efficiency [1]. Consequently, performance management has become a key issue in industry. The performance management system is important in several functional areas of management, such as operation, marketing and sales [2]. Companies, automotive enterprises, machine manufacturers and part suppliers need to measure their processes so that they can define their level of performance and can improve it [3]. Although there are many Key Performance Indicators (KPI), entrepreneurs use

just six up to ten, in general. A widely-used KPI for internal efficiency is Overall Equipment Efficiency (OEE). The OEE-indicator refers to the reliability of the entire production network [4].

Production processes consist of manufacturing and assembly processes. Assembly lines are widespread in manufacturing industries such as automotive, electronics, textile or furniture industry [5]. Assembly of manufactured products accounts for over 50% of the entire production time and for 20% of total production costs [6].

In the modern assembly environment, the vast amount of shop floor data is collected and recorded in digital format using the Manufacturing Execution System (MES) to ensure that parts and production steps can be traced [7]. MES can provide an appropriate database for production control [8]. Based on the smart manufacturing concept, one of the most important elements are data [9]. In the smart factory, the cyber-physical system continuously collects data from machines and assembly lines [10]. Based on production process data, output data, machine failures data, quality records, etc., the OEE-indicator can be calculated.

2. Literature review

2.1. Overview of OEE

In a factory, the following efficiency and productivity indicators are used in production and at the assembly lines:

- Overall Equipment Efficiency (OEE)
- Overall Equipment Efficiency of a Manufacturing Line (OEEML)
- Overall Line Effectiveness (OLE)
- Overall Factory Effectiveness (OFE)
- Overall Plant Effectiveness (OPE)
- Overall Throughput Effectiveness (OTE)
- Overall Resource Effectiveness (ORE)
- Production Equipment Effectiveness (PEE)
- Overall Asset Effectiveness (OAE)
- Total Equipment Effectiveness Performance (TEEP)
- Global Process Effectiveness (GPE)

In addition, Machine Utilization (MU) and Capacity Utilization (CU) also used.

The OEE indicator was introduced by Nakajima under the Total Productive Maintenance (TPM) concept in 1988 [11]. Hedman et al pointed out that OEE is a widely-used performance indicator and companies often invest in MES where OEE measurement is the key element [12]. Steenkamp et al. works with Haldan MES which collects OEE data in the factory in order to display information on different factory levels [13].

According to Mainea et al., OEE is used as an indicator of how well equipment is used in batch production [14]. The basic formula for calculating OEE is written as:

$$OEE = a\ p\ q\ \ [\%] \tag{1}$$

where a - availability [%]; p - performance [%]; q - quality [%].

Detailed calculus example is displayed with Fig. 1 [14].

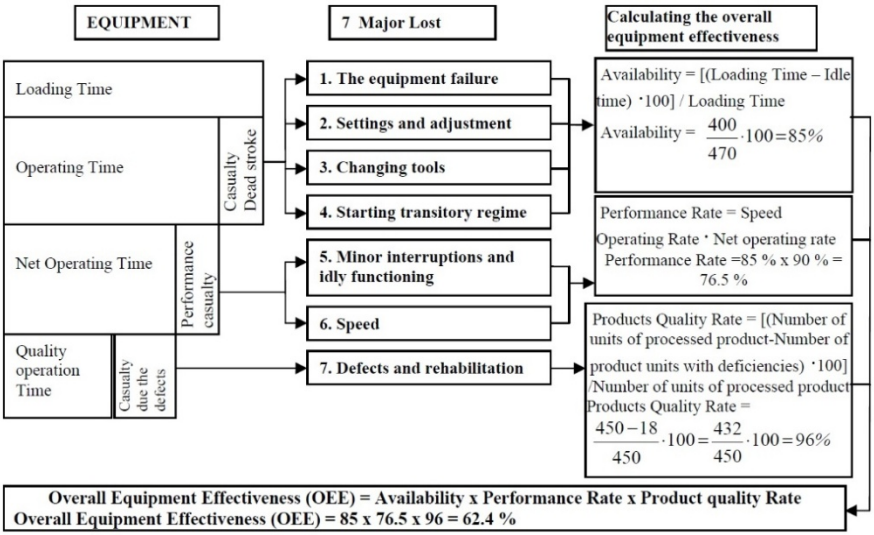

Figure 1. Detailed OEE calculus example [14]

De Grotte defined another OEE calculation method where the formula of availability, performance and quality was related to the production data [15]. From

the productivity side, Saito says that productivity can be enhanced through the improvement of the method (m), improving performance (p), and utilization (u) [16].

$$productivity = m\ p\ u\ [\%] \tag{2}$$

where m - method [%]; p - performance [%]; u - utilization [%].

2.2. OEE-values in the manufacturing industry

The role of the OEE indicator is to monitor and control operational efficiency and measure the effectiveness of decisions [17]. In the manufacturing industry the OEE values are measured thus can be raised and optimized. Under ideal circumstances availability should have greater than 90%, performance greater than 95% and quality rate greater than 99%. According to this conditions OEE values are greater than 84.6% [18]. Hansen determined the excellent OEE values in the following areas:

- batch type production: OEE > 85%
- discrete process: OEE > 90%
- continuous process: OEE > 95% [19].

Subramaniyan compared 884 machines used in 23 factories in 2014. Based on his research work, the average OEE-value is 74% in food and beverage industry, 65% in mechanical workshop, 61% in plastic industry and 59% in another discrete production [18]. Almström et al. defined different levels of automation. At semi-automatic machines, the average OEE-value is 61% and 69% at the automatic machines [20].

2.3. Possibilities to increase OEE-values in the manufacturing

At companies where OEE is measured, the primary goal is to improve the OEE-value continuously. The most common methods are as follows:

- apply lean manufacturing techniques, tools and focus on Total Productive Maintenance (TPM)
- apply six sigma tools
- quality improvement methodologies
- waterfall analysis (analysis and optimization of equipment failure, setup, minor stoppage, etc.)
- line balancing for identify bottleneck
- involve operator to influence OEE

- production logistic analysis, enhancing the performance in material supply
- zero defect manufacturing
- simulation

Silva et al. presented an OEE-improvement of 16% from 70% up to 86% with the standardization of the air-conditioning system production line [21]. Mourtzis et al. described an advanced engineering educational approach where thermosiphon production line efficiency was increased by 28% [22]. Permin et al. determined a self-optimizing assembly system with model-based interpretation in three steps [23].

3. OEE-values at the automotive semi-automatic assembly lines

This chapter presents comprehensive OEE data at the seat assembly lines and reveals connection between assembly and sub-assembly lines.

3.1. Effects of OEE

The OEE-value directly impacts EBITDA, one of the most important corporal KPI-s. For this reason, it is extremely significant for industrial companies to enhance this figure. The high OEE-value contributes to the stable operation of a company (e. g. plannable scrap cost, reliable on time delivery, stable and computable headcount, less overtime, etc.). The lean manufacturing system significantly contributes to the achievement of the expected OEE-values (e.g. 5S, SMED, VSM, Kanban, etc.).

3.2. Calculation errors

When doing the follow-up of the performance, it is essential to collect and process data using a pre-defined method. It is advisable not to change the method, otherwise interpretation of data and trends can cause trouble which may result in improper measures and actions. When calculating the OEE-values, the following mistakes can occur in the industrial practice:

- change and special interpretation of the calculation method (e.g.: long-term lack of material vs planned stoppage)
- there is a change in the production process
  - negative impacts (e.g.: new control measure that increases cycle-time and decreases OEE)

  - positive impacts (e.g.: omission of an action which does not influence product function, e.g.: visual marking, the OEE-value is increasing)

- job performance is done during the expected stoppage (e.g.: break, planned maintenance)
- measurement and calculation errors (the following criterium is not fulfilled: $0\% < OEE \leq 100\%$)
- accidental production and assembly of products with different cycle times

3.3. OEE of semi-automatic assembly lines

Big data of manufacturing processes consist of information system data, smart equipment data, product data, user data and public data. Big data provides appropriate technical support for monitoring assembly processes [24]. The shop floor data collection was supported by MES. Due to the high-level information system, the data was reliable [25]. When using the traditional data analysis and data processing method, special attention was paid to consistency, correctness, completeness of the data [26].

The data collection was possible by a common system and a same data collection process which gathered all OEE relevant data such as scheduled time, production time, downtime, scrape rate, norm, etc. After an SQL query, the data was processed in Excel and the most important production conditions are considered (e.g. ramp-up period, reduced production based on order, etc.) Fig. 2 shows a detail of dataset. Availability, performance and quality percentages are calculated and checked thus individual OEE values become reliable.

	June 2020				July 2020			
	OEE	Availability	Performance	Quality	OEE	Availability	Performance	Quality
Assembly line 1	82.10%	91.65%	90.28%	99.22%	80.73%	90.33%	90.53%	98.72%
Assembly line 2	77.37%	87.29%	89.29%	99.28%	80.52%	88.48%	92.40%	98.48%
Assembly line 3	80.62%	89.30%	91.03%	99.18%	81.98%	88.83%	93.52%	96.68%
Assembly line 4	84.47%	94.32%	90.38%	99.09%	83.64%	99.92%	84.45%	99.12%
Assembly line 5	86.57%	99.73%	86.87%	99.92%	84.58%	99.59%	86.80%	97.85%
⋮	⋮	⋮	⋮	⋮	⋮	⋮	⋮	⋮

Figure 2. Detail of values of OEE components

Analysing and comparing the OEE-values of 307 different assembly lines at 21 production facilities all over the world, the following thesis has been established. The OEE-value of semi-automatic assembly lines manufacturing the metal frame of car seats is always higher in a yearly period than the OEE-value of semi-automatic assembly lines manufacturing component equipment in the same period.

Frame construction of a seat is shown Fig. 3 together with the corresponding assembly lines where the components are made. In the production process, different component assembly actions are ahead of the assembly of the frame construction of the complete seat such as track assembly, recliner assembly, mechanism assembly (e.g. gear boxes).

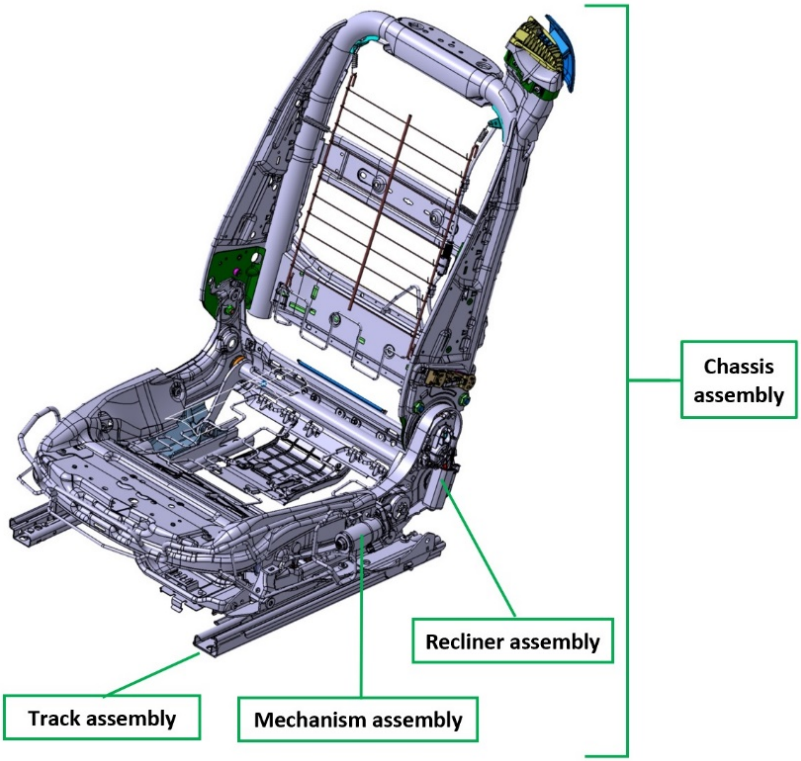

Figure 3. Seat structure assembly

A The average monthly OEE-value of the semi-automatic chassis assembly lines for October 2016 and August 2020 is shown in Fig. 4 OEE values are in the range of 8% from 82% up to 90%. The only salient rise and decline can be found in the environment of appearance COVID-19 in April 2020. In this period almost all of assembly lines suddenly finished the production for weeks with higher focus and this resulted better OEE values. This was followed by a short-term economic

setback. The decrease of OEE was mainly due to changes in demands and raw material supply in the form of unplanned change overs and unplanned downtimes.

Based on Fig. 5, it can be clearly seen that the OEE-value of a chassis assembly line is always higher than the OEE-value of actions performed by certain units at the assembly line in a period of 12 months.

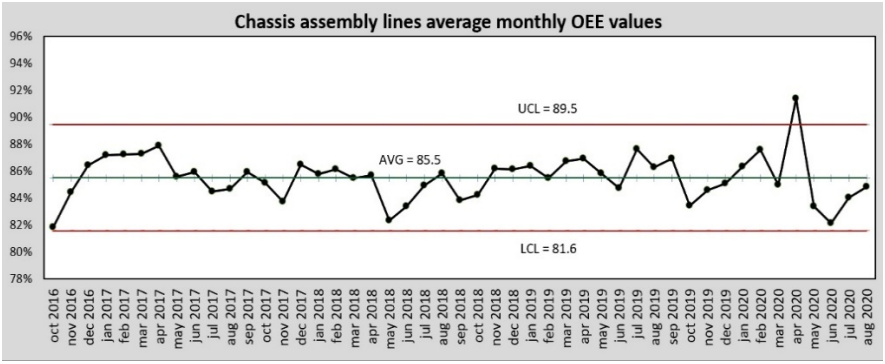

Figure 4. Chassis assembly lines average monthly OEE values

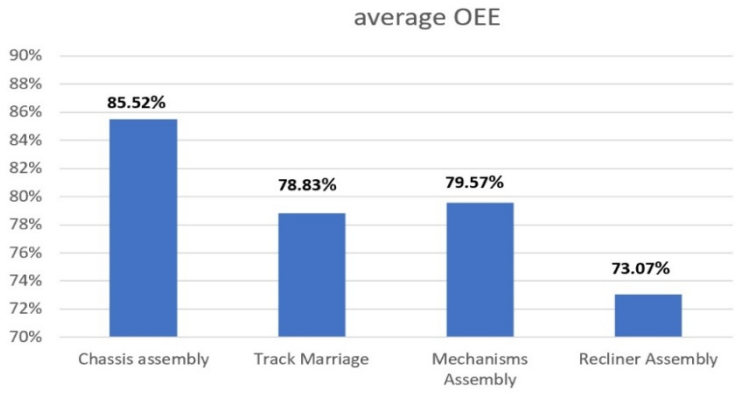

Figure 5. Average OEE values of different semiautomatic assembly lines

It can be identified, that the OEE-value of semi-automatic assembly lines manufacturing the metal frame of car seats depends on the number of workers. Final assembly lines with a staff of more than 10 employees have a higher OEE-value than semi-automatic assembly lines with less employees. The difference is at least 3% a year. The main reason for this difference is that more attention, control,

technological and engineering support are allocated to the assembly lines requiring more people because profit has to be maximized.

Based on the review of OEE-components (availability, performance, quality), the analysis has shown that the most focus is placed on quality resulting in the highest achievement. This component reaches the highest percentile rate in each semi-automatic assembly line. Performance ranks second and availability ranks in the last place. Figures of the OEE-components are shown in Table 1.

.

Table 1. OEE components values

	OEE	Availability	Performance	Quality	number of assembly lines	number of average person
Chassis assembly	85.52%	93.47% (3.)	94.01% (2.)	98.93% (1.)	127	10 - 40
Track Marriage	78.83%	85.89% (3.)	93.58% (2.)	98.93% (1.)	67	4 - 8
Mechanisms Assembly	79.57%	89.99% (3.)	90.62% (2.)	98.32% (1.)	61	3 - 6
Recliner Assembly	73.07%	84.30% (3.)	88.59% (2.)	97.70% (1.)	52	3 - 10

4. Conclusion

Considering a yearly period, the OEE-value of semi-automatic assembly lines manufacturing the metal frame of car seats is always higher than the OEE-value of semi-automatic assembly lines manufacturing component equipment in the same period of time. The average value of seat chassis assembly lines is 85.5%, the average value of sub-assembly lines is between 73% and 79.5%. In addition, the OEE-value depends on the size of the staff working at the assembly line. Final assembly lines with a staff of more than 10 employees have a higher OEE-value than semi-automatic assembly lines with less employees. The difference is at least 3% a year. It could be the subject of further analysis to compare other seat manufacturing technologies (e.g. welding, stamping, etc.) to assembly lines and big data research after pattern in the data for preactive measures.

References

[1] R. Glawar, F. Ansari, Cs. Kardos, K. Matyas, W. Sihn, Conceptual design of an integrated autonomous production control model in association with

a prescriptive maintenance model (PriMa), *Procedia CIRP* 80 (2019) pp. 482–487.
doi: https://doi.org/10.1016/j.procir.2019.01.047

[2] F. Antreter, The Possibilities of the Performance Measurement to the Estimating of the to Logistic Processes Joining Supplementary Work Hour Demand at the Automobile Manufacturer Factory, *Acta Technica Jaurinensis* 3 (3) (2010) pp. 267-283.

[3] M. Sokovic, D. Pavletic, K. K. Pipan, Quality improvement methodologies – PDCA Cycle, RADAR Matrix, DMAIC and DFSS, *Journal of Achievements in Materials and Manufacturing Engineering* 43 (2010) pp. 476-483.

[4] J. Oliveira, J.C. Sa, A. Fernandes, Continuous Improvement through 'Lean Tools': An Application in a Mechanical Company, *Procedia Manufacturing* 13 (2017) pp. 1082–1089.
doi: https://doi.org/10.1016/j.promfg.2017.09.139

[5] T. L. Nguyen, M. T. Le, T. T T.Vu, N. H. Do, Lean line balancing for an electronics assembly line, *Procedia CIRP* 40 (2016) pp. 437–442.
doi: https://doi.org/10.1016/j.procir.2016.01.089

[6] H. ElMaraghy, W. ElMaraghy, Smart Adaptable Assembly Systems, *Procedia CIRP* 44 (2016) pp. 4–13.
doi: https://doi.org/10.1016/j.procir.2016.04.107

[7] M. Subramaniyan, A. Skoogh, H. Salomonsson, P. Bangalore, J. Bokrantz, A data-driven algorithm to predict throughput bottlenecks in a production system based on active periods of the machines, *Computers & Industrial Engineering* 125 (2018) pp. 533–544.
doi: https://doi.org/10.1016/j.cie.2018.04.024

[8] B. Denkena, M.A. Dittrich, S. Wilmsmeier, Automated production data feedback for adaptive work planning and production control, *Procedia Manufacturing* 28 (2019) pp. 18–23.
doi: https://doi.org/10.1016/j.promfg.2018.12.004

[9] A. Kusiak, Smart manufacturing, *International Journal of Production Research* 56 1–2 (2018) pp. 508–517.

doi: https://doi.org/10.1080/00207543.2017.1351644

[10] C. L. Constantinescu, E. Francalanza, D. Matarazzo, O. Balkan, Information Support and Interactive Planning in the Digital Factory: Approach and Industry-Driven Evaluation, *Procedia CIRP* 25 (2014) pp. 269–275.
doi: https://doi.org/10.1016/j.procir.2014.10.038

[11] S. Nakajima, Introduction to TPM: Total Productive Maintenance, Productivity Press Cambridge, 1988.

[12] R. Hedman, M. Subramaniyan, P. Almström, Analysis of critical factors for automatic measurement of OEE, *Procedia CIRP* 57 (2016) pp. 128–133.
doi: https://doi.org/10.1016/j.procir.2016.11.023

[13] LP Steenkamp, D. Hagedorn-Hansen, G.A. Oosthuizen, Visual Management System to Manage Manufacturing Resources, *Procedia Manufacturing* 8 (2017) pp. 455–462.
doi: https://doi.org/10.1016/j.promfg.2017.02.058

[14] M. Mainea, L. Duta, Patic C., I. Caciula , A method to optimize the Overall Equipment Effectiveness, IFAC Proceedings (2010) pp. 237–241.
doi: https://doi.org/10.3182/20100908-3-PT-3007.00046

[15] P. De Grotte, Maintenance performance analysis: A practical approach, *Journal of Quality in Maintenance Engineering* 1 (2) (1995) pp. 4-24.

[16] S. Saito, Reducing labour costs using industrial engineering techniques, Maynard's Industrial Engineering Handbook, McGraw-Hill, New York, 2001.

[17] K. Mahmood, M. Lanz, V. Toivonen, T. Otto, A Performance Evaluation Concept for Production Systems in an SME Network, *Procedia CIRP* 72 (2018) pp.603–608.
doi: https://doi.org/10.1016/j.procir.2018.03.182

[18] M. Subramaniyan, Production Data Analytics – To identify productivity potentials, Chalmers University of Technology, Gothenburg, Sweden, 2015.

[19] R.C. Hansen, Overall Equipment Effectivness: A powerful production / maintenance tool for increased profits, New York Industrial Press, 2001.

[20] P. Almström, A. Kinnander, Productivity Potential Assessment of the Swedish Manufacturing Industry, Swedish Production Seminar, (2007)

[21] I. Antoniolli, P. Guariente, T. Pereira, L. P. Ferreira, F.J.G. Silva, Standardization and optimization of an automotive components production line, *Procedia Manufacturing* 13 (2017) pp. 1120–1127. doi: https://doi.org/10.1016/j.promfg.2017.09.173

[22] D. Mourtzis, D. Tsakalos, F. Xanthi, V. Zogopoulos, Optimization of highly automated production line: An advanced engineering educational approach, *Procedia Manufacturing* 31 (2019) pp. 45–51. doi: https://doi.org/10.1016/j.promfg.2019.03.008

[23] E. Permin, F. Bertelsmeier, M. Blum, J. Bützler, S. Haag, S. Kuz, D. Özdemir, Self-Optimizing Production Systems, *Procedia CIRP* 41 (2016) pp. 417–422. doi: https://doi.org/10.1016/j.procir.2015.12.114

[24] F. Tao, Q. Qi, A. Liu, A. Kusiak, Data-Driven Smart Manufacturing, *Journal of Manufacturing Systems* 48 (2018) pp. 157–169. doi: https://doi.org/10.1016/j.jmsy.2018.01.006

[25] G. Schuh, T. Potente, C. Thomas, F. Brambring, Improving data integrity in production control, *Procedia CIRP* 9 (2013) pp. 44–48. doi: https://doi.org/10.1016/j.procir.2013.06.166

[26] C. Reuter, F. Brambring, Improving data consistency in production control, *Procedia CIRP* 41 (2016) pp. 51–56. doi: https://doi.org/10.1016/j.procir.2015.12.116

Acta
Technica
Jaurinensis

Vol. 14, No. 1, pp. 36-59, 2021
DOI: 10.14513/actatechjaur.00566

Review of geosynthetic-reinforced pile-supported (GRPS) embankments - parametric study and design methods

R. Alsirawan [1,*]

[1] Széchenyi István University, Doctoral School of Multidisciplinary Engineering Sciences
Egyetem tér 1, 9026 Győr, Hungary
***e-mail: rashad.seirawan@gmail.com**

Submitted: 26/09/2020; Accepted: 03/12/2020; Available online: 14/12/2020

Abstract: Embankment construction on soft soil may result in excessive settlement, loss of bearing capacity, or sliding instability. However, geosynthetic-reinforced pile-supported (GRPS) embankments offer an effective technique to overcome the problems resulting from soft foundations soils. This paper presents a review of the most important parameters affecting the behaviour of GRPS embankments as well as design methods that estimate tensile forces in the geosynthetic layers and load efficiency. Results highlight the importance of using GRPS embankments, but also reveal the inconsistencies between design methods. Finally, general conclusions about the design and construction of GRPS systems are presented.

Keywords: *geosynthetic-reinforced pile-supported embankments; tensile forces; load efficiency*

1. Introduction

Embankments are a fast, inexpensive way to raise the grade of, highways and railways. However, their construction over soft soil with high compressibility and low shear strength, is a real challenge for geotechnical engineers. Nowadays this challenge is more urgent as a result of the shortage of available land for infrastructure and the location of urban centres along rivers and coastlines. Embankments on soft soils are possible through techniques such as: soft soil replacement, preloading, prefabricated vertical drains (PVDs), lightweight embankment materials, basal

reinforcement using geosynthetics, conventional columns (stone columns, deep soil mixing, etc.), and geosynthetics-reinforced platform and piles (GRPS).

The last technique has been widely used over the last three decades because of its advantages such as short waiting period for pore pressure dissipation, reduction of differential settlements at the embankment surface, and the ability to provide uniform support over heterogeneous foundation soils.

The typical GRPS embankment consists of a piles network and load transfer platform (LTP) located above the pile heads, Fig.1a. This platform generally includes one or more layers of geosynthetics (geogrid or geotextiles) underlain by piles that penetrate into firm ground. GRPS embankment systems are best suited for high loads and/or thick soft soil. This paper presents a review of the most important parameters affecting behaviour of GRPS embankments.

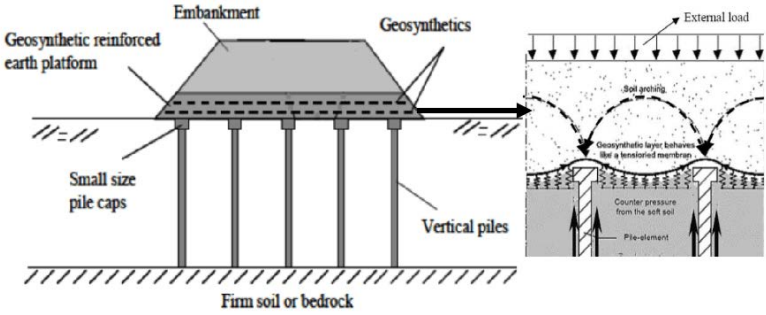

Figure 1. GRPS embankment [1]

2. Literature Review

2.1. The techniques of supporting embankments, an overview

Since the load transfer mechanism between the embankment, geogrid, piles and foundation soils is very complex, empirical approaches have been used to assess the practical design parameters for this technique. The general belief is that load is transferred to the piles via soil arching, Fig.1b where the geogrid further enhances this effect. A well-designed GRPS will transfer loads to the piles and underlying firm layers, creating only a tolerable magnitude of differential settlement and an acceptable margin of safety against slope or bearing capacity failure within the embankment. The studies discussed below use a wide variety of assumptions and methods to evaluate the performance of GRPS systems.

Sakleshpur and Madhav [1] described different techniques to support embankments on soft soil. These methods are:

1. Prefabricated vertical drains (PVDs): this technique is used to decrease the time required for soft soil to consolidate and strengthen itself.

2. Basal reinforcement with geosynthetics: this technique is used to increase the safety factor against failure through the tensile forces in the geosynthetics.

3. Stone columns: this technique is used in case of low loads to reduce the settlements and lateral deformations.

4. Piles: this technique is used over thick soft soil and/or high loads where the piles carry the major proportion of loads and that leads in turn to reduce the embankment surface settlements and soft soil settlement.

5. Piles with basal layers of geosynthetics: this technique is used to increase the proportion of loads carried by piles and thus decrease significantly the settlements.

Halder and Singh [2] explained the effect of using piles with one layer of geogrid, and found that the settlement and vertical stress applied on soft soil decrease about 65% relative to those without piles and geogrid. The lateral displacement at 1 m distance from the embankment toe decreases around 250%, which make the stability of the embankment in a safe side.

Liu and Rowe [3] compared different improvement options of the embankments (one unimproved, one with piles, one with piles and one layer of geogrid, one with piles and two layers of geogrid). According to this study, the settlements at the embankment surface after using the improvement options decreased to (60%, 41%, and 38%) respectively and the settlements at the soft soil surface decreased to (52%, 31%, and 28%) respectively. Inserting the first geosynthetic layer reduces the settlement about 20% while the effect of the second layer is very low.

2.2. Parametric study

Before starting the parametric study, some indicators using to evaluate the soil arching phenomenon must be defined:

- The soil arching ratio is defined as the ratio of the vertical stress applied on the soft soil between piles to the vertical stress resulting from the weight of embankment and surcharge.

$$\rho = \frac{\sigma_s}{\gamma H + q} \qquad (1)$$

where σ_s is the vertical stress on the soft soil, γ is the embankment fill unit weight, H is the embankment height, q is the uniform surcharge.

- The stress concentration ratio is defined as the ratio of the vertical stress applied on the piles to the stress applied on the soft soil.

$$SCR = \frac{\sigma_p}{\sigma_s} \qquad (2)$$

where σ_p is the vertical stress on the pile head.

- The cover rate is a ratio of the piles area (or pile caps area) to the area of the load transfer platform.
- The load efficiency is a ratio of the vertical stress applied on the pile to the vertical stress resulting from the embankment weight and uniform surcharge.

$$E = \frac{\sigma_p}{(\gamma H + q)} \qquad (3)$$

Han et al. [4] conducted a numerical study to examine the effect of several parameters on the performance of GRPS:

1. The number and stiffness of the geosynthetic layers.

2. The elastic moduli of deep-mixed columns and soft soil.

3. The pile spacing.

Their study demonstrated that inserting one geosynthetic layer in the platform decreased the maximum and differential settlements at the embankment surface (considering the settlement is the main problem of embankments on the soft soil) while the effect of more layers can be neglected. The geosynthetic stiffness was considered effective in reducing the settlements up to 4000 kN/m and after this value, the influence is not increase. The study also demonstrated that increasing the elastic moduli of piles and soft soil reduces both maximum and differential settlements, while the pile spacing has opposite effect.

Han and Gabr [5] conducted a numerical study on a GRPS embankment. The results showed that the soil arching ratio decreases with the increase of elastic modulus of piles. The stress concentration ratio increases with increasing the pile elastic modulus, embankment height, and geosynthetic stiffness.

Rathmayer [6] recommended using fill materials with good quality to decrease the cover rate. Han [7] found that the cover rate decreases to low values (around 40%) and ranging from 10% to 20% in the case of using geosynthetics reinforcement. Nuñez et al. [8] chose cement-treated fill instead of granular fill to use in the load transfer platform to find its effect on the load efficiency. The researchers found that the load efficiency increases by about 85% for the embankments with little height, less than 1.5m.

In the study described in Chevalier et al [9], a numerical method was used to understand the mechanism of load transfer through the granular platform. The results showed that the peak friction angle and thickness h_m of the platform play a main role in redirecting the load toward the piles. Fig. 2a shows that the load efficiency increases with increasing the platform thickness, $q_t$is defined as stress equivalent to the total load applied on the soft soil. The results in Fig. 2b show that the maximum settlement δ of the soft soil reduces when the platform thickness changes from 0.5 m to 1.0 m. Add to that, the inclusion of one layer of geosynthetic will lower this value further.

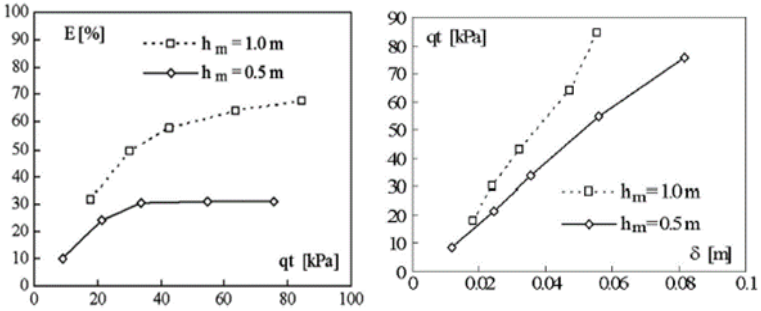

(a) *(b)*

Figure2. The influence of platform thickness on (a) load efficiency, (b) maximum settlement of soft soil [9]

In order to evaluate the most important parameters affecting GRPS behaviour, van Eekelen et al [10][11][12] carried out an extensive parametric study by conducting an experiment program that included twelve tests. The results were as follows:

1. The load efficiency increases (as a percentage) as the uniform surcharge increases
2. The use of granular fill (Ø=49°) instead of sand fill (Ø=40.88°) in the platform increases the load efficiency.
3. The maximum strains can be observed on the pile head and in the strip between two piles.
4. The vertical deflections of the geosynthetic are approximately the same in the case of using a geogrid or a geotextile.
5. The use of one biaxial layer or two uniaxial layers located above each other gives the same influence.
6. Inclusion one layer of the geosynthetic gives a relatively larger value of the load efficiency in comparison with using two layers apart.

Other researchers have supported the results obtained and demonstrated the effect of other parameters on the behavior of GRPS embankments:

Load efficiency is influenced by a host of parameters and increases with the uniform surcharge increases and with the use of high-quality fill material in the platform [13], and this is consistent with van Eekelen's results. Fagundes et al. [14] conducted a series of centrifuge tests. The results showed that the load efficiency reaches 100% in all the tests. Fig. 3 shows that the load efficiency increases with the settlement of soft soil Δw and the maximum deflection of the geosynthetic between two piles y_d. The maximum deflection of the geosynthetic y_d relies on the clear spacing between two piles (s-a), embankment thickness, and geosynthetics stiffness. While it is impossible to reach 100% efficiency without the geosynthetic layers.

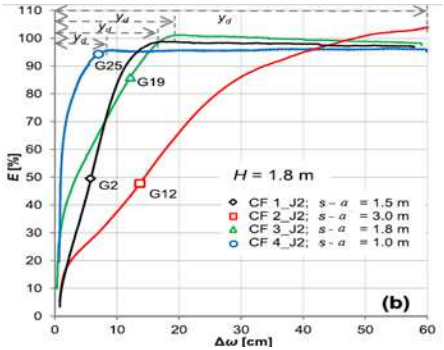

Figure3. Load efficiency versus settlements of soft soil [14]

The differential settlement at the embankment surface decreases as the embankment height increases, pile spacing decreases, and geosynthetic stiffness increases. The minimum embankment height to prevent the settlements equal to 2.1 (s-a) and the embankment height should be greater than 2.5 the height of a soil arch to avoid the differential settlements [14]. Al-Ani and based on a laboratory test model found that the settlement of the soft soil reduces when fill material with high effective friction angle is used while the effect of dilatancy angle (Ψ) on the soft soil settlements is small in comparison with that of effective friction angle [13]. Phutthananon et al. [15] have performed three physical model tests to investigate the effect of the pile cap size, pile strength, and thickness of soft soil on the differential settlements. The results indicated that enlarging the pile cap plays an important role in decreasing the differential settlements at the embankment surface. The results also indicated that the soft soil thickness has a little impact on the differential settlement but a significant impact on the maximum settlement, and the lower strength of the pile with small cap size leads to decrease differential settlement while has a negative influence on the maximum settlement. Thanh Truc et al. [16] carried out two-

dimensional and three-dimensional analyses by Plaxis 2-D and Plaxis 3-D to understand the behavior of GRPS embankment. They found that the differential settlements at the embankment base (over pile heads and in midpoints) are approximately the same under low surcharge values for low embankment heights, these settlements increase as the pile spacing increases; The analyses gave different results where Plaxis 2-D gave the largest values.

2.3. Design methods of GRPS embankments

The design of GRPS embankments is complicated due to different soil-structure interactions in this system. There are several empirical methods for the design focus on the load efficiency and tension in the geosynthetic layers. This paper addresses one side of the design related to tensile forces in the geosynthetics layers.

2.3.1. Terzaghi's design method (1943)

Terzaghi [17] presented soil arching theory based on a trap door experiment. This phenomenon occurs when one part of soil moves downward while another part remains in its place and shear forces are generated on the sliding surfaces between two parts of the soil. Fig. 4 shows soil Arching analysis with Terzaghi's method, the shearing resistance is given by the following equation:

$$\tau = c + \sigma \tan \emptyset \qquad (4)$$

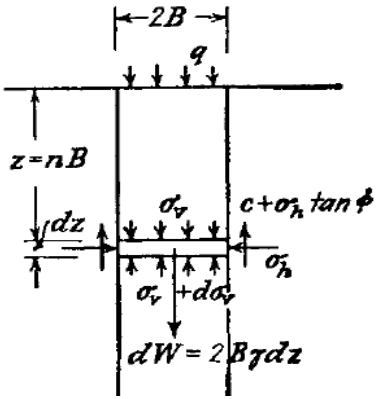

Figure 4. Soil arching phenomenon [17]

The requirement of equilibrium:

$$2B\gamma\, dz = 2B\,(\sigma_v + d\sigma_v) - 2B\sigma_v + 2c\, dz + 2K_0\, \sigma_v\, dz\, \tan \emptyset \qquad (5)$$

Or

$$\frac{d\sigma_v}{dz} = \gamma - \frac{c}{B} - K_0\,\sigma_v\,\frac{\tan\emptyset}{B} \qquad (6)$$

where τ is the shear stress, σ is the vertical stress, c, $\emptyset$ are friction angle and cohesion of the soil, 2B is the width of a trap door, γ is the soil unit weight, σ_v is the vertical stress, $K_0 = \sigma_h / \sigma_v$ is the earth pressure coefficient at rest, q is the uniform surcharge.

The solution to these equations is of the form:

$$\sigma_v = \frac{B\,(\gamma - c/B)}{K_0\,\tan\emptyset}\left(1 - e^{-K_0\tan\emptyset\;\; z/B}\right) + q\,e^{-K_0\tan\emptyset\;\; z/B} \qquad (7)$$

Russell and Pierpoint (1997) [18], using Terzaghi's analysis, described the arching phenomenon in a piled embankment. They calculate the tension in the geosynthetic as follows:

$$T = \frac{S_{3D}\gamma H(s^2 - a^2)}{4a}\sqrt{1 + \frac{1}{6\varepsilon}} \qquad (8)$$

where a is the pile cap width, s is the pile spacing, ε is the initial strain to generate tensile load and equal to 5%, S_{3D} is the stress reduction ratio and given by:

$$S_{3D} = \frac{(s^2 - a^2)}{4HaK_0 tan\emptyset}\left(1 - e^{\frac{-4HaK_0 tan\emptyset}{(s^2 - a^2)}}\right) \qquad (9)$$

where H is the embankment height.

2.3.2. Guido et al. design method (1987)

Guido et al. [19] have performed plate-loading tests and found that the load spreads in the load transfer platform at an angle of 45° from the LTP base in two-dimensional plane-strain condition. This method assumed that the geosynthetic layers and piles carried the full load while the soft soil does not carry any proportion of the load.

The geosynthetic tension is calculated as follow:

$$T = \frac{W}{2sin\delta} \qquad (10)$$

$$W = 0.525\,(\gamma H + q) \qquad (11)$$

where W is the load acting on geosynthetic, δ is the angle friction between soil and geosynthetic.

2.3.3. Carlson design method (1987)

Carlson [20] suggested a method to calculate the load resulting from the soil wedge which applied on the geosynthetic as shown in Fig. 5*a*.

Assumptions of the Carlson method include: the apex angle of the soil wedge is 30°, the soil wedge represents the area (A) between two piles and not the area (B) as shown in Fig. 5b, this is considered nonconservative and leads to underestimate the tensile forces.

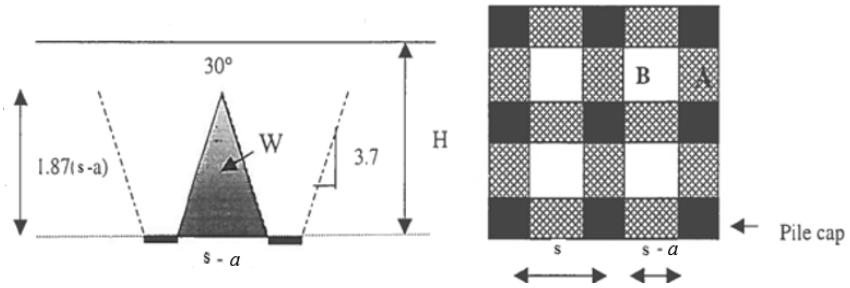

Figure 5. (a) Soil wedge, (b) A and B areas according to Carlson method [21].

They used equation (12) to calculate the weight of soil wedge:

$$W = \frac{(s-a)^2}{4\ tan15^\circ}\ \gamma \qquad (12)$$

Due to the applied load, the geosynthetic begins to deflect, and as a result, the strain ε increases as shown in Fig. 6. The geosynthetic deflection is given as follows:

$$d = (s-a)\sqrt{\frac{3}{8}\ \varepsilon} \qquad (13)$$

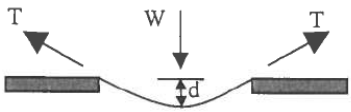

Figure 6. Deflection of geosynthetic *[21]*

The geosynthetic tension is given by the following equation:

$$T = \frac{(s-a)^3}{16\ tan15^\circ}\ \gamma\ \frac{1}{2d}\ \sqrt{1+\frac{16\ d^2}{(s-a)^2}} = W\ \frac{s-a}{8\ d}\ \sqrt{1+\frac{16\ d^2}{(s-a)^2}} \qquad (14)$$

2.3.4. Hewlett and Randolph design method (1988)

Hewlett and Randolph [22] [23] suggested that the proportion of the load is transferred to the pile heads as a form of hemispherical domes, and the rest is carried by the geosynthetic layer. This method supposed that the system may fail at the arch top (i.e. efficiency Ev) or at the pile heads (i.e. efficiency ET) as shown in Fig. 7. After determining the minimum efficiency between both of them, the maximum load carried by the geosynthetic is determined. In general, for the large embankment height, the efficiency at the pile heads is dominant, while for small embankment height, the efficiency at the top of the arch is dominant.

-Arching efficiency at the arch top [23]:

$$E_V = 1 - \left[1 - \left(\frac{a}{s}\right)^2\right] (A - AB + C) \qquad (15)$$

where:

$$A = \left[1 - \left(\frac{a}{s}\right)\right]^{-2(K_P - 1)} \qquad (16)$$

$$B = \frac{s}{\sqrt{2}H}\left[\frac{2\,K_P - 2}{2\,K_P - 3}\right] \qquad (17)$$

$$C = \frac{s - a}{\sqrt{2}H}\left[\frac{2\,K_P - 2}{2\,K_P - 3}\right] \qquad (18)$$

where, K_P is the passive earth pressure coefficient [23]:

$$K_P = \frac{1 + sin\emptyset}{1 - sin\emptyset} \qquad (19)$$

- Arching efficiency at the level of pile heads can be calculated by following equation [24]:

$$E_T = \frac{\beta}{1 + \beta} \qquad (20)$$

where β is a coefficient is given as follows [23]:

$$\beta = \frac{2\,K_P}{(2\,K_P + 1)\left(1 + \left(\frac{a}{s}\right)\right)}\left[\left(1 - \frac{a}{s}\right)^{-K_P} - (1 + K_P\,\frac{a}{s}\right] \qquad (21)$$

The proportion of the load applied on the geosynthetic between adjacent piles is given as follows [23]:

$$\sigma_{v,geo} = \frac{s^2}{s^2 - a^2}\ \sigma_v\ (1 - E_{min}) \qquad (22)$$

with $$\sigma_v = \gamma_\gamma\ \gamma_r\ H + \gamma_G\ g + \gamma_Q\ q \qquad (23)$$

where γ_γ is the partial factor on the soil unit weight, γ_r is the embankment unit weight, $\gamma_G$is the partial factor on the permanent actions, $g$is the permanent excess vertical load, γ_Q is the partial factor on the variable actions, q is the variable excess vertical load, E_{min}: is the minimum of $E_V\ and\ E_T$

British Standard BS8006 (2010) [24] used Hewlett and Randolph method to calculate the geosynthetic tension (per lineal meter) by the following equation:

$$T = \frac{(s-a)s\ \sigma_{v,geo}}{a}\ (1 + \frac{1}{6\varepsilon})^{0.5} \qquad (24)$$

2.3.5. Low et al. design method (1994)

Low et al. [26] developed Hewlett and Randolph method to investigate the arching phenomena in GRPS embankment where this method assumed semi-cylindrical sand arches are formed between pile walls. According to this method, cap-pile and geotextile contribute to decreasing embankment surface differential settlement. Low et al. developed charts and equations to estimate the strain and tension in the geosynthetic layers and the vertical stress applied on the soft soil. The results showed a partial agreement between theoretical and experimental analyses.

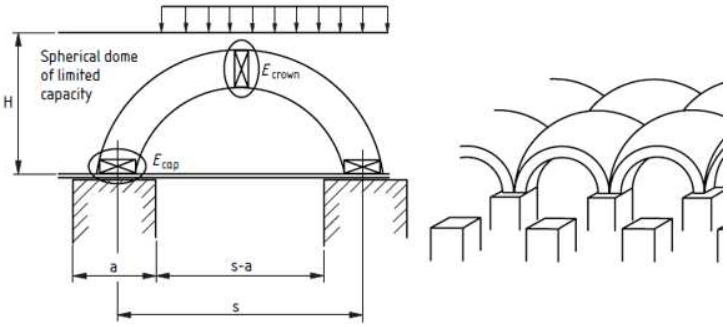

Figure 7. Soil arching according to Hewlett and Randolph [25]

The tension in the geosynthetics can be calculated by the following equation [27]:

$$T = J\ \varepsilon \qquad (25)$$

where $J\ is$ the tensile stiffness of geosynthetic, ε is the axial strain and given by:

$$\varepsilon = \frac{\theta - sin\theta}{sin\theta} \qquad (26)$$

where θ is the half the subtended angle of the geosynthetics arc after deformation and given by:

$$sin\theta = \frac{4(\frac{t}{s-a})}{1 + 4\,(\frac{t}{s-a})^2} \qquad (27)$$

where t is the maximum vertical displacement of soft soil in the midpoint between pile caps. The vertical stress applied on the soft soil in this point can be calculated as follows:

$$\sigma_s = \frac{\gamma(s-a)(K_P-1)}{2(K_P-2)} + (\frac{s-a}{s})^{K_P-1}\left[\gamma\, H - \frac{\gamma s}{2}(1 + \frac{1}{K_P-1}\right] \qquad (28)$$

Because of difficulty in finding the maximum displacement t, the appropriate solution is the reliance on the equilibrium of the vertical forces

$$T/R = \sigma_s - \frac{tE_c}{D} \qquad (29)$$

$$R = \frac{s-a}{2sin\theta} \qquad (30)$$

where E_c is the soft soil elastic modulus, D is the soft soil depth. Low et al. suggested using trial values of maximum displacement t to fulfil the equilibrium of vertical forces.

2.3.6. British Standards BS8006 design method (1995)

This method [25] relied on a variety of analytical, numerical, and physical models to understand the mechanism of load transferring through the load transfer platform to the pile caps. Marston (1913) presented the following equation to describe the ratio of vertical stress carried by piles to the vertical stress exerted on the embankment base:

$$\frac{P_c'}{\sigma_v'} = \left[\frac{C_c\, a}{H}\right]^2 \qquad (31)$$

where P_c' is the vertical stress applied on the pile caps, σ_v' is the vertical stress at the embankment base and equal to $f_{fs}\,\gamma\, H + f_q\, q$, ($f_{fs} = 1.3$ the partial factor for soil unit weight, $f_q = 1.3$ partial factor for surcharge load), γ is the unit weight of the

embankment fill, q is the uniform surcharge, C_c is the arching coefficient ($C_c = 1.95\ H/a - 0.18$ for end bearing piles, $C_c = 1.5\ H/a - 0.07$ for frictional piles.

The vertical load carried by geosynthetic between piles is calculated from:

For $H \geq 1.4\ (s-a)$;

$$W = \frac{1.4\ s\ f_{fs}\ \gamma\ (s-a)}{(s^2-a^2)} \left[s^2 - a^2(\frac{P_c'}{\sigma_v'})\right] \qquad (32)$$

For $0.7\ (s-a) \geq H \geq 1.4\ (s-a)$;

$$W = \frac{\mathrm{s}\ f_{fs}\ \gamma\ H + f_q\ q}{(s^2-a^2)} \left[s^2 - a^2(\frac{P_c'}{\sigma_v'})\right] \qquad (33)$$

The tension in the geosynthetic for each lineal meter can be calculated by the following equation:

$$T = 0.5\ W\ \frac{s-a}{a}\ (1 + \frac{1}{6\varepsilon})^{0.5} \qquad (34)$$

where the initial strain ε =6%.

Van Eekelen et al. [28] proposed that BS8006 designs a strong geosynthetic resulting in an expensive solution, and modified the load carried by geosynthetics. The results showed after comparison with the measurements that the modified BS8006 is more precise than BS8006.

2.3.7. Swedish design method (2002)

Rogbeck et al. [29] suggested that the vertical load, carried by geosynthetic, forms a pyramid of 75°wall inclination and this is also acceptable even if the height of the embankment is lower than the pyramid top, i.e. $(s-a)/2tan15°$as shown in Fig. 8a.

Assumptions of Swedish method include: one layer of geosynthetic is used and its position should be within 0.1 m above pile heads, the geosynthetic is deformed under loading (the initial strain ε =6% and strain at failure is less than 70%). Cover rate $\geq 10\%$ and the embankment height $H \geq (s-a)$.

The 2-D soil pyramid weight is calculated by the following equation:

$$W = \frac{(s-a)^2\ \gamma}{4 \tan 15°} \qquad (35)$$

The load is distributed over the surface with 3-D impacts as shown in Fig. 8b. the tension in the geosynthetic can be calculated for each lineal meter of depth by the following equation:

$$T = 0.5\left(1+\frac{s}{a}\right) W\,(1+\frac{1}{6\varepsilon})^{0.5} \qquad (36)$$

2.3.8. Collin design method (2004)

Collin et al. [29] recommended using a load transfer platform (LTP) under embankment with three layers of geosynthetic at least to create a stiffened beam.

Assumptions of Collin method include: the load transfer platform thickness $h \geq (s-a)$. The distance between geosynthetic layers $h_n \geq 200mm$. The initial strain in the geosynthetic ε =5%.

Fig. 9 shows the soil arching according to Collin method, where every layer of geosynthetic is subjected to a uniform vertical load from the soil wedge under the arch and can be calculated as follows:

$$W_n = \frac{[(s-a)_n^2 - (s-a)_{n+1}^2]h_n\gamma}{(s-a)_n^2} \qquad (37)$$

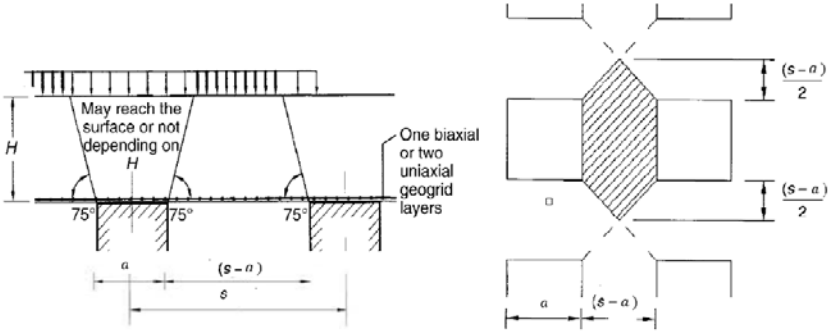

(a) *(b)*

Figure 8. (a) Arching according to Swedish method, (b) load distribution between piles [29]

The tension in the geosynthetic is calculated as follows:

$$T = \frac{W_n\,\Omega\,D}{2} \qquad (38)$$

where D is the design spanning for tension membrane and equal to $(s-a)_n$, Ω is the dimensionless factor and equal to 0.97 for geosynthetic strain ε =5%.

In 2005 Collin et al. modified this method by adding one layer of geosynthetic located directly above pile heads and this layer is designed as a catenary, the vertical load applied on this layer is given by:

$$W_n = \frac{h_n \gamma}{3} \qquad (39)$$

The tension in the geosynthetic is calculated as follows:

$$T = \frac{W_n \, \Omega \, D}{2} \qquad (40)$$

where D is the design span for tensioned membrane and equal to $1.41\{(s-a) - 2[\sum \text{vertical spacing}/tan45°]\}$, Ω is the dimensionless factor.

2.3.9. Kempfert et al. design method (2004)

Kempfert et al. [30] [31] relied on tests of a three-dimensional model, this model consists of four piles were installed in peat soil with reinforced or unreinforced load transfer platform LTP, to investigate the bearing and deformation behaviour of the supported embankment. The design approach of this method depends on determining the loads applied on the piles and soft soil, then the tension in the geosynthetic is calculated to carry the load applied on the soft soil. This method considers the soft soil support. The geosynthetic tension is given as follows:

$$T = J\varepsilon \qquad (41)$$

where J is the geosynthetic stiffness, ε is the maximum strain (the reference [31] to get more information on maximum strain)

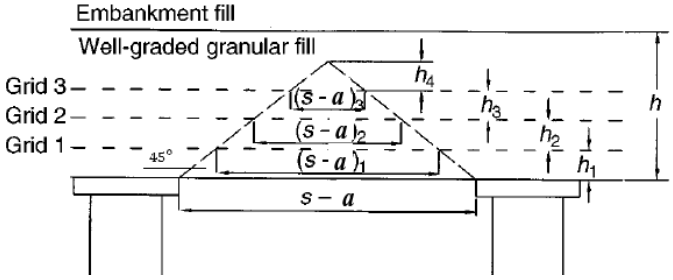

Figure 9. Soil arching according to Collin design method [29]

2.3.10. Abusharar et al. design method (2008)

Abusharar et al. [32] modified Low et al. method by adding the effect of uniform surcharge q on the embankment surface. In this method, the pile spacing is less than the embankment height and the vertical load is uniformly distributed on the geosynthetic as shown in Fig. 10*a*. The vertical stress applied on the middle of the soft soil between pile caps is given as follows:

$$\sigma_s = \frac{\gamma(s-a)(K_P-1)}{2(K_P-2)} + (\frac{s-a}{s})^{K_P-1}\left[q + \gamma H - \frac{\gamma s}{2}(1 + \frac{1}{K_P-1}\right] \qquad (42)$$

Fig. 10b shows a subtended angle2θ, radius of the geosynthetic arc after deformation, and maximum displacement at the middle of the soft soil t.

The geosynthetic tension is calculated as follow:

$$T = 4\beta^2 J + 0.25\, s'\lambda(\sigma_s\, tan\emptyset + \frac{tE_c}{D} tan\, \emptyset_c) \qquad (43)$$

where $\beta = \frac{t}{s'}$, $s' = (s-a)$, λ is the factor ranges between 0.7 and 0.9 (this value depends on the geosynthetic type), $\emptyset_c$ is the friction angle of soft soil. To solve equation (40), the first step is to find β and then the maximum displacement t:

$$a\beta^3 + b\beta^2 + c\beta + d = 0 \qquad (44)$$

where $a = 32DJ + 4s'^2E_c, b = 2s'^2\lambda E_c \tan\emptyset_c - 4s'D\sigma_s, c = 2s'D\sigma_s\lambda tan\emptyset + s'^2E_c, d = -s'D\sigma_s$.

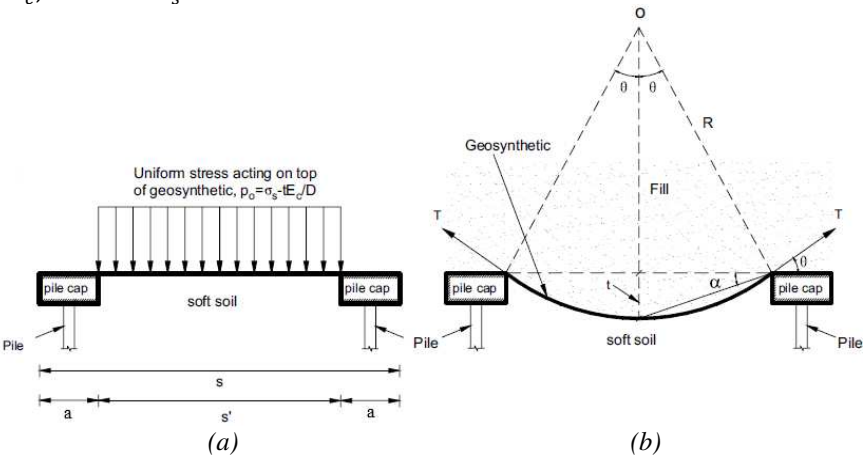

Figure 10. (a) Uniform stress acting on the geosynthetic, (b) deformed shape of geosynthetic [32]

3. Discussion

The results obtained from the review demonstrated that GPRS embankment is an effective solution to overcome the problems resulting from the soft soil such as insufficient bearing capacity and large settlements, especially over soft soil with large thickness and/or in case of the high loads. The mechanism of transferring the load through the embankment to the piles is a soil-arching mechanism and due to that, it can be observed the concentration of stresses over the pile heads and that is related to the different between piles stiffness and soft soil stiffness. Generally, increasing the geosynthetic stiffness, elastic modulus of piles and soft soil, friction angle of the load transfer platform and cover rate contributes in reducing the maximum and differential settlements at the embankment surface, which is the main objective.

The presence of many design methods indicates a lack of understanding of the precise load transfer mechanism to the piles and soft soil. The researchers relied on numerical and experimental models to calculate the tensile forces and loads acting on geosynthetic layers. (These methods are more extensive, but this paper presents the equations used to calculate the applied load on geosynthetic and tensile forces) and none of them used a comprehensive model to design GRPS embankment, this led to a significant difference between the results as shown in Fig 11.

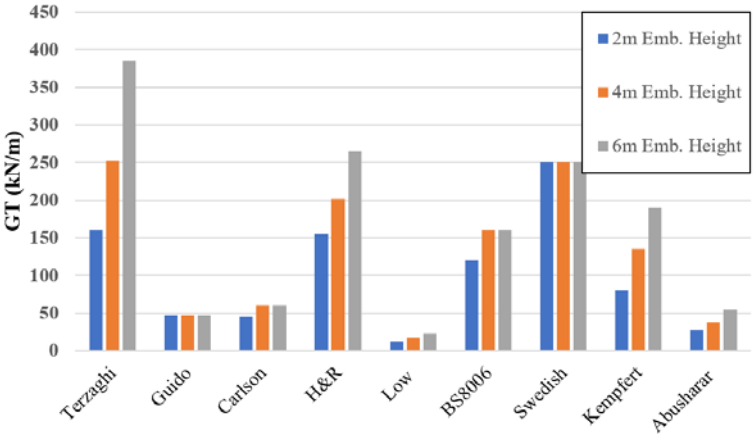

Figure 11. Geosynthetic tension according to design methods.

The design methods used different physical models, and some of them will be mentioned:

1. Low used a two-dimensional model of GRPS embankment where add caps to piles in his model.
2. Hewlett and Randolph developed a three-dimensional unreinforced experimental model.
3. Kempfert used a three-dimensional model, this model consists of four piles were installed in peat soil with reinforced or unreinforced load transfer platform LTP.

The previous examples demonstrate the difference between the physical models. add to that, some parameters (e.g. elastic modulus of piles and, soft soil and LTP material properties, surcharge loads, position of the geosynthetic layer) are not included in all design methods. Table 1. highlights a set of differences between design methods, it does not cover all the differences, but rather the most important ones. The development of GRPS embankment numerical models makes it possible to include the influence of all parameters in the design. The results of numerical simulation are supposed to give results close to reality in comparing with the analytical methods.

Finally, there are many differences between the methods and this can be justified due to the lack of a comprehensive model and the failure to include the influence of all parameters in the calculations. The literature review demonstrated a significant difference between the results of calculated geosynthetic tensile forces according to these methods.

Table 1. Differences between design methods, GS: Geosynthetic, (R&P)**: Russell and Pierpoint calculated the tension in the geosynthetic using Terzaghi's analysis, (J)***: If the stiffness is taken into consideration when calculating T, : Angle of arch from horizontal (deg).*

Design Method	Soil arch shape	GS* layer number	GS* stiffness (J)***	Soft soil support
Terzaghi	Rectangle-2D	1 layer (R&P)**	No	No
Guido	Triangle -2D $(45°)^{a}$	1 layer	No	No
Carlson	Triangle-2D $(75°)^{a}$	1 layer	No	Yes
Hewllet and Randolph	hemispherical dome - 3D	1 layer	No	No
Low	semi-circle-2D	1 layer	Yes	Yes
BS8006	semi-circle-2D	1 layer	No	No
Swedish	Pyramid-3D $(75°)^{a}$	1 layer	No	No
Collin	Pyramid-3D $(45°)^{a}$	≥ 3 layers	No	Yes
Kempfert	multi-shell domes with different centres- 3D	1 layer	Yes	Yes
Abusharar	semi-circle -2D	1 layer	Yes	Yes

4. Conclusions

The aim of this paper is conducting an overview of GRPS embankments, and the results can be summarized as follows:

- ✓ The geosynthetic layers with piles network technique is used to support embankments over thick soft soil and/or high loads where it is difficult to use other techniques under these conditions. GPRS embankment is an effective solution to overcome the problems resulting from the soft soil such as insufficient bearing capacity and large settlements.
- ✓ The load efficiency increases with increasing the platform thickness, geosynthetic stiffness, cover rate, and uniform surcharge, and decreasing the pile spacing. The load efficiency also increases by using fill material with good quality and using one geosynthetic layer.
- ✓ The settlements at the embankment surface decrease with increasing the stiffness of piles and soft soil, geosynthetic stiffness, cover rate, and

embankment thickness. Add to that, inserting the geosynthetic layers and using fill material with good quality decrease the settlements.

- ✓ The design methods of GRPS embankments are generally used to calculate the tension in the geosynthetics, and the load efficiency.
- ✓ The design methods are similar in describing the mechanism of load transferring and differ in the soil arch shape, for example, Hewlett and Randolph supposed that the soil arch shape is semi-spherical; Abusharar et al., Low et al. and BS 8006 supposed that the shape of soil arch is a semi-cylindrical.
- ✓ Some methods considered the influence of soft soil such as Low et al. and Kempfert et al. while others neglected this influence such as Hewlett and Randolph and BS 8006. Some methods assumed inserting one geosynthetic layer in the load transfer platform to act as a catenary such as Swedish and BS8006 while others assumed using three layers to act as beam such as the Collin method.
- ✓ The design methods give a significant difference between the results of calculated geosynthetic tensile forces due to the lack of a comprehensive model and the failure to include the influence of all parameters in the calculations.
- ✓ Due to varied interactions between elements in the system, none of the design methods could cover all these interactions. In this case, a development of finite element model is considered as an effective method to include the influence of all parameters in the design. The results of numerical simulation are supposed to give results close to reality in comparing with the analytical methods.

References

[1] A. Sakleshpur, M. Madhav, Embankments on Soft Ground: An Overview, 1st International Conference on Foundation and Soft Ground Engineering, Thu Dau Mot University, Binh Duong, Vietnam, 2013, pp. 27-44.
URL *https://www.researchgate.net/publication/306107953*

[2] P. Halder, B. Singh, Soft Soil Response and Behaviour of Piles Under a Geotextile Reinforced Embankment, Indian Geotechnical Conference IGC2016, IIT Madras, Chennai, India, 2016.
URL *https://www.researchgate.net/publication/329170394*

[3] K. Liu, R. Rowe, Three-dimensional finite element modelling of a full-scale geosynthetic-reinforced, pile-supported embankment, *Canadian Geotechnical Journal* 52 (12) (2015) pp. 2041-2054.
doi: https://doi.org/10.1139/cgj-2014-0506

[4] J. Han, L. Yan, J. Yang, Parametric study on geosynthetic- reinforced pile supported embankment, GeoShanghai International Conference, 2006, pp. 255-261.
doi: https://doi.org/10.1061/40863(195)28

[5] J. Han, A. Gabr, Numerical Analysis of Geosynthetic-Reinforced and Pile-Supported Earth Platforms over Soft Soil, *Journal of Geotechnical and Geoenviromental Engineering 128* (1) (2002) pp. 44-53.
doi: https://doi.org/10.1061/(ASCE)1090-0241(2002)128:1(44)

[6] H. Rathmayer, Piled embankment supported by single pile caps, Istanbul Conference on Soil Mechanics and Foundation, Istanbul, 1975, pp. 283-290.

[7] J. Han, Design and construction of embankments on geosynthetic reinforced platforms supported by piles, Proceeding of 1999 ASCE/ PaDOT Geotechnical Seminar, Central Pennsylvania Section, ASCE and Pennsylvania Department of Transportation, 1999, pp. 66-84.

[8] M. Nuñez, D. Dias, R. Kastner, C. Poilpré, Soft Ground Improved by Rigid Vertical Piles. Experimental and Numerical Study of Two Real Cases in France, 6th Conference of the International Conference on Case Histories in Geotechnical Engineering, Arlington, Virginia, 2008, pp. 40-49.
URL
https://scholarsmine.mst.edu/icchge/6icchge/session07/40

[9] B. Chevalier, P. Villard, G. Combe, Investigation of Load-Transfer Mechanisms in Geotechnical Earth Structures with Thin Fill Platforms Reinforced by Rigid Inclusions, *International Journal of Geomechanic* 11 (3) (2011) pp. 239-250.
doi: https://doi.org/10.1061/(ASCE)GM.1943-5622.0000083

[10] S.J.M van Eekelen, A. Bezuijen, H.J. Lodder, A.F. van Tol, Model experiments on piled embankments. Part I, *Geotextiles and Geomembranes Journal* 32 (2012) pp. 69-81.
doi: https://doi.org/10.1016/j.geotexmem.2011.11.002

[11] S.J.M van Eekelen, A. Bezuijen, A.F. van Tol, Model experiments on piled embankments. Part II, *Geotextiles and Geomembranes Journal* 32 (2012) pp. 82-94.
doi: https://doi.org/10.1016/j.geotexmem.2011.11.003

[12] S.J.M van Eekelen, A. Bezuijen, A.F. van Tol, An analytical model for arching in piled embankments, *Geotextiles and Geomembranes Journal* 39 (2013) pp. 78-102.
doi: https://doi.org/10.1016/j.geotexmem.2013.07.005

[13] W. Al-Ani, D. Wanatowski, H. Chan, Numerical Analysis of Piled Embankments on Soft Soils, Geo-Shanghai Conference, 2014, Shanghai, pp. 30-39.
doi: https://doi.org/10.1061/9780784413401.003

[14] D.F. Fagundes, M.S.S. Almeida et al., Load transfer mechanism and deformation of reinforced piled embankments, *Geotextiles and Geomembranes Journal* 45 (2) (2017) pp.1-10.
doi: https://doi.org/10.1016/j.geotexmem.2016.11.002

[15] C. Phutthananon, P. Jongpradist, P. Jamsawang, Influence of cap size and strength on settlements of TDM-piled embankments over soft ground, *Marine Georesources & Geotechnology* (2019) pp.1-20.
doi: https://doi.org/10.1080/1064119X.2019.1613700

[16] P.T. Thanh Truc, L.L. Gia, T. Hino, Valuate the effect of embankment height and pile spacing to the behaviour of the Geosynthetic Reinforced Piled embankment using FEM, NAG2018 conference, University of Technology, Ho Chi Minh City, Vietnam, 2018.
URL https://www.researchgate.net/publication/327834113

[17] K. Terzaghi, Theoretical Soil Mechanics, John Wiley & Sons, Inc, New York, USA, 1943, p. 526.

[18] D. Russell, N. Pierpoint, An assessment of design methods for piled embankments. *Ground Engineering* 30 (11) (1997) pp. 39–44.
URL https://trid.trb.org/view/476724

[19] V.A. Guido, J.D. Kneuppel, M.A. Sweeney, Plate loading tests on geogrid reinforced earth slabs. Geosynthetic‘87 Conference 87 (1) (1987) pp.216–225.

[20] B. Carlson, Reinforced soil, principles for calculation, Terratema AB, Linköping, Swedish, 1987.

[21] G. SvanØ, T. Ilstad et al., Alternative calculation principle for design of piled embankments with base reinforcement, 4th International Conference on Ground Improvement Geosystems, Helsinki, 2000.
URL *https://www.researchgate.net/publication/327652189*

[22] W.J. Hewlett, M.F. Randolph, Analysis of piled embankments, *Ground Engineering* 22 (3) (1988) pp.12-18.

[23] P. Berthelot, T. Bret et al. Recommendations for the Design, Construction and Control of Rigid Inclusion Ground Improvements. Presses des Ponts, Paris, 2012, p. 316.

[24] BS 8006, Code of Practice for Strengthened /Reinforced Soils and Other Fills, British Standard Institution, London, UK, 2010.
URL *http://worldcat.org/isbn/0580242161*

[25] BS 8006, Code of Practice for Strengthened /Reinforced Soils and Other Fills, British Standard Institution, London, UK, 1995.
URL *https://webstore.ansi.org/standards/bsi/bs80061995*

[26] B.K. Low, S.K. Tang, V. Choa, Arching in piled embankments, *Journal of Geotechnical Engineering* 120 (11) (1994) pp.1917–1938.

[27] P. Ariyarathne, D.S. Liyanapathirana, Review of existing design methods for geosynthetic-reinforced pile-supported embankments, *Soils and Foundations* 55 (1) (2015) pp.17–34.
doi: *https://doi.org/10.1016/j.sandf.2014.12.002*

[28] S.J.M. van Eekelen, A. Bezuijen, A.F van Tol, Analysis and modification of the British Standard BS8006 for the design of piled embankments, *Geotextiles and Geomembranes Journal* 29 (3) (2011) pp.345-359.
doi: *https://doi.org/*10.1016/j.geotexmem.2011.02.001

[29] R.W. Sarsby, Geosynthetics in civil engineering, Wood head Publishing Limited in association with The Textile Institute, Cambridge, England, 2007, 308p.
URL https://www.pdfdrive.com/geosynthetics-in-civil-engineering-e185194584.html

[30] H.G. Kempfert, C. Gobel et al., German recommendations for the reinforced embankments on pile-similar elements. *Geosynthetics in Civil and Environmental Engineering* (2004) pp.697–702.
doi: https://doi.org/10.1007/978-3-540-69313-0_128

[31] The German Geotechnical Society, Recommendations for Design and Analysis of Earth Structures using Geosynthetic Reinforcements – EBGEO, 2st Edition, Munich, Germany, 2012, p. 324.
doi: https://doi.org/10.1002/9783433600931

[32] S.W. Abusharar, J. JZheng, B.G. Chen, J.H. Yin, A simplified method for analysis of a piled embankment reinforced with geosynthetics, *Geotextiles and Geomembranes Journal* 27 (1) (2008) pp. 39-52.
doi: https://doi.org/10.1016/j.geotexmem.2008.05.002

Acta
Technica
Jaurinensis

Vol. 14, No. 1, pp. 60-79, 2021
DOI: 10.14513/actatechjaur.00570

Literature review on steel fibre, silica fume and fly ash: improving methods for recycled and multiple recycled aggregate concretes

M. Shmlls[1,*], D. Bozsaky[1], T. Horváth[1]

[1]Széchenyi István University,
Department of Architecture and Building Construction
Egyetem tér 1, 9026 Győr, Hungary
***E-mail: maysamshmlls@gmail.com**

Submitted: 19/10/2020; Accepted: 03/12/2020; Available online: 14/12/2020

Abstract: If all concrete is to be recycled in a future scenario, recycled concrete will be needed. Usually concrete recycling causes loss of properties, but this does not have to be truth for all the mixtures. This paper shows a comprehensive knowledge about the improving methods used to keep the properties of the recycled aggregate concrete (RAC). In the reviewed literature several kinds of RAC were tested with various replacement ratios. The effect of adding steel fibres, silica fume or fly ash to the mixture were also examined both separately and together. Most of the experiments demonstrated excellent mechanical properties of the RAC compared with ordinary concretes. Based on these results the ideal RAC composition can be deduced and a future can be imagined when concrete can be recycled multiple times (MRAC).

Keywords: *recycled coarse aggregate; steel fibre; silica fume; fly ash; multiple recycled aggregate concrete*

1. Introduction

Concrete is a global and basic construction material primarily used at civil engineering works. Aggregate gives about 70-80% of the concrete. There is shortage of aggregate materials due to the increasing demand of this raw material in all over

the world. Therefore, it is important and beneficial to focus on recycling this material and to solve the environmental problems by reducing the use of conventional concrete. Scarcity of natural resources and impacts of climate change have made the increasing consumption of resources an important issue, especially in the case of building materials such as cement, fine and coarse aggregate. Simultaneously, there are massive amounts of waste materials generating from demolitions of old buildings or remaining as debris after the wars all over the world.

Because of these two points, the definition of recycled coarse aggregate was created to reach sustainable construction and to decrease the cost of aggregates. Many researchers have studied recycled aggregate concrete (RAC) and the effects of recycling on the fresh and hardened properties of concrete. The results were different in the cases of different concrete types containing cement replacement materials and other additions such as superplasticizer and steel fibres. For many decades, steel fibres have been used in reinforced concrete to reduce the numbers of cracks and provide ductility inside the concrete. However, just a few studies focused on the effect of steel fibres on durability and compressive strength of RAC containing cement replacement materials such as fly ash and silica fume.

This paper reviews what scientific knowledge found about recycled aggregate concrete and what the fresh and hardened properties of different concrete admixtures are, compared with the case of the controlled concrete. In addition, it answers these questions: Do the cement replacement materials (fly ash or silica fume) (Fig. 1) play a significant role in the concrete field? What kind of materials can be used effectively? What is their effect on the properties of normal and recycled aggregate concrete? Can the RAC properties improve with the addition of steel fibres, or not?

Figure 1. Fly ash (left) and silica fume (right) supplement materials [1][2]

Silica fume is a by-product in the processing of simple silicone or silicone alloys in electric arc furnaces. The reduction of high pure quartz into silicone at a temperature of about 2000 °C creates silicone dioxide vapor that changes its physical

state and becomes silica smoke at low temperatures. Silica fumes have a solid surface and extremely fine average size 0.1–0.3 μm [1]. The early slump of fresh concrete is to be raised to improve the workability. The silica fume has been proven to lower bleeding by its impact on rheological products [3] [4]. Test results revealed that silica fumes have limited significance in the development and stabilization of the air avoidance system. Resistance experiments (ASTM C666) on silica concrete produced reasonable results like the average factor of longevity was above 99%.

Waste fly ash (WFA) typically consists of small carbon-burned fragments and has many uses. Its material content thus depends on the origin and nature of the coal used. In many countries, fly ash formed by the burning of coal in power stations presents large environmental and economic problems. Snelson and Kinuthia [5] proposed the addition of WFA as a partial replacement of cement to enhance properties of concrete. In addition, they studied WFA with cement paste to confirm the ability of using WFA on physical, mechanical and activation behaviour of concrete. The typically specified rate of substitution of fly ash for Portland cement is 1 to 1 1/2 pounds fly ash for 1-pound cement. Nevertheless, it depends on the researcher's experiments and what kind of mixtures are to be tested.

2. Types of steel fibres and an its use in concrete

In order to improve the properties of concrete, several types of fibres are used in the construction practice an in research. Fibres can be made of plastic, glass, carbon, or steel (Fig. 2). Steel fibre is a small piece of metal reinforcement with different aspect ratio (length, diameter) that can reach up to 100 mm length, having different forms and endings (straight, crimped, stranded, hooked, and twisted fibre), as it is shown in Fig. 3 [6].

Figure 2. Fibres commonly used to reinforce concrete [6]

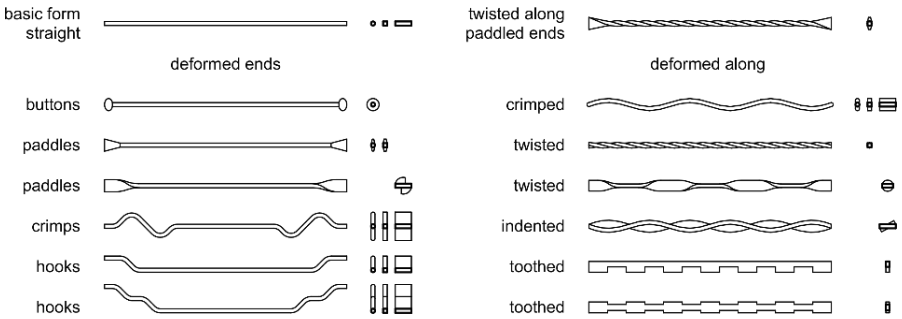

Figure 3. Types of steel fibres [original drawing]

There are five groups of steel fibres based on the shape and industrial process of production: mill cut, melt-extracted, cut sheet, cold-drawn wire, modified cold-drawn wire. The greatest benefits of steel fibre utilization in concrete is to reduce the number of cracks which can happen on the surface of concrete, to increase its resistance on high temperatures and against exterior impacts, to improve other concrete properties such as banding capability, durability, weakness, and fatigue.

2.1.1. Steel fibres in ultra-high-performance concrete (UHPC)

In different fields of civil engineering (construction of bridges, decks, slabs, industrial pavements) steel fibres play an important role. Brandt's study [7] focuses on the production of the evolving ultra-fibre reinforced concrete and explains that

steel fibres can reduce the amount of cement in concrete and thus its carbon footprint and environmental impact can be reduced. This experiment substituted the 50% weight of Portland cement with fly ash and ground granulated blast-furnace slag in half proportion, and the results showed that UHPC mixtures approached 125 and 140 MPa compression strengths at the ages 28 and 56 days. The flexural strength test results showed that UHPC with the maximal fibre fraction (i.e. 2.5% by volume, comprising 1.5% hooked fibres, and 0.5+0.5% long and short micro wire fibres) attained adequate flexural and uniaxial compressive strength for post cracking ductility and sub-peak load holding. Brandt [8] explained that steel fibre reinforced high-strength concretes can be excellent solutions in critical areas where earthquakes are frequent because of their high compressive strength, ductility, and adequate seismic structure.

2.1.2. Steel fibres in light-weight concrete (LWC)

Kalpana and Tayu [8] described their study about the incorporation of the waste steel fibres in lightweight concrete. Their results showed that even a small quantity of fibre is able to improve the composition of lightweight concrete and prevent it from the brittle failure, and the effect of steel fibres on the flexural strength is far greater than their direct stress or compression influence. Moreover, it was observed that the LWC strength was found to depend on the quantity of fibre content, the best fibre ingredients vary with the quality demands to achieve the greatest profit in diverse strengths. As the fibre content increases, failure mode is changed from brittle to ductile once subjected to compression and bending. The incorporation of steel fibre is an important factor in fragility reducing.

Rico et al. [9] added steel fibres into a delicate cement matrix, according to their research, in order to increase the break resistance of the LWC by the split capture process and to improve the tensile and flexural properties. The results showed that steel fibre played a connection role inside the concrete thus helping to raise the resistance of the concrete against cracks and mentioned that increased toughness is a consequence of increased fibre.

2.1.3. Steel fibre in self-compacting concrete (SCC)

In the study described in Ramesh et al. [10], different rates of steel fibres (0.3, 0.6, 0.9, 1.2%) had been used in self-compacting concrete mixtures to measure the effects of the fibres for the mixtures, to study the workability and the strength properties. According to the results, the flexural and break tensile strength improved for the 7th day in case of SCC incorporation and steel fibres compared to the control concrete (with no steel fibres), but the improvement was not considerable. For the 28th day, the bending intensity and the split tensile strength improved significantly (15-21%) when fibres were applied compared to the reference concrete.

Dhaher [11] presented his experimental investigation on the fracture behaviour of hybrid fibre reinforced self-compacted concrete. In the experiments, two forms of fibres were used: steel and polypropylene fibres. Volumetric fibre percentages were implemented: 0.75, 1.0 and 1.15% for steel; 0.10, 0.15 and 0.25% for polypropylene. In comparison, a 0.75% (0,65% steel and 0,10% polypropylene fibre) combination mix of the above-listed forms have been used. This was the only formula that managed to meet the new demands of self-compacting concrete. The test results show that the fresh-state properties considerably decreased if fibres are incorporated into the SCC blends. The SCC criteria could be achieved only by the mixtures of volumetric percentages of 0.75-1.00% steel and 0.10-0.15% polypropylene fibres. The use of steel fibres also works more than the use of polypropylene fibres regarding all forms of strength. The increase in-group intensity for any measured combination was far greater than that of compressive strength. During the experiments, Dhaher [11] also observed that a link-cracking area evolved due to the incorporation of fibres regardless of the type and amount.

3. The necessity of recycled coarse aggregate (RCA)

Concrete is in the first place among the list of construction materials because of its massive advantages. However, concrete production also emits immense amount of CO_2, which affects the environment and climate. Moreover, researchers estimate the amount of raw concrete materials, such as cement, fine and coarse aggregate, water, to be about 20 billion tons per year with increasing demand year by year [12]. Zhang et al. [13] mentioned that the global concrete production in each year is between 13-21 billion tons, and in this amount 49% is the aggregate (gravel and fine), and 16% is water.

Concrete demolition waste to be recycled is estimated about 850 million tons/year in European countries and about 200 million in China. The challenge is the same in the Middle East countries, such as Gaza strip and Syria where a huge amount of debris resulted from the ruined buildings due to the constant wars. The estimated concrete debris amount is about 2 million tons in the Gaza strip after the war in 2014, and until now, there are no statistics on the extent of huge destruction in Syria, which can be seen in Fig. 4.

Figure 4. Destroyed place in Syria, with concrete debris [14]

Aggregate as the biggest part of the concrete (usually about two-thirds) is an essential element that needs to be highlighted by doing lots of experiments and detailed research to sustain the balance in the construction trade taking into consideration the growing demand of this material. In addition, some countries are struggling to obtain this raw material because it is not available in a sufficient quantity and quality from domestic sources for the continuous constructions (Fig. 5). Based on all these factors, the recycled coarse aggregate (RCA) is playing a significant role in the construction field, which still needs more future studies.

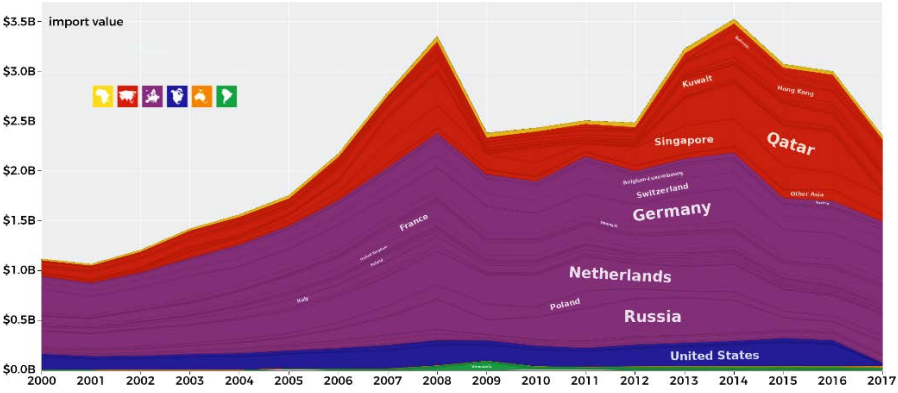

Figure 5. Crushed stone and gravel import between 2000-2017 [15]

4. The recycled aggregate concrete and its improvement

RCA is not a brand-new concept; it was used during and after the World War II to get rid of the tremendous amount of debris generated from demolitions and construction waste. Firstly, instead of natural aggregate (NA), used recycled aggregate (RA) was applied as a bedding in the substructure of a road in England [16]. Then researchers initiated the investigations of the possibilities for the replacement of NA with RA in the building structures. Rahal [17] found, during his experiments, that the compressive strength of the recycled aggregate concrete (RAC) was reduced and the same thing happened for modulus of elasticity. However, researchers continued in this field to improve and adopt RCA by adding an unprocessed material to provide a concrete admixture, which can be similar to the control concrete with same properties.

4.1. Using fly ash (FA) in RAC

Recycled aggregate concrete also reduces the cost of making concrete up to 30% [18]. Many researchers studied the ability of RAC with different replacement amount of natural aggregate. These studies usually confirmed the reduction of the compressive and tensile strength [19] [20] [21]. However, some of them found the opposite results [22]. To decrease this effect on the strength of RAC, some researchers used cement replacement materials such as fly ash, waste cellular concrete or waste perlite powder to modify the strength of RAC. Snelson and Kinuthia [5] explained the positive effect of fly ash on the mechanical properties and durability when fly ash was partially replaced with cement. There are also different names for this supplementary material such as unprocessed material, rejected material, low-quality material, or raw material.

Abed and Nemes [23] added three type of supplementary materials to the cement in different admixtures with different replacement amount of recycled aggregate (RA). The most important points in their results showed: (1) There is some increase in the compressive strength at the age of 90 and 270 days, when the fly ash ratio was 15% and the RA replacement was 50% of the NA. (2) Result is almost the same by using waste perlite powder in 15% ratio. (3) But for the splitting tensile strength, their experiments showed that 15% waste perlite powder made the RAC with 25% and 50% of NA replacement slightly stronger than adding the same dosage of fly ash or the waste cellular concrete.

Chandragiri and Cao [24], Vieira et al. [25] and Laneyrie et al. [26] found that after exposure to elevated temperature, the properties of concrete were affected and the residual mechanical properties became enhancing, and the explosive spalling of concrete decreased. The incorporation of pulverized fly ash and the slag in two separate admixtures showed an important effect to save the residual mechanical

properties, to reduce the exterior cracks and to decrease the possibility of spalling after the concrete's exposure to high temperature [27] [28].

4.2. Using silica fume (SF) in RAC

In the research of Pilehvar et al. [29] demolition structure waste is used as RA in concrete mixtures, with or without SF. The mechanical properties of the concrete specimens are defined in three groups, such as compression strength, tensile strength, and physical properties of the specific concrete specimens, such as the density of the water absorption rate. The optimal ratio in concrete combinations is implemented as 30% of RA. Low RAC regression factor with SF is observed in the short term. It has been found that the 5% SF content of the RAC improves the low features of the RAC more easily.

The effects of SF in the concrete blend are described by Cakir and Sofyanli [30], to improve the quality of recycled concrete. Portland cement has been replaced at 0%, 5% and 10% by SF. Specimens were produced by substituting natural aggregates for recycled aggregates. Four group of concrete mixtures and two size fractions (4/12 and 8/22 mm) were used. A consistent water / binder proportion of 0.50 has been used in all mixtures and concrete were prepared with a preliminary target slump of the class S4 (16 to 21 cm). The results showed that mechanical and physical characteristics of concrete were enhanced by 10% SF as cement replacement for RAC. The tensile strength increases in the NA concrete mix with and without SF was higher during all the test times than that of the RAC mixtures. The strength of the RAC incorporating SF was observed for continuous and significant improvement. Concrete with 10% SF and 4/12 mm fraction RA have shown improved performance between recycled compound concretes.

Contrary to the above-mentioned studies, Adebakin and Piaye [31] noticed in their study that adding silica fume has negatively affected on the residual strength and raised the surface cracks on the concrete.

4.3. Using steel fibre in RAC

Gao et al. [32] investigated the durability of steel fibre reinforced recycled coarse aggregate concrete (SFRRAC) by doing carbonization, quick freeze-thaw, and chloride penetration tests. Different replacement amounts of coarse aggregate were used, which were made of waste old mixture concrete with compressive strength from 30 to 50 MPa. The replacement ratio was 0, 30, 50, 100% of the normal coarse aggregate. Steel fibre was used as reinforcement with the ratio 0, 0.5, 1, 1.5, 2%. The experimental results showed that: carbon tolerance, freeze-thaw resistance, and anti-chloride permeability improved with compressive strength. SFRRAC's durability indicators were more susceptible to water binding than to compression strength. A

less water-cement ratio improved the durability. The experimental results showed the followings: (1) The recycled aggregate replacement ratio had a low effect on carbonate strength, freeze-thaw resistance and anti-chloride permeability with the same compressive strength and steel fibre volume fraction. SFRRAC's durability is like normal concrete. (2) Steel fibres also increased the durability of SFRRAC as they did for ordinary concrete. If the fraction of steel fibre was less than 1.5%, SFRRAC's durability increase with the fraction of stainless fibre volume. Nevertheless, the durability became slightly lower with the rising fibre amount of steel, when the steel fibre fraction was higher than 1.5%. (3) The 5% weight loss was not an adequate failure standard for the SFRRAC rapid freeze-thaw test. A further study is required to determine the suitable failure test of the SFRRAC fast freeze-thaw test. (4) Concrete compactness was the main factor that affected the SFRRAC's durability. SFRRAC is a long-lasting material and can be applied successfully as structural elements with good blending design.

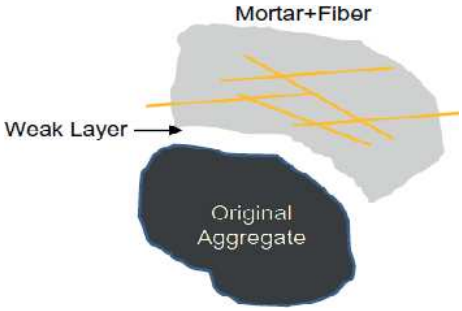

Figure 6. Composition of recycled concrete with steel fibres [33]

Kunieda et al. [33] investigated the possibilities of recycling fibre concrete, which included different types of fibres, as well as steel fibres. The content of fibres had different ratios: 0.2%, 0.5%, 1.0% polypropylene, and 1.0% steel fibre. The crushing process was made by a jaw crusher machine, which had 38 ton/h capacity. The findings of these recycling experiments were the followings: (1) With an increase in the fibre content, the size of crushed concrete in recycled fibre concrete decreased, because the fibre in the mortar reinforced the cracked parts and caused other damage. They also noticed that the distribution of particle size did not significantly differ between the normal and PP fibre concrete, only by 0.2 percent. (2) The crushing phase was performed in this experiment by using a jaw crusher, which is ordinary, used to produce recycled aggregate from concrete. The fibre content can be easily removed through the operation. Fibres are stored in the mortar and the processing of admixture is the same as that in the control concrete, as it is shown in the Fig. 6. (3) Researchers noticed that adding the steel fibres caused reduction in the compressive

strength but slightly increased the flexural strength and toughness. (4) During the experiments, the air content increased from 3.8% to 9.8% in the new mixture with steel fibre. The 1% fibre content could lower the water absorbance ratio by more than 1% compared to regulated concrete and thus decrease the installed mortar around the recycled coarse aggregate.

4.4. Using couple effect of silica fume and steel fibre in RAC

Adding steel fibre with silica fume to RAC can lead to a future structural material with less crack in the RAC, reduction in the water permeability, increasing in both compressive and flexural strength [34]. Xie et al. [35] used the pair effect of silica fume and steel fibre to experiment the compressive strength and flexural performance of RAC. Adding of silica fume had done with two ways: the equal quantity substitution was 0, 5, 10% (depending on normal performance and cost calculation), or the straight addition was 3%. Steel fibre ratio was 1% and polypropylene ratio was 0.13% of the concrete volume. The replacement amount of recycled aggregate was 100%. 39 cylinders (150×300 mm) and 39 prisms (100×100×515 mm) have been made for testing. At the age of 90 days, the experiments were made on the samples, and these showed that: (1) The perfect percentage of silica fume is 10% to improve the compressive and flexural strength of SFRRAC. (2) The pair effect of silica fume and steel fibre is stronger than the pair effect of silica fume and polypropylene. (3) Adding the silica fume can improve the interfacial bonding between the cement paste and the thick steel fibres. (4) 1.5% of steel fibre had improved the flexural strength. Table 1. shows the most important results for this couple effect of silica fume and steel fibres demonstrated in this study.

Table 1. Couple effect of steel fibres and silica fume on RAC properties

Properties of RAC	Adding only steel fibres to RAC	Adding steel fibres and silica fume to RAC
Compressive strength	Reduced up to 10.8%	Increased up to 9.1%
Flexural strength	Slight effect	Significant effect
Modulus of elasticity	Reduced up to 13.9%	Increased up to 5.0%
Toughness	Increased with 9%	Increased over 50%

5. Multiple recycled concrete aggregate (MRCA)

Recycling of concrete as aggregate should be an essential method in the building industry. In this way, the CO_2 emissions of natural stone extraction can be reduced [36], as well as the cost of construction of new buildings. Especially in developing

countries which have been facing tough circumstances over the past few years, such as Syria which suffers from an economic crisis due to the second local war since 1980. Wars have produced a lot of construction debris and wastes. The reconstruction cost is estimated at 250 billion dollars by the United Nation. The demolition and construction wastes, which need many landfills, have an increasing amount each year. 850 million tons is the yearly generation of C&D waste in European countries, while the annual amount in China is 200 million tons [13]. These facts explain the necessity for the research of recycled coarse aggregate and even the possibility of multiple recycling.

Only a few studies investigated the mechanical and other properties of the multiple recycling coarse aggregate concrete (MRAC) with different replacement amounts. Thomas et al. [36] presented by using computerized microtomography that the adhered mortar volume of multiple recycled coarse aggregate (MRA) could be up to 80%. When the mechanical and physical properties were compared between the first generation and the multiple recycled concrete in the precast industry, the findings of Salesa et al. [37] showed perfect mechanical performance of MRAC. The results showed that MRAC was superior to the control concrete of precast concrete samples and they supported the idea of adopting MRAC as a sustainable method of recycling.

Huda and Alam [38] presented different conclusion when they used replacement up to 100% in the MRAC: the compressive strength was marginally reduced. Marie and Quiasrawi [39] used only 20% replacement of MRA to study the closed-loop conduct. Their results also showed some reduction in the tensile and compressive strengths. In general, they proved that the performance and the possibility of using MRA were still satisfactory. They used MRA's closed-loop process, because recycling was important to compensate the natural scarcity, to achieve sustainability, and to reduce climatic changes at least in the construction field as it is shown in the Fig. 7. The experimental results of Abed et al. [40] showed less porosity and the same pressure resistance for the second-generation of recycling in comparison to those shown by the normal control concrete.

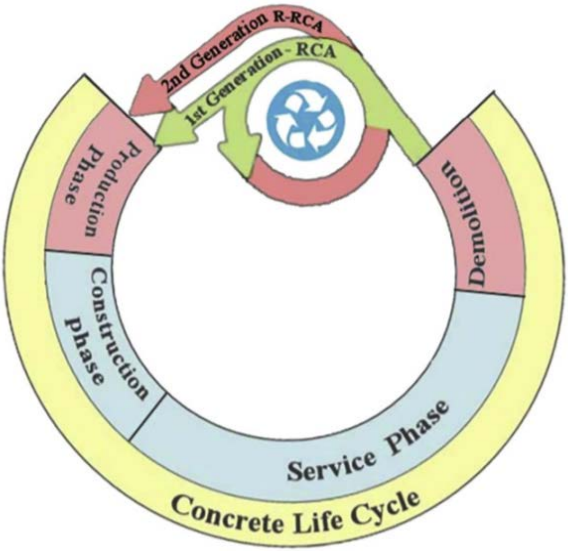

Figure 7. Closed-loop recycling of coarse aggregate [39]

6. Discussion

The aim of this paper was to review what the researchers have discovered so far in the concrete field about the impact of steel fibre on the concrete types, especially in the two generations of recycled concretes (RAC and MRAC). It also showed what the effect of additional materials such as (fly ash, silica fume and steel fibre) is on the recycled concrete's properties.

Using 2.5% volume of steel fibre in ultra-high-performance admixture provided a perfect concrete with high compressive and flexural strength in the regions exposed to earthquakes constantly. Lightweight concrete interacted with the steel fibre in a perfect admixture causing some increase in the crack resistance and playing a connecting role among the concrete particles. For self-compacting concrete, different rates and types of steel fibre were tested to measure the impact of these materials in this kind of concrete. Table 2. presents a summary of the effect of steel fibre on mechanical properties of each concrete category.

Table 2. Effect of steel fibre on properties of different concretes

Types of concrete	The effect of steel fibre on mechanical properties	
	Compressive strength and crack reduction	**Tensile strength**
Ultra-high-performance concrete	High compressive strength up to 140 MPa	Adequate flexure and uniaxial strength
Light weight concrete	Prevent from brittle failure and turn into ductile / reduce	Increase the break resistance
Self-compacting concrete	Link-cracking area had been improved	Significantly improvement

Fly ash with 15% replacement of cement was the best ratio, it had a positive effect on mechanical properties and the durability of RAC and saved the residual mechanical when RAC was exposed to high temperatures. Silica fume was observed in the short term. It has been found that the 5% silica fume content of the RAC improves the low features of the RAC more easily. Adding 5% of silica fume resulted satisfactory properties in the RAC, but another researcher tried a different ratios of silica fume (0%, 5%, 10%) and found that 10% was a perfect ratio to improve the properties of RAC. Unlike others who noticed in their study, that adding silica fume negatively affected the residual strength and raised the surface cracks on the concrete. Main findings from the studies:

- Adding the steel fibres to RAC caused a reduction in the compressive strength and slightly increased the flexural strength and toughness. In addition, air content inside the samples increases from 3.8% to 9.8% after the new mixture with steel fibre. Another researcher noticed that 1.5% of steel fibre improved flexural strength.
- The combined effects of steel fibres and the 10% silica fume will contribute to the potential structural material of RAC with less cracking.
- The pairing effect of silica fume and steel fibre is stronger than the pairing effect of silica fume and polypropylene.
- Adding silica fume can improve the interfacial bonding between the cement paste and the thick steel fibres.
- The compression and strength tests on the MRAC proved close results to those tests performed on the control concrete.

As a result of reviewing the scientific literature of the recycled aggregate concrete topic, some research directions can be inferred for future researches:

- Using the triple effect of steel fibre, fly ash and silica fume can provide an optimum concrete admixture with excellent compressive and flexural strength, minimum cracks on the surface and high-temperature resistance.
- Multiple coarse aggregate concrete still needs further research and more laboratory experiments to test the fire resistance and freeze/thaw effect.
- Using supplementary materials, the properties of MRAC can be improved and the missing properties can be defined in a future research.

Acknowledgement

The author would like to acknowledge the financial support of the project EFOP-3.6.1-16-2016-00017 - Internationalization, initiatives to establish a new source of researchers and graduates, and development of knowledge and technological transfer as instruments of intelligent specializations at Széchenyi István University.

References

[1] D. K. Panesar, Supplementary cementing materials, in: S. Mindess (ed.), Developments in the Formulation and Reinforcement of Concrete, Woodhead Publishing, 2019, pp. 55–85.
doi: https://doi.org/10.1016/B978-0-08-102616-8.00003-4

[2] M. Pigeon, R. Cantin, Flexural properties of steel fibre-reinforced concretes at low temperatures, *Cement and Concrete Composites* 20 (5) (1998) pp. 365–375.
doi: https://doi.org/10.1016/S0958-9465(98)00017-1

[3] R. Pérez-López, J. M. Nieto, G. R. de Almodóvar, Utilization of fly ash to improve the quality of the acid mine drainage generated by oxidation of a sulphide-rich mining waste: Column experiments, *Chemosphere* 67 (8) (2007) pp. 1637–1646.
doi: https://doi.org/10.1016/j.chemosphere.2006.10.009

[4] S. M. Levy, Calculations Relating to Concrete and Masonry, in: Construction Calculations Manual, Butterworth-Heinemann, 2012, pp. 211–264.
doi: https://doi.org/10.1016/B978-0-12-382243-7.00005-X

[5] D. G. Snelson, J. M. Kinuthia, Characterisation of an unprocessed landfill ash for application in concrete, *Journal of Environmental Management* 91 (11) (2010) pp. 2117–2125.
doi: https://doi.org/10.1016/j.jenvman.2010.04.015

[6] T. E. T. Buttignol, J. L. A. O. Sousa, T. N. Bittencourt, Ultra-high-performance fibre-reinforced concrete (UHPFRC): a review of material properties and design procedures, *Revista IBRACON de Estruturas e Materiais* 10 (4) (2017) pp. 957–971.
doi: https://doi.org/10.1590/s1983-41952017000400011

[7] A. M. Brandt, Fibre reinforced cement based (FRC) composites after over 40 years of development in building and civil engineering, *Composite Structures* 86 (1–3) (2008) pp. 3–9.
doi: https://doi.org/10.1016/j.compstruct.2008.03.006

[8] M. Kalpana, A. Tayu, Experimental investigation on lightweight concrete added with industrial waste (steel waste), *Materials Today: Proceedings* 22 (3) (2020) pp. 887–889.
doi: https://doi.org/10.1016/j.matpr.2019.11.096

[9] S. Rico, R. Farshidpour, F. M. Tehrani, State-of-the-art report on fiber-reinforced lightweight aggregate concrete masonry, *Advances in Civil Engineering* (Special Issue) (2017) p. 9.
doi: https://doi.org/10.1155/2017/8078346

[10] B. Ramesh, Review on the flexural properties of fibre reinforced self-compacting concrete by the addition of M-sand. *Materials Today: Proceedings* 22 (3) (2020) pp. 1155–1160.
doi: https://doi.org/10.1016/j.matpr.2019.12.041

[11] A. S. Dhaher, Fracture behaviour of reinforced self-compacting concrete with hybrid fibres, M.Sc. thesis, University of Technology, Iraq, (2016).
URL https://www.researchgate.net/publication/292157685

[12] A. M. Wagih, H. Z. El-Karmoty, M. Ebid, S. H. Okba, Recycled construction and demolition concrete waste as aggregate for structural concrete, *HBRC Journal* 9 (3) (2013) pp. 193–200.
doi: https://doi.org/10.1016/j.hbrcj.2013.08.007

[13] Y. Zhang, W. Luo, J. Wang, Y. Wang, Y. Xu, J. Xiao,
A review of life cycle assessment of recycled aggregate concrete,
Construction and Building Materials 209 (2019) pp. 115–125.
doi: https://doi.org/10.1016/j.conbuildmat.2019.03.078

[14] L. Vignal, Destruction-in-Progress: revolution, repression and war planning in Syria, *Built Environment* 40 (3) (2014) pp 326–341.
doi: https://doi.org/10.2148/benv.40.3.326

[15] The Observatory of Economic Complexity: Which countries import Gravel and Crushed Stone? (2000-2017) [cited 2020-09-25].
URL https://oec.world/en/visualize/stacked/hs92/import/show/all/2517/2000.2017/

[16] N. Kisku, H. Joshi, M. Ansari, S. K. Panda, S. Nayak, S. C. Dutta,
A critical review and assessment for usage of recycled aggregate as sustainable construction material, *Construction and Building Materials* 131 (2017) pp 721–740.
doi: https://doi.org/10.1016/j.conbuildmat.2016.11.029

[17] K. Rahal, Mechanical properties of concrete with recycled coarse aggregate, *Building and Environment* 42 (1) (2007) pp. 407–415.
doi: https://doi.org/10.1016/j.buildenv.2005.07.033

[18] M. Rakshvir, S. V. Barai, Studies on recycled aggregates-based concrete, *Waste Management and Research* 24 (3) (2006) pp. 225–233.
doi: https://doi.org/10.1177/0734242X06064820

[19] J. Sharma, S. Singla, Study of recycled concrete aggregates, International *Journal of Engineering Trends and Technology* 13 (3) (2014) pp. 1–5.
doi: https://doi.org/10.14445/22315381/IJETT-V13P226

[20] C. S. Poon, Z. H. Shui, L. Lam, H. Fok, S. C. Kou, Influence of moisture states of natural and recycled aggregates on the slump and compressive strength of concrete, *Cement and Concrete Research* 34 (1) (2004) pp. 31–36.
doi: https://doi.org/10.1016/j.cemconres.2003.12.019

[21] I. B. Topcu, S. Sengel, Properties of concretes produced with waste concrete aggregate, Cement and Concrete Research 34 (8) (2004) pp. 1307–1312.
doi: https://doi.org/10.1016/j.cemconres.2003.12.019

[22] N. Fonseca, J. de Brito, L. Evangelista, The influence of curing conditions on the mechanical performance of concrete made with recycled concrete waste, *Cement and Concrete Composites* 33 (6) (2011) pp. 637–643. doi: https://doi.org/10.1016/j.cemconcomp.2011.04.002

[23] M. Abed, R. Nemes, Long-term durability of self-compacting high-performance concrete produced with waste materials, *Construction and Building Materials* 212 (2019) pp. 350–361. doi: https://doi.org/10.1016/j.conbuildmat.2019.04.004

[24] P. Chindaprasirt, T. Cao, Reuse of recycled aggregate in the production of alkali-activated concrete, in: Handbook of Alkali-Activated Cements, Mortars and Concretes, Woodhead Publishing, 2015, pp. 519–538. doi: https://doi.org/10.1533/9781782422884.4.519

[25] J. P. B. Vieira, J.R. Correia, J. de Brito, Post-fire residual mechanical properties of concrete made with recycled concrete coarse aggregates, *Cement and Concrete Research* 41 (5) (2011) pp. 533–541. doi: https://doi.org/10.1016/j.cemconres.2011.02.002

[26] C. Laneyrie, A. Beaucour, M. F. Green, R. L. Hebert, B. Ledesert, A. Noumowe, Influence of recycled coarse aggregates on normal and high-performance concrete subjected to elevated temperatures, *Construction and Building Materials* 111 (2016) pp. 368–378. doi: https://doi.org/10.1016/j.conbuildmat.2016.02.056

[27] J. Z. Xiao, J. B. Li, C. Zhang, On relationships between the mechanical properties of recycled aggregate concrete: An overview, *Materials and Structures* 39 (2006) pp. 655–664. doi: https://doi.org/10.1617/s11527-006-9093-0

[28] J. Xiao, D. Lu, J. Ying, Durability of recycled aggregate concrete: An overview, *Journal of Advanced Concrete Technology* 11 (12) (2013) pp. 347–359. doi: https://doi.org/10.3151/jact.11.347

[29] S. Pilehvar, A. M. Szczotok, J. F. Rodríguez, L. Valentini, M. Lanzón, R. Pamies, A. Kjøniksen, Effect of freeze-thaw cycles on the mechanical behaviour of geopolymer concrete and Portland cement concrete containing micro-encapsulated phase change materials, *Construction and Building Materials* 200 (2019) pp. 94–103. doi: https://doi.org/10.1016/j.conbuildmat.2018.12.057

[30] Ö. Çakır, Ö. Ö. Sofyanlı, Influence of silica fume on mechanical and physical properties of recycled aggregate concrete, *HBRC Journal* 11 (2) (2015) pp. 157-166. doi: https://doi.org/10.1016/j.hbrcj.2014.06.002

[31] I. H. Adebakin, T. O. Ipaye, Effect of elevated temperature on the compressive strength of recycled aggregate concrete, *Research Journal of Engineering Sciences* 5 (9) (2016) pp. 1–4. URL http://www.isca.in/IJES/Archive/v5/i9/1.ISCA-RJEngS-2016-119.pdf

[32] D. Gao, L. Zhang, J. Zhao, P. You, Durability of steel fibre-reinforced recycled coarse aggregate concrete, *Construction and Building Materials* 232 (2020) Paper Nr. 117119 doi: https://doi.org/10.1016/j.conbuildmat.2019.117119

[33] M. Kunieda, N. Ueda, H. Nakamura, Ability of recycling on fibre reinforced concrete, *Construction and Building Materials* 67 (C) (2014) pp. 315–320. doi: http://dx.doi.org/10.1016/j.conbuildmat.2014.01.060

[34] W. M. Shaban, J. Yang, H. Su, K. H. Mo, L. Li, J. Xie, Quality improvement techniques for recycled concrete aggregate: A review, *Journal of Advanced Concrete Technology* 17 (2019) pp. 151–167. doi: https://doi.org/10.3151/jact.17.4.151

[35] J. Xie, C. Fang, Z. Lu, Z. Li, L. Li, Effects of the addition of silica fume and rubber particles on the compressive behaviour of recycled aggregate concrete with steel fibres, *Journal of Cleaner Production* 197 (1) (2018) pp. 656-667. doi: https://doi.org/10.1016/j.jclepro.2018.06.237

[36] C. Thomas, J. de Brito, A. Cimentada, J. A. Sainz-Aja, Macro- and micro- properties of multi-recycled aggregate concrete, *Journal of Cleaner Production* 245 (2020) Paper Nr. 118843. doi: https://doi.org/10.1016/j.jclepro.2019.118843

[37] Á. Salesa, J. A. Pérez-Benedicto, D. Colorado-Aranguren, P. L. López-Julián, L. M. Esteban, L. J. Sánz-Baldúz, J. L. Sáez-Hostaled, J. Ramis, D. Olivares, Physio – mechanical properties of multi – recycled concrete from precast concrete industry, *Journal of Cleaner Production* 141 (2017) pp. 248-255. doi: http://dx.doi.org/10.1016/j.jclepro.2016.09.058

[38] S. B. Huda, M. S. Aram, Mechanical behavior of three generations of 100% repeated recycled coarse aggregate concrete, *Construction and Building Materials* 65 (2014) pp. 574-582. doi: https://doi.org/10.1016/j.conbuildmat.2014.05.010

[39] I. Marie, H. Quiasrawi, Closed-loop recycling of recycled concrete aggregates, *Journal of Cleaner Production* 37 (2012) pp. 243-248. doi: http://dx.doi.org/10.1016/j.jclepro.2012.07.020

[40] M. Abed, R. Nemes, B. A. Tayeh, Properties of self-compacting high-strength concrete containing multiple use of recycled aggregate, *Journal of King Saud University – Engineering Sciences* 32 (2) (2020) pp. 108-114. doi: https://doi.org/10.1016/j.jksues.2018.12.002

Acta
Technica
Jaurinensis

Vol. 14, No. 1, pp. 80-103, 2021
DOI: 10.14513/actatechjaur.00565

Tutorial on the emergence of local substructure failures in the railway track structure and their renewal with existing and new methodologies

B. Eller[1], Sz. Fischer[1,*]

[1]Széchenyi István University, Department of Transport Infrastructure and Water Resources Engineering
Egyetem tér 1., 9026 Győr, Hungary
[*]e-mail: fischersz@sze.hu

Submitted: 18/09/2020; Accepted: 27/10/2020; Available online: 04/12/2020

Abstract The construction and maintenance of a railway track is an expensive process. Therefore, nowadays, except for advanced countries, considerable attention must be paid to apply the optimal maintenance of railway lines. In Hungary, until 2020 nearly 11% of railway tracks were renewed and rehabilitated from EU support, which means millions of Euros, i.e. billions of Hungarian Forints. It also follows from the support that planned preventive maintenance works must be performed on the renewed and rehabilitated lines. On the other hand, it takes away significant costs from the non-renewed (non-rehabilitated) lines maintenance works, but naturally, less money does not mean less failures, so cost-effective technologies are needed. A segment of maintenance is the local substructure problem(s). In this article, this segment will be mentioned from the development of the failures, through the applied technologies, to the possible new solutions like injection and the using of geosynthetic cementitious composite mats (so called GCCMs).

Keywords: substructure; local failure; protection layer; injection; concrete canvas

1. Introduction

The deterioration of the railway (track) is only to be shown with a genuinely complex correlation. The pressure that the loads of the railway generates is divided amongst the elements until it reaches a lower level exerted on the substructure than on the rails, for instance (Fig. 1). In conclusion, this load transfer does not inflict serious obsolescence; however, the dynamically arriving loads do. The dynamic loads can cause a slight bend even on high quality railways, both in the railway track and at its joints. That is what the saying is for: there is no such perfect track because there can be occurring problems in all kind of aspects. As the elements in the system of the railway's structure are correlating with each other, some of them even contribute in the initiation of some of its fellow's obsolescence, hence it can be seen at the term 'obsolescence' as a self-initiating exponential procedure. The load transfer can be seen in Figure 1. [1, 2].

One of the railway's cardinal spots is the substructure. When a problem occurs with the substructure it might not be only because of the load (from the vehicles and dead load), but environmental effects, like the consistence of the soil can affect it as well. Either the not properly constructed, or not of proper, materials-built support can cause some reoccurring problems in the long term and also maintaining it in some cases is nearly impossible. That is why solutions are needed, that can increase the longevity of the whole track by opting to use long lasting and appropriate supports. Problems that are only appearing at one particular spot in the railway and can be traced back to the substructure are called local substructural problems [3].

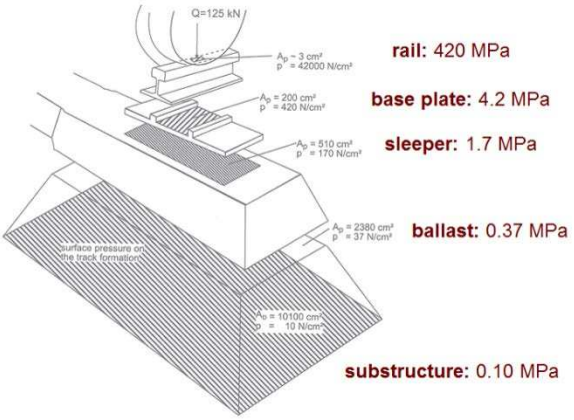

Figure 1. The load distribution in the railway superstructure based on [2]

2. Formation of local substructure failures

Speed restrictions made by problems in the railway result in the need of more dragging force in order to reattain the original velocity. This extra energy expressed monetarily is many billion Hungarian Forints annually [4], in addition to the already extent problems that are already expensive. If they increase the axle load by 2 and a half tons the extra cost would be an additional 4.2% to the maintenance fee [5]. If the substructure does not have enough load capacity and proper soil mechanical features, then soil swap or installing a defensive layer is in need. Speaking of a local substructural problem, full interference depending on access might be expensive, let alone technical barriers.

2.1. Questions of design

Functions of the railway substructure's reinforcing layers [6]:

- securing load carrying base layer for the ballast (middle layer's main task),
- preventing frost effect in the track (frost protection layer's main task),
- load distribution in the subsoil,
- making sure that the rail and its other parts provide proper flexibility,
- avoiding the blending amongst the middle layers and the ballast with the lower weaker layers,
- avoiding the blending between the anti-freeze layer and the subsoil's material (filtering layer).

A properly constructed railway embankment provides homogeneous support for the railway superstructure.

At designing a substructure for a railway, the following aspects you should consider:

- axle load,
- design velocity,
- subsoil's consistence, quality, etc.

Economically the substructure has to last at least 40 years and needs to be capable of going under maintenance any time. In Hungary, the planned nominal axle loads are mostly from 210 kN through 225 kN, whereas in other countries it can go a lot higher, even up to 360 kN in North and South America or 440 kN in Australia [7].

Speaking of track system in the aspect of continuity there are traditionally joint and also gapless tracks (CWR track that means continuously welded rail tracks). In

these cases, it is needed to create dilatative gaps accordingly to the laying rail temperature, so when it comes to colder weather the gap expands, which is succeeded by continuous dynamic additional effects towards the rails. Other solution would be a rail expansion device that is meant to operate the rail dilatation due to how its shape transforms when interacting with objects with a given rail temperature.

2.2. Reasons of emergence

Main reasons that contribute to the emergence of problems in the subgroup can be categorized into three classes [8]:

- loading factor (failures from deteriorated structure elements)
- features of the soil / and/or design / (poor quality, consistence of the soil),
- environmental factors (soil moisture content, soil temperature).

There are two types of load in the railway tracks:

- the dead load of the structure (so called static load),
- the dynamic load from the traffic/vehicle (static value + dynamic addition).

Although problems that may occur are divided into three groups, yet they appear together often, therefore every local substructural error demand to be taken seriously when investigated.

2.2.1. Loading factors

The dead load causes less amount of complications than the dynamic effects, however, when the filling has not been properly built or designed, it may inflict serious damage regarding stability or shearing. The dynamically emerging traffic load is a repeating, cyclic type of load. The effects of the static and dynamic loads differ on the lower layers, even if the axle load is the same [8, 9].

When it comes to traditional railway tracks where the joints are situated 21-24 meters apart from each other the amount of problems by dynamic collisions are occurring more often, however, the speed limit on these tracks are a lot more strict (in Hungary it is 80 km/h top). These dynamic collisions may result in some loose fastenings, a sunken substructure and even the ballast wears down a lot faster. On top of those faults/errors, there are a lot more in addition: the end of the rails can bend down. In order to recover their original shapes a particular technology has to

be used. The errors are situated according to the locations of the gaps (standard is 1 per every 24 meters) [1, 10].

Hypothetically, it is impossible that there would be a load caused by similar dynamic collisions in the tracks due to the welded rails placed in them. Nowadays there have been a couple of welding methods in use when it comes to constructing major railways [2]:

- flash butt welding (either in a welding plant or by a moving machine),
- aluminothermic welding (thermit welding or AT welding).

This is claimed to be true hypothetically, however, in practice, especially on old weldings the wear can be faster (an outcrop emerges) than on the surface of the rails. The main reason for that is that the AT (aluminothermic) welding is about the correspondence of "three different type of materials" (the two rails and the welding material), and the steel that supports the joints wears down faster than the steel that makes the rails because the former one's features are weaker. There is no publication about that, so what the authors asserted is only based on their experience. The reason why it is important to emphasize that problem is that when short-railed tracks are constructed to CWR tracks nowadays it is sure that these weldings are 24 (or 21) meters apart from each other. The outcropped weldings cause smaller but similar problems than the weldings on traditional railways. The collision is smaller, even though, these types of problems mean larger dynamic addition load at higher track velocity.

The deflection, the substructural deformations at the supporting tracks with different stiffness occur either where the bridge and the railway tracks meet (Fig. 2), or where the tunnel and the railway track join each other are making another focal spot. The stiffness of the support by the bridge abutment suddenly changes which results in the moving train accelerating vertically that generates addition-of-use in the tracks. These problems can cause serious distortion in the track geometry on tracks that were not properly constructed or are already deteriorated, additionally mudding may occur when it does not have appropriate drainage. Therefore, the main problem is from geotechnical/loading and either from structural or design causes. The primary reason why temporary tracks are needed is to reduce travel time that increases the design velocity, which results in the tendency of addition-of-use and obsolescence. [11, 12] The problem is mainly depending on the soil's factor, however, it is mainly

because of the addition-of use by the change of stiffness, therefore it goes to the loading factors when classifying.

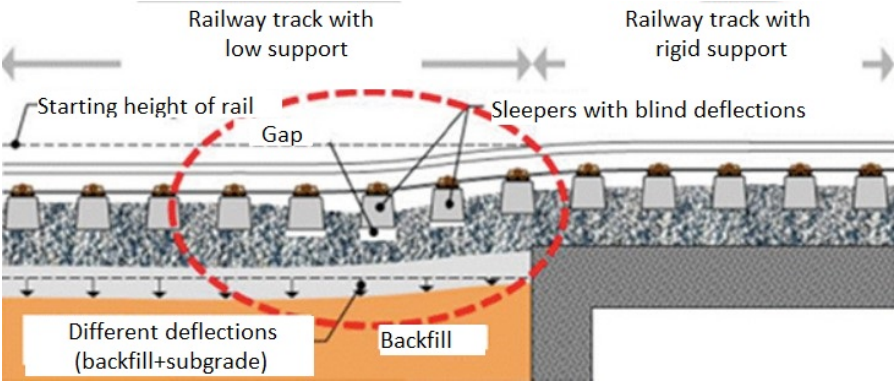

Figure 2. Track failure in the track-bridge transition zone based on [12]

2.2.2. The consistence of the substructural embankment = Soil factors

There were numerous publications conceived regarding the consistence of the embankment that have an elaborate description on the principles of design, construction, as well as maintenance in connection with geotechnics [13, 14, 15, 16]. An important thing in the railway is the proper support that can be achieved with a substructure that meets the requirements in both the aspects of compressibility and load capacity. Even if these factors are given the work is not entirely done because the drainage is still to be emphasized, moreover, the layer separation mustn't be left out either.

When a problem occurs, the soil factor means that it does not have adequate mechanical characteristics, like fine clay or mud. The change of moisture content (water content) in these types of soils usually results in expansion, so they would be a poor solution when it comes to load capacity. On top of that the previously mentioned loading factor by weak soils is significantly important because blending and compression are expectable on the surface when it is under dynamic load in such moisture content. That is why it is emphasized to apply either granular soils or complementary layers because they secure the evaporation and the drainage of the water.

The embankment's width is another factor in restricting the ballast's deformation under the vehicles' loads throughout its lifespan. In order to save money, these embankments are constructed relatively narrow with an inappropriate ratio of 1:1.5 sloping. On the other hand, there are embankments, which were constructed decades ago with a paving of lateral support that has already been either eroded, or lost. This might cause improper lateral support and excessive permanent distortion in the structure of the embankment [6]. In Hungary there has been numerous amount of precedents, where the sloping of the embankment eroded after installing a complementary layer, that later got fragmented vertically due to support deficiency. Therefore, the width of the paving decreased or got lost [17].

2.2.3. Environmental factors

As far as the ballast fragmented, got stained or due to substructural deformation the water's drainage from the surface of the substructure is not secured (Fig. 3), the muddy residue of precipitation pumps up as a result of each and every dynamic force. The soil particles are still staining the ballast and keep the water back from flowing (Fig. 4.) [18].

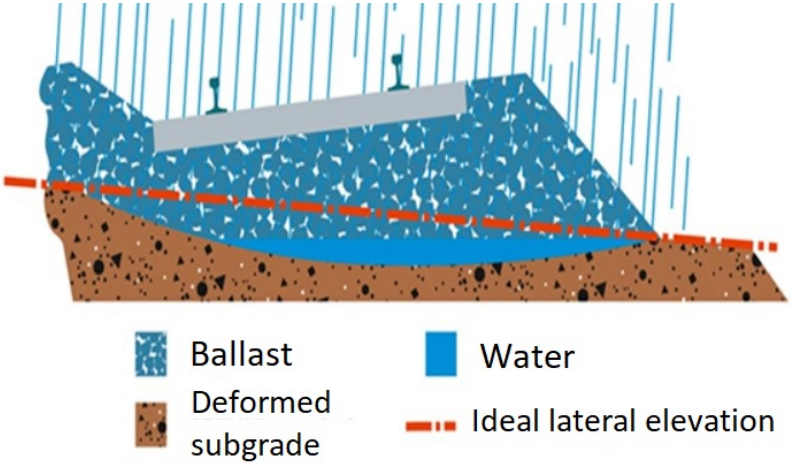

Figure 3. Dewatering is not working on the deflected substructure based on [18]

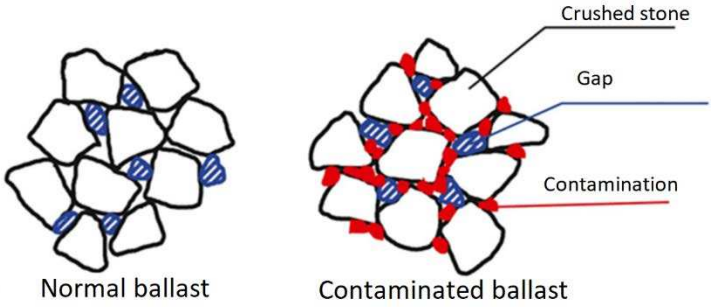

Figure 4. The contamination of the ballast based on [18]

As the soil and the ballast settle, even a couple meter deep-water pocket can emerge that is induced by the precipitation penetrating from above. The water pocket is officially defined as embankment range or deterioration form in which the stone material of the ballast and the substructure are settling due to the dynamic and/or hydraulic procedures [3]. The water pocket itself is a typical locally emerging problem, that's removal is really expensive. In the aspect of drainage, it does not matter how clear the ditch is next to the railway when it is not able to exit the railway structure as it can be seen in the Fig. 5.

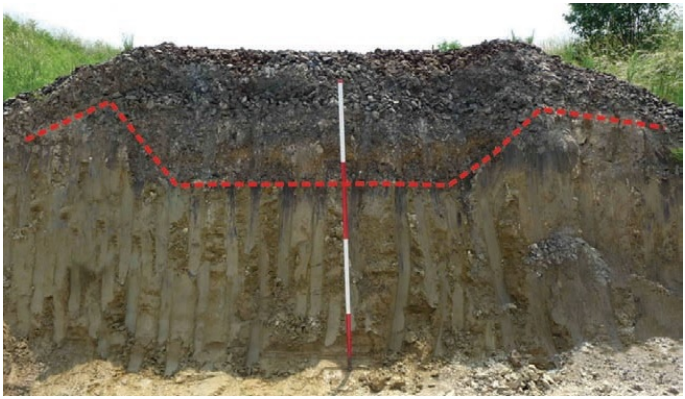

Figure 5. Water pocket in the substructure in initial stage [19]

Apparently, due to the dynamic addition loads, the ballast particles get pushed in and settle with the embankment material that was softened by precipitation and a temporary streak between the ballast and the embankment emerges where the

settlement of the materials provides a descending support in practice. In a case like this, layer separating complementary layers are to be applied.

The particles in the ballast are getting indented in a particular manner, because the position of the ballast doesn't cover the substructural embankment entirely, so the transferred load shares the mass through less amount of particles than the area of the ballast would. This is justified by the research made on the subconcrete's position [20].

Other local problem opportunity in addition is a more seldom occurring, even though there were numerous cases of substructural indentions of animal origin. Some mammals carve out tunnels in the embankment that later on collapses and causes lots of distortion in the tracks (Fig. 6.), which can only be repaired by spending a lot of money by having someone fix it with a special repairing method [21]. This type of repair is elaborated in Chapter 4.2.

Figure 6. Local substructure fault due to cavity rupture [21]

3. Diagnostics of the substructure failures

According to the new order D.5 by MÁV Zrt., the registration of local substructural problems is to be done at the annual walk-ins, while the tracing has to be constantly in progress [22]. The tracing and the evaluation is to be completed when doing the observing and the examination of subsidence under loads measured by track-geometry.

While doing track diagnostics, where small frequented, great amplitude waves emerge at a point are referring to the interruption of the substructure. Depending on this when examining diagrams these problems [23].

Thorough analysis can be done from the deflections moving spread. Those are local problems regarding railway diagnostics when among the measured railway diagnostic parameters, in a particular moment/point either of those exceeds the prescribed measuring range. A local substructural problem can be inferred when the moving standard deviation of the draft parameter differs from the surrounding values based on a graph and to a significant extent during the track diagnostic measurement. The subsidence moving spread is to be evaluated by in a mathematical way [24]. Efforts have already been made to propose the classification of value into size limits [25], but no formal size limits have been set until the writing of this article. However, as the authors wrote earlier, these procedures can only be used to infer the origin of the substructural problem. The more precise definition of the problem can be done by excavations, trenching and soil mechanical drilling.

Another accurate method for concluding is the usage of georadar (GPR-Ground Penetrating Radar). Their application has been thoroughly investigated in [26] and [27] literatures, among others. The electromagnetic shortwaves emitted by the georadar are reflected from the different dielectric layers, and thus revealing the thickness and location of the given layers (Fig. 7). The soils' dielectric constants of different qualities are determined by moisture content, soil density and structure. A further development of this became a radar-detectable geotextile to which a 20 cm wide aluminum sensor was attached. This got integrated into the railway track structure, provides better reflection of the electromagnetic signals and makes any structural deformations more detectable. The method assists with georadar tests performed in subsequent operations and provides long-term controllability [28].

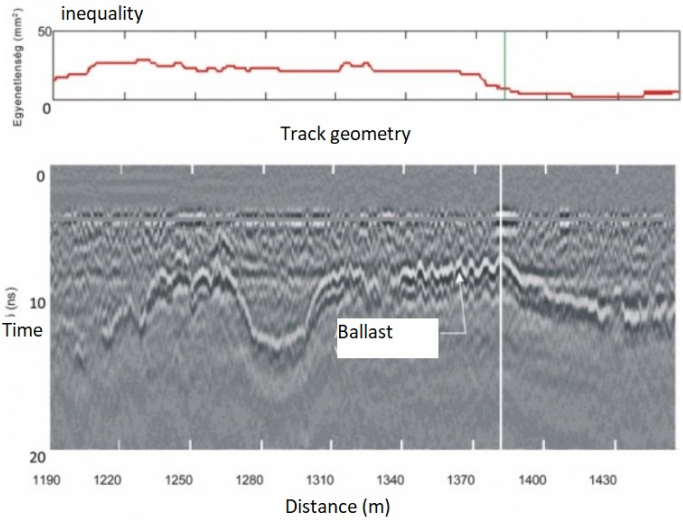

Figure 7. Evaluation of the georadar's measurement based on [28]

4. The possible renewing technologies of the local substructure failures

The authors have already written in the previous part of the article that the examination of each local substructural problem's location requires a complex task. This is really important to emphasize because it is common for certain problems to be corrected simply by ballast screening and possible trenching, and then the problem returns in several cases. Geogrid and geotextile will be installed at the same time as ballast screening. The complex test should therefore include the inspection of the drainage facilities because if the rainwater receiver is not available, the drainage will not be complete. Another problem is if the screened material is deposited directly next to the track, as water on the already contaminated material either does not flow and can leak towards the track or flow back towards the track.

4.1. Renewing by mostly used technologies

Usually, a multifunctional protective layer is built in between the ballast and the substructure crown (upper plane of the embankment). It is made up of natural and /

or artificial materials. The applied technology must be determined depending on the needed functions to be performed and the technical parameters of the used materials [9].

Generally, the following solutions are used to reinforce the structure or substructure of a railway track [3]:

- CGM1, CGM2, sandy gravel, etc .;
- soil stabilization,
- geosynthetics (geogrid, geotextile, geocomposite, etc.),
- asphalt protection layer,
- XPS extruded polystyrene slabs.

4.1.1. Coarse grained mixture (CGM)

By constructing a granular layer, the problem can be improved in the medium term. Mixtures of CGM1 and CGM2 have been transposed from the German Railway Construction Directive Ril.836 [29] into Hungarian standards [3]. The CGM1 layer is quasi-water sealing, so it can provide a suitable solution with proper drainage. The CGM2 layer functions as a load-bearing layer similarly to the CGM1 but acts as a water-permeable layer due to its particle size distribution [3]. This ability is also true for sandy gravel with the required particle size distribution. The efficiency of the latter materials in the case of water-related problems is questionable, other materials with a layer-separating role (e.g. geotextiles) can be said to be obligatory.

However, this requires a machine such as PM1000-URM [30], which is able to build in the granular layer and perform the screening process in one time. From an economic point of view, it is questionable whether the application of such a technology is necessary if the substructure faults occur only locally within just over a few hundred meters.

4.1.2. Stabilizations

The stabilization of the subgrade on the old embankment can be done with different binders and (partly) different technologies. The applicable materials depend on the soil's consistence, that can be lime, cement or chemical stabilization, and without any binder, they are so called mechanical stabilization.

For the mentioned main problem, none of the listed stabilization solutions are adequate, because there are many physically and approach aspects which needs

higher space and more technological time. Due to this, that would not be an economical and good solution to fix a local failure.

Another type of stabilization is the application of glue material in the ballast. In [31] improvement was shown at the bridge ends in terms of reduced track settlements and the stability of track surface geometry. In [32] more investigations and results were published. On the other hand, the glued ballast does not solve fully the drainage problems, thus, it is not a good solution for renewing local substructure failures.

4.1.3. Geosynthetics

From the aspect of railway construction, the following geosynthetics are used [3]:

- geotextile,
- geogrid,
- geocomposite,
- geomembrane.

The primary aspect of renewing local substructure failures is the good drainage, the full covering of a water-sensitive embankment, and the prevention of further mixing. If a geotextile is laid on a deformed surface, it will pick up the plane of the surface due to the ballast. In this case, if there is no adequate “cross-slope” on the surface, the water will seep through the geotextile and remain in the substructure in the same way.

By using the geogrid, the load bearing capacity is increased, the shear resistance in the lower part of the ballast increases and making the ballast “beam” less sensitive to deflection. However, at this solution the drainage is not solved. As a result, the “movement” (settlement) of the substructure is continuous because of the change of volume due to moisture. So highly probable, the base length of the deflection is extended in longitudinal direction.

For the reasons described above, laying a geocomposite (geogrid + geotextile) may be a sufficient solution, as it bears beneficial effects together. However, on an especially weak section, this provides only a short-term solution, because the dewatering does not work well.

The application of geomembrane can be a suitable solution as complete water exclusion can be achieved by laying it on the plane of the already reinforced substructure. By doing this, the moisture content of the water-sensitive substructure

can only be affected by the capillary water pressure. However, it should also be noted that in the case of a substructure with inadequate load capacity, if a deflection occurs, it restrains the water as a "trough".

In conclusion, geosynthetics that can be incorporated during ballast screening can provide an economically efficient solution, but a long-term solution can only be achieved by installing geomembranes that seal the substructure, and thus preventing the infiltration of precipitation and the associated volume change, siltation and crushing. However, for the reasons mentioned earlier, this would only be a suitable solution if the load capacity of the substructure is also appropriate.

4.1.4. Asphalt protection layer

The asphalt protection layer could be an excellent solution, because its separation function is perfect, while it provides significant increase in load bearing capacity. In many countries, the technology is applied in both high-speed rail traffic and on lines where higher axle loads are required due to significant freight traffic [33, 34].

However, similar to stabilizations, there are physical conditions in the approach that would not be an economical solution to renew a local failure and could only be built in inaccessible places by manual installation and compaction.

4.1.5. XPS polystyrene slabs

The advantage of extruded polystyrene slabs is that these are a highly flexible material with thermal insulation properties. It has high compressive and flexural strength. Its water uptake is negligible, which also means that its resistance to freeze-thaw cycle changes is appropriate. Aging and dry rot are not to be expected. The low dead weight and easy machinability make it suitable for use to protect the railway substructure. Experiences have shown that by modifying the screening machine during the renewing, the sandy gravel layers can be neglected, but damage can happen while laying [9]. It has been used in a few places in Hungary so far (railway line 40. between Szentlőrinc and Pécs; Budapest tramway line 1), but the experiences were adequate [2].

If polystyrene slabs were installed, the falling rainwater would be drained until there is no defect in the substructure. On the other hand, easy to imagine that the slabs could bend and break locally, then the falling rainwater collects in one smaller territory in the superstructure and the substructure is soaked at one point. For these

reasons, their installation would only be ideal if a granular layer were to be built in before laying, as a reinforcement of the railway track.

4.2. Possible new solutions

In the case of local substructure faults, optimal solutions are needed, which provides drainage on the substructure crown, give reinforcing effect, and are easy to build in. None of the listed technologies guarantee these requirements. Therefore, the application and experimentation of new technologies is justified.

4.2.1. Injection

Two types of injection methods are applied in the construction industry, "cement milk" injection and polyurethane injection. In the case of both technologies, the approach to the construction site is less of a problem, the injected substructure is sufficiently strengthened, and the drainage is also solved.

The "cement milk" injection solution is also used in China, where substructure of high-speed railways is the weak and the substructure and its foundation are strengthened with it. [35,36] The solution has also been applied in Hungary several times, including at the mentioned animal substructure fault of main line 41 in chapter 2.3.3. [21], at the reconstruction of the main line 30 at Dél-Balaton (South-Balaton) section to strengthen the backfilling of a bridge, and at the railway line 36 to locally strengthen some sections. Based on short-term experience, the solutions proved to be appropriate. The disadvantage of the technology is that the amount of the required material is unpredictable. On the other hand, rigid points can be developed, which can be followed by failures at the transition sections, like at the already explained.

The injection of polyurethane foam into the railway substructure has been studied in [37], and the injection of ballast has been discussed inter alia in [38] (Fig. 8). The theory of the installation is the same as for the injection of "cement milk", but while the "cement milk" solidifies, the polyurethane foam (RPF) expands, thus filling the pores, narrow gaps.

Therefore, the injection reinforcement causes a long-term increase in load capacity, improves the properties of the substructure, and fills the pores thus reducing the water absorption capacity/possibility of the railway substructure material. The solution could be cost-effective and would provide an additional tool for railway maintenance by demonstrating its impact.

Figure 8. Injectioned ballast bed sample [38]

Due to the disadvantages of the technology, it may be risky to install on higher speed railway lines, but on those inferior railway lines where the problem is serious, but because of the underutilization and other reasons, it would be a waste of money to spend, these solutions could be good maintenance options.

4.2.2. Geosynthetic cementitious composite mats (GCCMs)

This technology has entered into the construction industry in the last decade. By building in it, mainly layer separation and drainage problems can be solved. These materials are cement impregnated fabrics that would harden when they are being hydrated with water, thus, providing high rigidity and strength [39,40]. GCCM is commonly applied as an alternative solution of shotcrete [40]. Several variants were invented, however, the most effective solution proved to be a cementitious material impregnated between two layers of geotextile, thus forming a "sandwich" structure. The upper geotextile is non-woven, while the lower is of the woven type. Its installation does not require serious expertise, and transportation to difficult places is also easier.

Among the mentioned products, one of the most promising one is Concrete Canvas (CC) (Fig. 9). The upper fibrous fabric and the lower PVC waterproofing layer are connected by a 3D fiber matrix, and a special cement mixture is filled between the two layers [41]. According to official data scripts, the compressive strength of the hardened concrete slab is 80 MPa after a setting time of 28 days. Its 80% (but at least 50 MPa) is reached 24 hours after hydration. After bonding, the fiber structure

strengthens the concrete, avoiding cracking. Its lifespan is roughly 50 years [42]. Its effectiveness has been presented in several case studies [41].

Figure 9. Installing of CC for experimental mobile building foundation [43]

The material can be built in easier by hand or machine when a local substructure failure is being renewed, because the material is delivered in scrolled up formation like geosynthetics, so the screening machine can pull it in under the ballast bed. Based on the authors' theory, CC conforms to the bending (settlement) and deformations of the terrain (Fig. 10). If the cement in the layer is bonded only after the ballast has been screened, the rigid layer will be deformed, while suiting to the shape of the ballast bed particles, to some extent. Due to this, it can be assumed that in this way, compared to the application of geogrids, some amount of "interlocking" effect is created. Thanks to this, the internal shear resistance of the ballast increases at the lower part of the thickness. [4, 44]

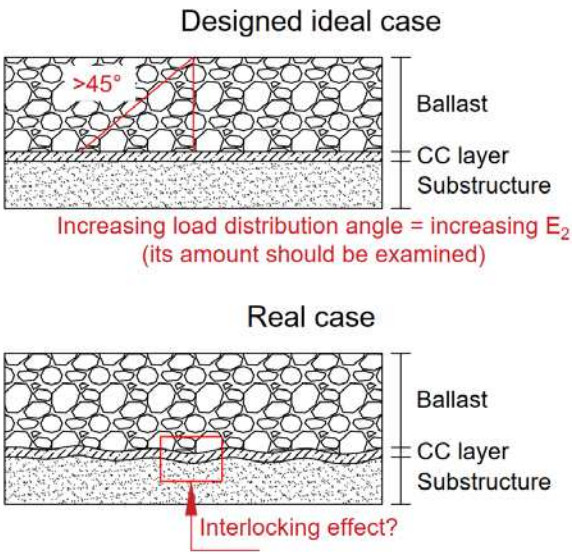

Figure 10. Laying of CC on the substructure crown while ballast screening [44]

To connect the main topic, with usage of the cementitious geosynthetic composite mats the local substructure failures can be improved with good chance. Thanks to the ability of the adequate dewatering, the substructure's water supply from the weather is nearly ended, the rigid layer can give more stability to the track structure, and the built in is easier, more cost efficient.

The authors still have to investigate its behavior in the railway track structure (especially the effect of the dynamical loads), but direction of the research can be assessed as good.

4.2.3. Other technologies

Few years ago, the Hungarian State Railways (MÁV) worked on a project, which wanted to develop a mobile screening technology. The base of this idea is the application of the amphibian mobile vehicles. Unfortunately, the project has been paused before time.

5. Summary

In this paper the factors were showed, which can cause local substructure failures, and the applied diagnostic methods in Hungary. The railway protection layers were also showed which are capable for railway structures, and these were analyzed from the aspect of the improvement of the local failures. Summarized the material properties, the functions and the experiences, it was cleared that the often-used technologies do not give cost efficiently improving solution for local substructure problems.

To be able to solve this problem, the authors investigated the built-in eligibility of the mentioned new technologies. The injection technologies are not new solutions, there are many foreign and home experiences to show. Next to this technology, the cementitious geosynthetic composite mats could be potential key, because thanks to the materials properties and the experiences are deservedly thought it could give cost efficiently improving manner for the mentioned local problems. The authors are working to verify this.

Acknowledgements

The paper was written with the support of the project titled "Internationalisation, initiatives to establish a new source of researchers and graduates and development of knowledge and technological transfer as instruments of intelligent specialisations at Széchenyi István University" (project number: EFOP-3.6.1-16-2016-00017).

References

[1] MÁV, Railway construction and railway maintenance Vol. 1-2. Mezei, I., Horváth, F. (eds.), Magyar Államvasutak Rt., (1999), in Hungarian.

[2] Sz. Fischer, B. Eller et al., Railway construction, Universitas-Győr Nonprofit Kft., Győr, 2015.
URL
https://www.researchgate.net/publication/282246421_Railway_construction

[3] MÁV, D.11 Regulation: Design, construction, maintenance and renewing of railway substructures. Vol. 1., MÁV, Budapest, 2014, in Hungarian.

[4] Sz. Fischer, Investigation of railway track geometry stabilization effects of geogrid layers under ballast bed PhD Thesis. Széchenyi István University, Győr, 2012, 148 p. in Hungarian.
doi: https://doi.org/10.13140/RG.2.1.4958.9921

[5] D. Larsson, A Study of the Track Degradation Process Related to Changes in Railway Traffic. PhD Thesis, Luleå University of Technology, Luleå, 2014.
URL https://www.dissertations.se/dissertation/bec6dd1fd0/

[6] A. Nurmikolu, P. Kolisoja, Extruded polystyrene (XPS) foam frost insulation boards in railway structures. 16th International Conference on Soil Mechanics and Geotechnical Engineering, Osaka, 2005, pp. 1761–1764.
doi: https://doi.org/10.3233/978-1-61499-656-9-1761

[7] M. D. Roney, Heavy Hauling: A Worldwide Update and Highlights from IHHA2015. Heavy Haul Seminar WRI2016, 2016
URL https://www.wheel-rail-seminars.com/archives/2016/hh-papers/HH%2002%20Highlights%20of%20IHHA2015.pdf

[8] D. Li, E. T. Selig, Evaluation of Railway Subgrade Problems. Transportation research Record 1489 (1995), pp. 17–25.
URL
http://onlinepubs.trb.org/Onlinepubs/trr/1995/1489/1489-003.pdf

[9] B. Eller, Sz. Fischer, Review of the modern ballasted railway tracks' substructure and further investigations, *Nauka ta Progres Transportu* 84 (6) (2019) pp. 72–85.
doi: https://doi.org/10.15802/stp2019/195831

[10] S. Kaewunruen, C. Chiengson, Railway track inspection and maintenance priorities due to dynamic coupling effects of dipped rails and differential track settlements. *Engineering Failure Analysis* 93 (2018), pp. 157–171.
doi: 10.1016/j.engfailanal.2018.07.009

[11] F. Horvát, E. Koch et al. Establishment of transitional sections between a bridge and railway track. *Sínek Világa* 60 (4-5) (2018). pp. 89–97, in Hungarian.

[12] E. Koch, Geotechnical impact assessment of bridge construction schedule, *Sínek Világa* 61 (3) (2019) pp. 9–17, in Hungarian.

[13] E. T. Selig, J. M. Waters, Track geotechnology and substructure management, Thomas Telford Publications, London, 1994.

[14] B. Indraratna, W. Sahim et al., Advanced Rail Geotechnology – Ballasted Track, Professional book, Taylor & Francis Group, London, 2011.

[15] E. T. Selig, D. D. Cantrell, Track Substructure Maintenace – From Theory to Practice. American Railway Engineering and Maintenance-of-Way Association Annual Conference, Chicago, Illinois, 2001

[16] B. Indraratna, J. Chu et al., Ground Improvement Case Histories: Compaction, Butterworth-Heinemann, Grouting and Geosynthetics, Oxford, 2015.

[17] B. Eller, Efficiency of the asphalt protection layer, cataloguing of its failures and technological suggestion for the renewing of the Dombóvár- Godisa railway track section, MSc Thesis, Széchenyi István University, 2016, in Hungarian

[18] N. Waldhör, As you make your bed so you must lie on it, *Innorail Magazin* 2 (1) (2015) pp. 48–52, in Hungarian.

[19] O. Szengofszky, How to terminate the velocity limits. *Sínek Világa* 56 (3) (2014) pp. 37–39, in Hungarian.

[20] V. Sárik, Examination of railway under-sleeper pads, Scientific Student Work, University of Technology and Economics of Budapest, 2014, in Hungarian.

[21] I. Simon, B. Eller, Mammals in the railway substructure, *Sínek Világa* 61 (2) (2019) pp. 25–28, in Hungarian.

[22] MÁV, D.5 Regulation: Track maintenance, MÁV, Budapest, 2017, in Hungarian.

[23] I. Zobory, Dynamics - measurement - qualification of the railway track-vehicle system, *Közlekedéstudományi Szemle* 65 (1) (2015) pp. 6–19, in Hungarian

[24] Cs. Ágh, Modern methods of examining railway tracks, *Military Technical Bulletin* 29 (2019) pp. 219–230, in Hungarian.
doi: https://doi.org/10.32562/mkk.2019.1.18

[25] D. Krózser, Proposing the size limit of the standard deviation-based track geometry parameter, MSc Thesis, Széchenyi István University, 2019, in Hungarian.

[26] J. Hugenschmidt, Railway track inspection using GPR. *Journal of Applied Geophysics* 43 (2-4) (2000) pp. 147–155.
doi: https://doi.org/10.1016/s0926-9851(99)00054-3

[27] R. M. Narayanan, J. W. Jakub et al., Railroad track modulus estimation using ground penetrating radar measurements. *NDT and E International* 37 (2) (2004) pp. 141–151.
doi: https://doi.org/10.1016/j.ndteint.2003.05.003

[28] E. Gönczi, Application of radar detected geotextile in Hungarian. *Sínek Világa* 56 (3) (2014) pp. 21–24, in Hungarian.

[29] DB, Ril. 836: Earthwork and special geotechnic structures, design, construction and maintenance ("Erdbauwerke und sonstige geotechnische Bauwerke planen, bauen und instand halten"), in German.
URL https://dvlv.eu/interessante-links/db-dokumente/

[30] Plasser & Theurer webpage [cited 2020-07-06].
URL https://www.plassertheurer.com/en/machines-systems/formation-rehabilitation-pm-1000-urm.html

[31] S. Kaewunruen, Dynamic responses of railway bridge ends: A systems performance improvement by application of ballast glue/bond. Massachusetts Institute of Technology, 2014
URL http://works.bepress.com/sakdirat_kaewunruen/46/

[32] J. Szabó, Investigation and analysis of the behavior of ballasted railway superstructure stabilized with bed gluing technology on static and dynamic loads. PhD Thesis. University of Technology and Economics of Budapest, 2011, in Hungarian.
URL https://repozitorium.omikk.bme.hu/handle/10890/5597

[33] J. Rose, P. Teixeira et al., International design practices, applications, and performances of asphalt/bituminous railway trackbeds, GeoRail 2011 International, Paris, 2011.
URL
https://web.engr.uky.edu/~jrose/papers/GeoRail%202011%20International.pdf

[34] J. Rose, P. Teixeira et al., Utilization of asphalt/bituminous layers and coatings in railway trackbeds – a compendium of international applications, Joint Rail Conference, Urbana, Illinois, 2010
URL
https://web.engr.uky.edu/~jrose/papers/JRC_2010_International.pdf

[35] Y. Tan, Research on Application of Cement Mortar Pile in Reinforcing Soft Foundation of High-speed Railway, *Journal of Railway Engineering Society* 2010 (10) (2010).
URL https://en.cnki.com.cn/Article_en/CJFDTotal-TDGC201010006.htm

[36] S. Li, The application of cement injection pile in soft soil foundation reinforcement of existing railway line, *Shanxi Architecture* 2007 (8) 2007.
URL https://en.cnki.com.cn/Article_en/CJFDTotal-JZSX200708071.htm

[37] B. J. Warren, Field application of expanding rigid polyurethane stabilization of railway track substructure, MSc Thesis, University of Wisconsin-Madison, 2015.
URL https://minds.wisconsin.edu/handle/1793/72861

[38] A. Keene, J. M. Tinjum et al., Mechanical Properties of Polyurethane-Stabilized Ballast, *Geotechnical Engineering Journal of the SEAGS & AGSSEA* 45 (1) (2015) pp.67–73.
URL
https://www.researchgate.net/publication/273958170_Mechanical_Properties_of_Polyurethane-Stabilized_Ballast

[39] T. Jirawattanasomkul, N. Kongwang et al., Finite element analysis of tensile and puncture behaviours of geosynthetic cementitious composite mat (GCCM). *Composites Part B* 154 (2018) pp. 33–42.
doi: https://doi.org/10.1016/j.compositesb.2019.02.037

[40] P. Jongvivatsakul, T. Ramdit et al., Experimental investigation on mechanical properties of geosynthetic cementitious composite mat (GCCM). *Construction and Building Materials* 166 (2019) pp. 956–965.
doi: https://doi.org/10.1016/j.conbuildmat.2018.01.185

[41] Concrete Canvas Ltd. [cited 2020-09-15].
URL https://www.concretecanvas.com

[42] H. Li, H. Chen et al.,. Application design of concrete canvas (CC) in soil reinforced structure. *Geotextiles and Geomembranes* 44 (2016) pp.557–567. doi: https://doi.org/10.1016/j.geotexmem.2016.03.003

[43] Trackway Trial: Melk, Austria (2011) Case Studies of CC. [cited 2020-06-15].
URL https://www.concretecanvas.com

[44] B. Eller, Sz. Fischer, New possibilities of application of geosynthetic cementitious composite mats (GCCM) in railway substructure, Transport Science Conference, Győr, 2020, (accepted manuscript) in Hungarian.
URL
https://www.researchgate.net/publication/339366238_New_application_possibilities_of_geosynthetic_cementious_composite_mat_layers_for_railway_substructure_in_Hungarian_-_Betonpaplan_reteg_ujfajta_alkalmazasi_lehetosegei_a_vasuti_alepitmenyben

Acta
Technica
Jaurinensis

Vol. 14, No. 1, p. 104-122, 2021
DOI: 10.14513/actatechjaur.00569

Tutorial on the fragmentation of the railway ballast particles and calibration methods in discrete element modelling

E. Juhász[1], Sz. Fischer[1,*]

[1]Széchenyi István University, Department of Transport Infrastructure and Water Resources Engineering
Egyetem tér 1, 9026 Győr, Hungary
[*]e-mail: fischersz@sze.hu

Submitted: 23/11/2020; Accepted: 01/02/2021; Published online: 05/02/2021

Abstract: This paper presents a short literature review related to the fragmentation of the railway crushed ballast particles. With the help of the processed articles with the main topic of discrete element modelling (DEM) we aim to provide some insight into the international achievements and forward progress of the subject. Rock materials as granular elements can be investigated from several perspectives. The elements can be examined in laboratory conditions purely from the quarry, or even by obtaining already fragmented particles from the real railway tracks. In addition, DEM models can be created by using computer software. This article tackles only a small segment of the literature. Though each DEM topic was unique, they all involved examination of degradation of particles in some way. This review focuses on model building, including particle construction and calibration. The selected publications do not cover the current state of the entire DEM research related to ballast degradation.

Keywords: *ballast; degradation; DEM modelling*

1. Introduction

Railroads ensure the biggest network for quick and secure, public and freight transportation on rails over the world [1].

Ballast bed is one of the most important railway track structural elements; it is composed of (mainly deep magmatic) rock particles built-in beneath the railway track, i.e. crossties (sleepers) and rails [2]. The aim of ballast is to ensure water drainage (dewatering) and structural support against loading due to railway vehicles, i.e. trains. Base rock type, rock quality, particle size distribution (i.e., gradation), as well as grain shape are the main characteristics of railway ballast materials that have to be considered during design process. Hard and strong ballast aggregates with preferable shape characteristics, i.e., angular 'stones', are high-priority for adequate strength and stability [3].

Railway ballast aggregates regularly consist of dolomite, rhyolite, andesite, gneiss, basalt, granite and also quartzite [4]; and they include medium to coarse gravel sized grains (i.e., 10-60 mm) with a lower quantity of pebble-sized grains [5, 6]. Good quality ballast material must contain angular grains, a high density, high shear strength, high persistence and hardness, high resistance against weathering, a rough surface, and a minimum of hairline cracks inside [7, 8]. The most important roles of ballast materials are to distribute and reduce forces affecting sleepers, provide horizontal resistance, and ensure quick dewatering. Ballast for high loads and stability must be angular, well graded, and dense (i.e., well compacted), but this structure hinders drainage [1].

The form of the particles keeps changing: the corners and edges brake from the particles and fine particles are modified, the result is a reduction of track quality (structural as well as geometrical). Finally, ballast screening and/or replacement will be required [9].

The railway track with all of its elements becomes continuously obsolete during usage. In addition to increasingly noticeable signs of slow failure on track elements, e.g., wear of rails, muddy area, etc. it is important to examine the causes of each problem and draw conclusions about the life expectancy associated with the causes and their prevention. Many authors around the world are concerned with the obsolescence of railway tracks, including degradation of ballast bed.

On a daily basis, more and more papers appear on the topic that help a lot in the research of the authors who concern similar research topic all over the world.

Articles on various topics mainly include the construction of new DEM models and the results of the running.

These will not be covered in these articles, because they have been presented in several of our previous publications, but the following factors also influence the ballast degradation:

- strength, hardness and durability of the grains,

- density, and water absorption of the grains,
- the PSD (particle size distribution) of the particles,
- formal properties (which kind of particle form is dominant in the sets).

Naturally, a lot of other factors affect the lifetime of railway ballast beds, which are also at least as important as the DEM, but they cannot be completely modelled by using the DEM software.

The listed properties connect to the ballast grain form. Similar results can be achieved in literature published on granular materials, e.g., sand or concrete mixtures. Morphology as well as degradation are the most important factors to determine the deformation of railway ballast beds. However, these two factors can (and should) be examined in a number of ways, for which computer software is not necessarily the most ideal.

2. Discrete Element Modelling (DEM)

The DEM method is applied to model granular materials. This kind of computer-based simulation allows to virtually track the behaviour of the particles in the aggregate. Behaviour of the aggregate as a whole set is greatly influenced by the behaviour of the individual particles. With the help of this method, it is possible to take into account the element shape, which could be also one the most important physical parameters of the aggregate, and to determine the physical parameters of the model. When judging behaviour, it is necessary to simulate the element shape [10-16].

2.1. Review of calibration approaches

For model, exact prognoses can only be obtained if the values of the input parameters are precisely calibrated. All authors publishing on the topic apply various ways and methods to calibrate or determine the values of the parameters, however, relatively few authors have focused on improving and validating them [10].

There are two approaches in the literature for calibrating the input DEM parameters. The first way is to apply a method in which field tests or lab tests are executed to determine the main properties of a given substance. The test is then repeated numerically, with the parameters and results of lab and in situ test settings and procedures with the most accurate way [10].

The values of the DEM parameter are later iteratively modified until the expected mass ‘reaction’ is equal to the previously recorded one(s). A probable issue with this method is the mass ‘reaction’ of a numerical test may be affected by more than one parameter. This means: no individual solution is available because more than one

combo of parameter values will occur in the same macro-mechanical behaviour. In this case, there is no guarantee that if the material is calibrated for one purpose, it will be exact and precise for the other one [10].

DEM models have been improved by presenting physical explanation to the parameters, but if this method is applied, the physical content of the parameters may be lost to some range [10].

2.2. Modelling of element shape and size

The particle size and shape distribution needs to be also taken into account as input parameters. Particle shape is one of the most relevant parameters to consider in DEM and must be precisely recorded if DEM is to be applied as a prognostic 'device'.

In nearly all DEM software, sphere-shaped (circles in 2D) elements are promoted because the contact is perceptible with efficiency and there is no need to determine the orientation of the particles. However, when spherical particles are used, the mass (inner) frictional or shear strength of the assembly is regularly set too low against the true particulate material [11]. The shear strength can be developed in several ways: using non-spherical particles, and/or by applying contact rolling friction [11, 12, 13]. Among many other constitutive laws, for example rolling friction straightly limits the rotation of the elements by using a moment that resists rotation [11].

By increasing the particles' interlocking effect, non-spherical particles achieve this indirectly [14]. Particle rotation influences not only shear strength but also the expansion and localization of shear belts, so this parameter is not negligible [15].

Zhou et al. [15] compared 2D circular particles (disks) in detail against friction (i.e., rolling one) with non-spherical particles (nodules) without friction and stated that these two anti-rotation workings affected the macroscopic and microscopic action of particles [10].

2.2.1. Shape of the particles

Several parameters are important during the designing of the model, such as the shape modelling method, the usage, and the modelled particles. Nevertheless, it should be noted that the emphasis is on modelling the shape of the particles, combined with calibration steps, validating, and sensitivity phases, and not on the computative equations or formulas of various shape simulation methodologies [16].

Shapes experienced during the classification of the particles in ballast sets like flaky, rod-like and compact are also important types. To define the forms (morphology) several parameters need to be taken into consideration as follows: axis lengths, perimeter, volume, surface, etc. Furthermore, when the particles are

designed roundness also matters. The surface of each particle can also be made up of polygons in DEM software in which a generalized version of the so-called area-weighted fabric tensor has been applied to a smooth surface. The tensor has several advantages over bounding box methods and based on the three eigenvalues of the tensor, the characteristics were proposed to serve classification. [17, 18]

Angularity of particles is a main shape parameter that influences the mechanical characteristics (micro as well as macro ones) of particulate materials. Nearly all the actual particle angularity methodologies are founded on two-dimensional methods using grain predictions [16].

When analysing the particle shape, parameters are categorised into 3 groups: form, roundness and roughness. These are shown in *Fig. 1.*

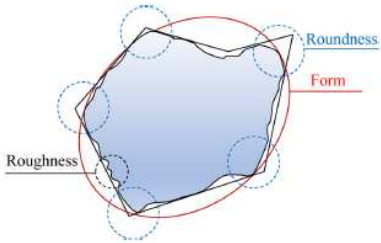

Figure 1. Presentation of the difference parameters [16]

According to some authors, the key to angularity is to identify the corner. The angle is defined by examination in contrast to the curvature of the grain face with the maximum inscribed circle (in three-dimensional cases: the maximum inscribed sphere, ball). The curvature of the grain face becomes one of the most relevant necessity for both edge/corner identification and angularity assessment [16].

Edge/corner identification process created on the scheduled interpretation (three-dimensional mode of Wadell's definition):

- reconstructs the surface of the particle using a triangular mesh,
- calculates the local curvature of all vertices on the reconstructed surface,
- check that the vertex meets both the curvature and the associated relative conditions
- the vertex is considered to be a vertex,
- the corner vertices and the vertices within the single ring are defined as corner portions [16].

A new 3D particle angularity estimation method is proposed for triangle mesh three-dimensional particle models. First, the edges (corners) of the particle are referred by admitting the concepts of surface curvature and relative related area. The sphere is then evaluated with a ball filling approach. With respect to edge/corner identification, the concept of RSt (Ci) relative related area has been shown to adequately differentiate between angularity and confined features, allowing the expected methodology to reject confined high curvature features and thereby necessarily improve its certainty. To test the dependability of the proposed method, three-dimensional elements were generated from the 2-contour by application of an amorphological preservation principle [16].

There are plenty of methods to describing particles, only one source document contains 42 different quantities and their interpretation, usability, and practical application which are adaptable to research. These descriptions could be categorized qualitative or quantitative. [17]

2.3. Comparison of 2D and 3D angularity

The outcomes of the expected methodology are consistent with the outcomes of the corresponding 2D contour. In addition, the proposed method is examined in contrast with other three-dimensional angularity estimation methodologies, and the outcome looks promising. The advantage of the expected methodology is that its computation is not affected by subjective factors such as projective direction, optic contrasting, or non-objectively collected corner sections.

In addition, the expected methodology can be used to various particle models. The main goal of the expected methodology is to help engineers and scientists investigate the relationships between particle angularity and the mechanic behaviour of granular materials.

Two disadvantages need to be optimized in this regard:

a) accuracy of the assessment is affected by the curvature assessment algorithm performed. To be able to lower this effect, a high density triagonal mesh has to be used, that will increase the time-consumption of the calculation.

b) when applying the ball filling methodology, a high density ball assembly is needed to derive adequate corner spheres for accurate angularity estimation and thus increase the calculation effort.

The expected methodology is going to be farther optimized in the future. Future investigation will focus on combining this methodology with other DEM programs,

such as the Particle Flow Code (PFC), to study whether the characteristics of particulate matter are affected by particle morphology [19].

2.4. Particle generation with clumping

There are several available programs, e.g. PFC [20], EDEM Simulation [21], Yade-DEM [22], etc., which have already been presented by the authors in their previous publications [10]. Some of these software are very costly, the others can be regulated by very complicated form. The authors applied PFC^{3D} software to build and run their model. The test bases are quite analogous, in this way in the first step the authors found PFC^{3D} 4.0 adequate for "testing" DEM and are familiar with this methodology. As the modelling of granular materials (i.e., railway ballast) as balls showed non-correct behaviour (singularities in the computations), the application of clusters was necessary in order to achieve more realistic outcome. [23].

The model was approximated based on an existing laboratory examination, which are shown in *Fig. 2* and *Fig. 3.*

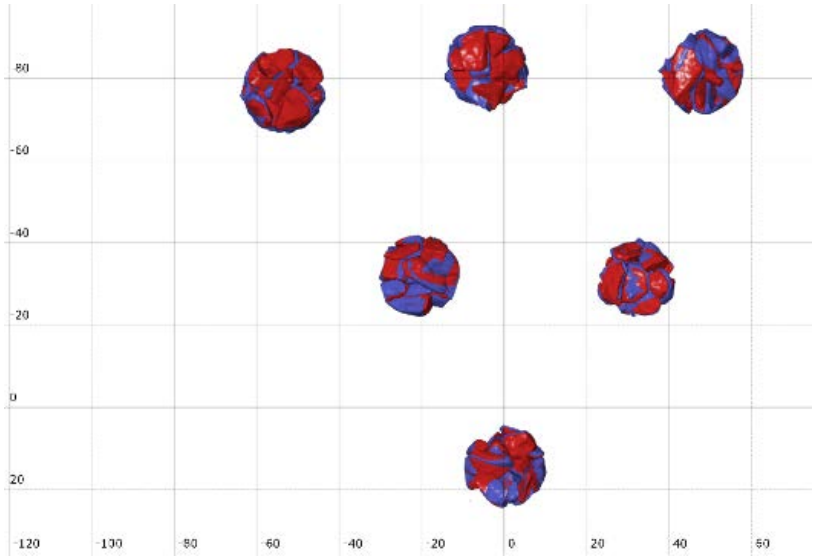

Figure 2. CT scans from the uniaxial compression tests with granules 4/8 mm material (top view) – red colour for before load and blue colour for after load [23]

Figure 3. The laboratory test assembly [23]

The images after the model and the load steps are shown below on *Fig. 4.*

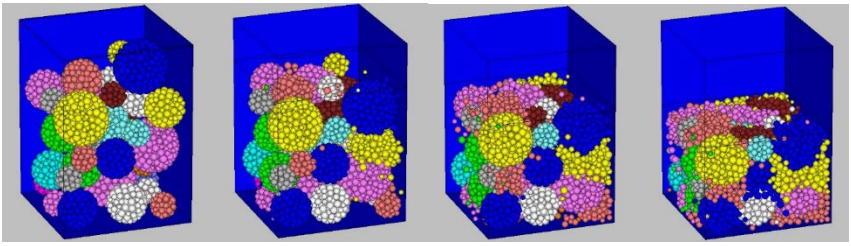

Figure 4. The gradual compression, in which the macroparticles are reduced to microparticles [23]

Scientists can model grains more realistically by creating polyhedral shaped elements. They can be created manually or randomly (e.g., with 3D scanner, shown in *Fig. 5.*), estimating the geometry of rocks. An entire set of individual elements can be assembled. Individual grains can be formed both randomly and manually, with significant similarity observed. The average number of vertices and sides and the size of the areas and angles were approximately the same. In random form, the particles are formed from convex polyhedrons. It is simple to detect concave regions on the face of particles that are points with stress concentration [24].

Figure 5. Digitizing a particle using 3D scanner [24]

A complete set of individual elements was created and loaded through a top plate. The plate moves down with constant velocity.

During the time period, the particles are able to move simply due to the high porosity of the sample. The lower the porosity, the less space the elements have for moving, and with this in parallel the percentage of breakage "action" is higher. During the unloading period, the forces (normal direction) decrease to null. Breakage can result peak values in forces that disappear in a few timesteps and they do not have relevant effect on the loading mechanism [24].

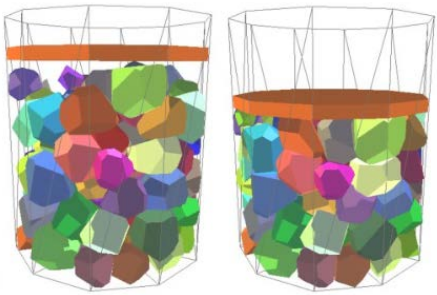

Figure 6. Loading a set of polyhedral individual particles in a vessel Left: Before load condition of the assembled model, Right: After load condition of the assembled model [25]

The model showed results close to reality and shown in *Fig. 6* [25].

An assembly of ballast grains of unconventional shapes was taken into account and the angularity of the particles was simulated by grains: 2…9 regular (circle) grains were applied to formulate single grains of 12 various volumes. The grains are generated into random places. The assembly was calculated by PFC^{2D} (3.1), and the forces in the contacts were considered by gravity and compaction [26].

Using grains in the software, an initial analysis was made applying four various grain shapes (*Fig. 7*). Taking into account various value of radius of the component circle disks, the dimension of the grains was also modified to create the assembly of a requested grain size distribution. The grain generation in the PFC software can be

of random or fixed sizes. In this research, the grain sizes were 19…53 mm. A box with dimensions 300×600 mm was used.

Railway ballast material needs be considered according to their particle size distribution (PSD), with random manner (*Fig. 8*) [26].

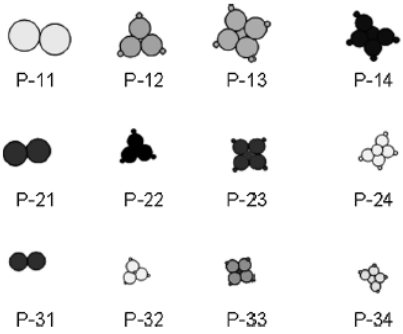

Figure 7. Particle sizes and shapes considered in the numerical modelling [26]

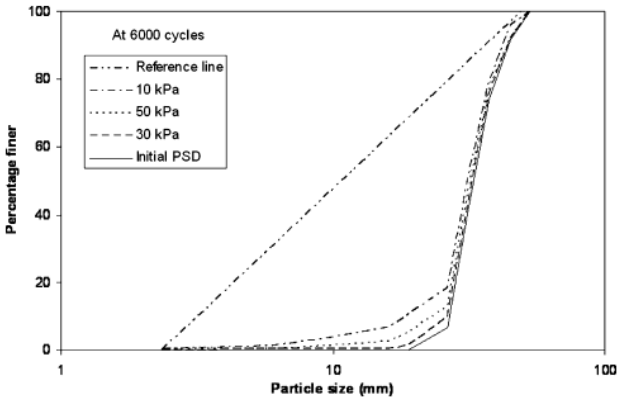

Figure 8. PSD at different confining pressure [26]

A cyclic loading analysis was executed for non-spherical grains. Relative low confining stress values were applied (10, 30, as well as 50 kPa) in accordance with real circumstances. The PSD at different confining pressure is shown in *Fig 8*. The generated assembly of non-spherical grains under and after breakage can be seen in *Fig. 9.*

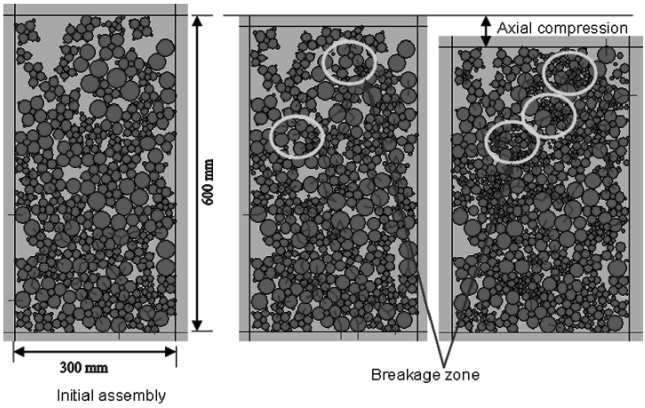

Figure 9. Some shots of assembly deformation including breakage [26]

In case the axial strain is higher than 4%, dilatation of the grains can be discovered, because at low confining stress value (e.g., 5-10 kPa), high dilatation and breakage are referred primarily to the shearing and depreciation of angular projections regarding the significant high axial and radial strains [26]. The results are in accordance with experiments [26].

Higher degradation is obtained at a lower confining stress (i.e., 10 kPa). This trend is also similar to that of the results of esteemed authors. It was mentioned that at quite low confining stresses (and at places with the higher dilatation), grain degradation arisen primarily in this dilatation area, and it is only at much higher confining stress (σ_3=50 kPa) that degradation developed under compression [26].

2.5. Numerical investigation of the material and tamping

Ballast breakage and irrecoverable malformation (defect) occurred in ballasted tracks in case of high-speed and heavy loading railway vehicles. With EDEM 2.4. software, the authors documented a new numerical research of bulk material dynamics and the transient impaction of a system of non-regular polyhedral grains enclosed with a brick-shape box with a retaining wall applying them to simulate and model cyclic tamping. Ball packing methodology was used to simulate conventional real-size ballast grains. The methodology aimed to establish firm-soft coupling particle-flow tamping operation simulation numerical model based on contact dynamics theory.

Authors both introduced the contact dynamics (CD) methodology with both balls and also grains of balls. EDEM program can be applied for assembly of grains modelling and firm-soft coupling particle-flow tamping operation numerical model.

They apply the ball grains stacking methodology to simulate the common grain model in EDEM program, which are shown in *Fig. 10*.

Figure 10. The particle models [27]

The main work when creating the system model included two parts and are shown in *Fig. 11.*:

- created a tamping bank 3D model
- choosing a track section unit with 3 ties as tamping simulation area and confine a particle factory with rectangular section in EDEM.

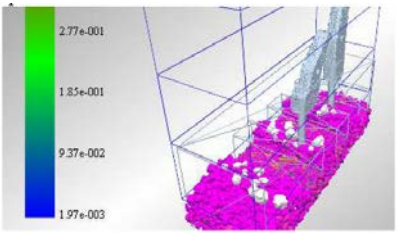

Figure 11. Simulation results of an assembled model in EDEM from tamping vibration [27]

Tamping hammers infiltrate into the ballast and press the grains under the ties in tamping cycle (the time consumption of one cycle is approximately 4 secs, the whole process contains 10 cycles). In reality, ties are buried on more than 15 cm depth general under the ballast track, but in the simulations a tie is on the top of the ballast [27].

The ball clump methodology is the basis grain modelling for DEM, i.e., ballast breakage during dynamic loadings. The simulation of this methodology illustrates the compression pressure during the cycle(s) and the local points of the railway track where the pressure is applied. Holding the purpose in sight, all of the transport modes and their specialities, and also to meet the increasing demand of public and freight transport, railway has a big challenge to develop the efficiency and lower its costs (maintenance, infrastructure). [28, 29].

2.6. Summary of recent results

Granular materials like railway ballast have plastic deformation caused by traffic load. DEM method can help reduce the rate of ballast bed obsolescence by creating simulations. This can also be used to reduce maintenance costs. DEM simulation has already been created for box tests with different layered ballast sets built up from clumps of particle shape. The displacements of the particles under the sleepers can be examined. [30]

Some studies suggest an analysis method for the interaction of the ballast and wheel based on DEM. Finite-element analysis (FEA) cannot be used for analysing track ballast because it consists of small separable particles. In contrast, other authors used the finite element method (FEM) to model and simulate the ballasted track for its reliability and convenience. Using the conventional FEM approach, the ballast is modelled as a shell or solid element, with the same material properties as the gravel layers in the two- or three-dimensional range. [31]

With the well-known Itasca PFC^{3D} software a series of DEM models were created. The set of the ballast was created from particles by clumping around 100 spheres together. The authors examined their macro- and microscopic performance by shearing with four different loads. Complex calibration procedures were performed to operate the simulations. [32]

Related to discrete element simulations, a lot of laboratory or field tests have to be conducted [33-37], these articles deal with the ballast, ballasted tracks as well as track-vehicle interaction. These kind of models can be simulated in sophisticated computer programs. To be able to achieve it, the micro- and macromechanical parameters have to be determined, after that calibration and validation of the model should be performed. A well-calibrated and validated model is suitable for calculation of special behaviour of ballast as well as ballasted tracks, e.g. stresses, strains, deformation, settlements, particle breakage, etc.

3. Conclusions

There is a very extensive literature on the subject, of which only a very tiny slice can be presented by the authors.

Numerous methods and methodologies are available thanks to the world's researchers. Based on the experience, both the researchers and the authors of this article are looking for correlations between the results experienced in real life and the simulations and constructed models developed using the computerized DEM method. It will be appreciated that laboratory and computer systems, although highly advanced, contain limitations and conditions. Users almost always must prepare a long list of which parameters they can take into account and which cannot.

In many cases, measurements are difficult to reproduce due to individual laboratory and modelling conditions.

Since every research is different, the authors believe that it is always advisable to use a particular, ideal research method as there is no exact result or it is not clear which is the best solution first. They need to be personalized.

Ideally, characterizations are deterministic and human subjectivity is excluded. Furthermore, if the tools used are objective, they allow the production of repeatable results and work with as much information as possible.

Recent international literature [30-32] suggests that discrete element modelling will be indispensable for sophisticated modelling of granular sets in the future: both mechanically (micro as well as macro) and in terms of fragmentation.

Up-to-date articles [33-37] can be base of further, special numerical modelling problems.

Acknowledgements

The paper was written with the support of the project titled "Internationalisation, initiatives to establish a new source of researchers and graduates and development of knowledge and technological transfer as instruments of intelligent specialisations at Széchenyi István University" (project number: EFOP-3.6.1-16-2016-00017).

References

[1] B. Indraratna, N. T. Ngo, S. Nimbalkar, C. Rujikiatkamjorn, Two Decades of Advancement in Process Simulation Testing of Ballast Strength, Deformation and Degradation. In T. D. Stark, R. H. Swan & R. Szecsy (Eds.), Railroad Ballast Testing and Properties, West Conshohocken, United States: *ASTM International* (2018) pp. 11–38. [cited 2021-01-30]
URL `www.astm.org`

[2] T. D. Stark, S. T. Wilk et al., Fouled Ballast Definitions and Parameters, *American Railway Engineering and Maintenance of Way Association Annual Meeting 2017,* Indianapolis, 2017 [cited 2021-01-30]
URL
`https://www.researchgate.net/publication/319981870_Fouled_Ballast_Definitions_and_Parameters`

[3] M. A. Wnek, E. Tutumluer et al., Investigation of Aggregate Properties Influencing Railroad Ballast Performance, *Transportation Research Record:*

Journal of the Transportation Research Board, Transportation Research Board of the National Academies, No. 2374 (2013) pp. 180–189.
doi: https://doi.org/10.3141/2374-21

[4] G. P. Raymond, V. A. Diyaljee, Railroad ballast sizing and grading, *Journal of the Geotechnical Engineering Division*, 105(GT5) (1979) pp. 676–681.
doi: https://doi.org/10.1061/(ASCE)GT.1943-5606.0001710

[5] E. T. Selig, J. M. Waters, Track Geotechnology and Substructure Management. *Thomas Telford Publications*, London, 1994.

[6] N. T. Ngo, B. Indraratna, C. Rujikiatkamjorn, Micromechanics-based investigation of fouled ballast using large-scale triaxial tests and discrete element modeling, *Journal of Geotechnical and Geoenvironmental Engineering*, 143 (2) (2017) pp. 04016089-1– 04016089-16.
doi: https://doi.org/10.1061/(ASCE)GT.1943-5606.0001587

[7] R. J. Marsal R. J., Large scale testing of rockfill materials, *Journal of Soil Mechanics and Foundation Engineering*, 93(SM2) (1967) pp. 27-43.

[8] B. Indraratna, N. T. Ngo, C. Rujikiatkamjorn, Behavior of geogrid-reinforced ballast under various levels of fouling, *Geotextiles and Geomembranes* 29 (3) (2011) pp. 313–322.
doi: https://doi.org/10.1016/j.geotexmem.2011.01.015

[9] I. Deiros, C. Voivret et al.. Quantifying Degradation of Railway Ballast using Numerical Simulations of Micro-Deval Test and In-situ conditions, *Procedia Engineering* (143) (2016) pp. 1016–1023.
doi: https://doi.org/10.1016/j.proeng.2016.06.096

[10] C. J. Coetzee, Review: Calibration of the discrete element method, *Powder Technology*, 310 (2017) pp. 104–142
doi: https://doi.org/10.1016/j.powtec.2017.01.015

[11] J.-P. Plassiard, N. Belheine, F.-V. Donze, A spherical discrete element model: calibration procedure and incremental response, *Granular Matter* 11 (5) (2009) pp. 293–306.
doi: https://doi.org/10.1007/s10035-009-0130-x

[12] J. Ai, J. F. Chen et al., Assessment of rolling resistance models in discrete element simulations, *Powder Technology* 206 (3) (2011) pp. 269-282. doi: https://doi.org/10.1016/j.powtec.2010.09.030

[13] D. Markauskas, A. Ramirez-Gomez et al., Maize grain shape approaches for DEM modelling, *Computers and Electronics in Agriculture* 118 (2015) pp. 247–258. doi: https://doi.org/10.1016/j.compag.2015.09.004.

[14] B. Saint-Cyr, E. Azema, J.-Y. Delenne, F. Radjai, P. Sornay, Effect of particle shape non-convexity on the rheology of granular media: 3D contact dynamics simulations, *II. International Conference on Particle-based Methods – Fundamentals and Applications*, Barcelona, 2011, pp. 1–8. [cited 2021-01-30] URL https://www.researchgate.net/publication/267985633_Effect_of_Particle_Shape_non-Convexity_on_the_Rheology_of_Granular_Media_3D_Contact_Dynamics_Simulations

[15] B. Zhou, R. Huang et al., DEM investigation of particle anti-rotation effects on the micromechanical response of granular materials, *Granular Matter* 15 (3) (2013) pp. 315–326. doi: https://doi.org/10.1007/s10035-013-0409-9

[16] H. Li, G. R. McDowell, Discrete element modeling of under sleeper pads using a box test, Springer, Nottingham Centre for Geomechanics, *Granular Matter* 20 (2018) pp. 1–12. doi: https://doi.org/10.1007/s10035-018-0795-0

[17] K. Bagi, Á. Orosz, A new variable for characterising irregular element geometries in experiments and DEM simulations, *Communications of the ECMS*, Proceedings, 2020 ISBN 978-3-937436-68-5/978-3-937436-69-2(CD)

[18] J. M Rodriguez, T. Edeskär, S. Knutsson, Particle Shape Quantities and Measurement Techniques – A Review, *EJGE* (18) (2013) pp. 169–198. [cited 2021-01-30] URL https://www.diva-portal.org/smash/get/diva2:976352/FULLTEXT01.pdf

[19] Z. Nie, Z. Liang, X. Wang, A three-dimensional particle roundness evaluation method, Springer, *Granular Matter* 20 (2018) pp. 1–11.
doi: https://doi.org/10.1007/s10035-018-0802-5

[20] ITASCA Consultants GmbH, PFCTM Particle Flow Code software [cited 2021-01-30]
URL https://www.itasca.de/software/PFC

[21] DEM Solutions Ltd., EDEM Software software [cited 2021-01-30]
URL https://www.edemsimulation.com/software/

[22] YADE-DEM [cited 2021-01-30]
URL https://yade-dem.org/doc/

[23] E. Juhasz, R. M. Movahedi, I. Fekete, Sz. Fischer, Discrete Element Modelling of particle degradation of railway ballast material with PFC^{3D} software, *Nauka Ta Progres Transportu* 84 (6) (2019) pp. 103–116.
doi: https://doi.org/10.15802/stp2019/194472

[24] Á. Orosz, J. P. Rádics, K. Tamás, Calibration of railway ballast DEM model, *31st European Conference on Modelling and Simulation*, Budapest, 2017, pp. 1–6.
doi: https://doi.org/10.7148/2017-0523

[25] Z. Hossain, B. Indraratna et al., DEM analysis of angular ballast breakage under cyclic loading, *Geomechanics and Geoengineering: International Journal* 2 (3) (2007) pp. 175–182.
doi: https://doi.org/10.1080/17486020701474962

[26] X. Wang, B. Hua et al., The Research on the DEM Simulation of the Railway Ballast Tamping Process, *Advanced Materials Research* 724-725 (2013) pp. 1723–1726
doi: https://doi.org/10.4028/www.scientific.net/AMR.724-725.1723

[27] X. Wang, B. Hua et al., Study on the Cyclic Loading Effects to the Railway Ballast, *Advanced Materials Research* 724-725 (2013) pp. 1736–1739
doi: https://doi.org/10.4028/www.scientific.net/AMR.724-725.1736

[28] G. R. McDowell, W. L. Lim, A. C. Collop, R. Armitage, N. H. Thom, Comparison of ballast index tests for railway trackbeds, *Geotechnical Engineering* 157(3) (2008) pp. 151–161.
doi: https://doi.org/10.1680/geng.2004.157.3.151

[29] N. T. Ngo, B. Indraratna, C. Rujikiatkamjorn, DEM simulation of the behavior of geogrid stabilised ballast fouled with coal, *Computers and Geotechnics* 55 (2014) pp. 224–231.
doi: https://doi.org/10.1016/j.compgeo.2013.09.008

[30] H. Li, G. McDowell, Discrete element modelling of two-layered ballast in a box test, *Granular Matter* 22 (2020) pp. 1–14.
doi: https://doi.org/10.1007/s10035-020-01046-6

[31] L. Nam-Hyoung, K. Kyoung-Ju et al., DEM Analysis of Track Ballast Track Ballast-Wheel Interaction Simulation, *Applied Sciences* 10 (8) (2020) pp. 1–19.
doi: https://doi.org/10.3390/app10082717

[32] Z. Hongyi, C. Jing, Numerical Study of Railway Ballast Subjected to Direct Shearing Using the Discrete Element Method, *Advances in Materials Science and Engineering* 20 (2020) pp. 1–13.
doi: https://doi.org/10.1155/2020/3404208

[33] M. Sysyn, U. Gerber et al., A laboratory study of pressure distribution and residual settlements in wide grading double layer railway ballast under long-term cyclic loading, *Archives of Civil Engineering* 66 (4) (2020) pp. 561–578.
doi: https://doi.org/10.24425/ace.2020.135237

[34] M. Przybylowicz,, M. Sysyn et al., Experimental and theoretical evaluation of side tamping method for ballasted railway track maintenance, *Transport Problems* 15 (3) (2020) pp. 93–106.
doi: https://doi.org/10.21307/tp-2020-036

[35] M. Sysyn, O. Nabochenko, V. Kovalchuk, Experimental investigation of the dynamic behavior of railwaytrack with sleeper voids, *Railway Engineering Science* 28 (2) (2020) pp. 290–304.
doi: https://doi.org/10.1007/s40534-020-00217-8

[36] D. Kurhan, Y. Leibuk, Research of the Reduced Mass of the Railway Track, *Acta Technica Jaurinensis* 13 (4) (2020) pp. 324–341. doi: https://doi.org/10.14513/actatechjaur.v13.n4.563

[37] D. Kurhan, Determination of Load for Quasi-static Calculations of Railway Track Stress-strain State, *Acta Technica Jaurinensis* 9 (1) (2016) pp. 83–96. doi: https://doi.org/10.14513/actatechjaur.v9.n1.400